Università degli Studi di Torino

Scuola di Dottorato in

Scienze della Natura e Tecnologie Innovative

Dottorato in Scienze Farmaceutiche e Biomolecolari (XXXIII ciclo)

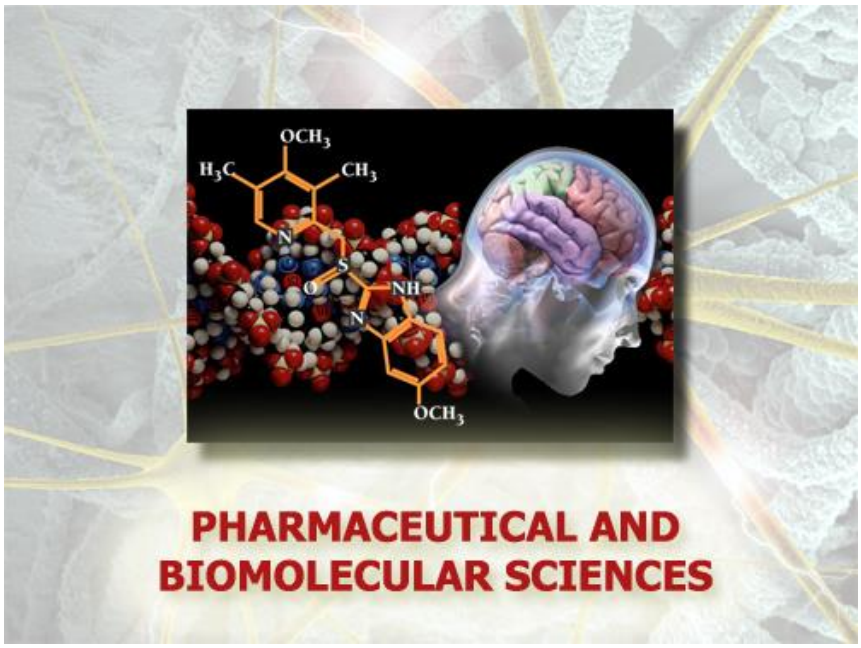

Effect of Protein Dynamics on the Activity of Aromatase

Candidato: Chao Zhang **Tutor: Professor Gianfranco Gilardi**

Università degli Studi di Torino

Dottorato in

Scienze Farmaceutiche e Biomolecolari

Tesi svolta presso il

Dipartimento di Scienze della Vita e Biologia dei Sistemi

CICLO: XXXIII

TITOLO DELLA TESI: Effect of Protein Dynamics on the Activity of Aromatase

TESI PRESENTATA DA: Chao Zhang

TUTOR: Prof. Gianfranco Gilardi

COORDINATORE DEL DOTTORATO: Prof. Roberta Cavalli

ANNI ACCADEMICI: 2017-2018, 2018-2019, 2019-2020

SETTORE SCIENTIFICO-DISCIPLINARE DI AFFERENZA: BIO/10

ACKNOWLEDGMENTS

It has been a long journey and an unforgettable experience for me to pursue a doctorate degree as an international student. It would be an impossible task for me to finish my PhD study without help from many people in my life.

First, I would like to thank my supervisor, Professor Gianfranco Gilardi, for his guidance and encouragement during the course of my PhD. Without his support, I doubt I would have been able to reach this point. Especially his experience and guidance, together with the most advanced equipment and facilities, provided the greatest supports for my project. I consider myself very lucky to have been part of such a great group.

I would like to thank Professor Giovanna di Nardo for bringing me on the CYP19 project, helping me along the way and teaching me so much. I have enjoyed this time and learned a lot from her experiences and rigorous scientific attitudes. In addition, I am very grateful for her patient guidance, proofreading and editing in the process of writing this thesis. I'm glad to have the opportunity to work closely with her.

I am also very thankful for Dr. Gianluca Catucci, who is one of the nicest people I have ever known. He not only taught me to use different instruments but also taught me the mindset necessary to succeed in doing research in the lab. His patience and care were inspiring and encouraging, especially as I was starting out in research.

I would also like to thank Professor Sheila Sadeghi. I will never forget her celebrating the Chinese New Year for me, and I feel the warmth of my home.

I would also like to thank Professor Francesca Valetti. She was always very generous and provided a wealth of knowledge and advice on my experiments.

I am also indebted to Dr. Silvia Castrignanò, who is always so eager to help with anything I need in the lab and provide any support necessary for my experiments to succeed.

I also want to thank the other members of the lab. Dr. Oleksii Skorokhod, Dr. Elena Gazzano, Dr. Arianna Marucco, Dr. Danilo Correddu, Dr. Jose Francisco Gasteazoro Pineiro, Alessandro Della Costa, Hanna Cheropkina, Claudia Grillo and Rossella Scardaci. Especially the people in our office, thank you for your encouragement and company.

I would be remiss if I didn't thank former lab members and my friends Dr. Alberto Ciaramella, Loris Catizzone and Francesca Baj. I will cherish all the fun conversations and internet videos we shared.

Finally, I would like to thank my mother and father. Without your endless love and support, there is no way I would be here. Thank you for always treating me like an adult and letting me find my own way.

Again thank you very much to everyone.

Abstract

Cytochrome P450 aromatase (CYP19A1) is a human steroidogenic cytochrome P450 responsible for the conversion of androgens into estrogens through the aromatization of the A-ring of the steroid molecule. Although aromatase has been studied for decades, many details about its catalytic mechanism are missing. Moreover, the enzyme is polymorphic, it is involved in different estrogen-dependent pathologies and it is a target for the so-called endocrine disrupting chemicals, a series of compounds that are toxic due to their interference with the hormonal system.

The first part of the thesis is focused on the study of how oxygen is activated by human aromatase and on the role of the redox partner cytochrome P450 reductase (CPR). In particular, the oxoferryl reactive species Compound I was obtained by the peroxides pathway and its spectral properties were characterized. Since the formation of Compound I depends on the proton transport network, the role of key amino acids was studied. It was found that Asp-309, part of the conserved "acid-alcohol" pair (Asp-309, Thr-310), plays a key role in proton transfer, whereas Thr-310 has a gating role by stabilizing both Compound 0 and Compound I. The results strongly support that Compound I is the reactive species responsible for C-C cleavage on the aromatization reaction.

Since aromatase requires cytochrome P450 reductase (CPR) as a redox partner to provide electrons required for catalysis, its possible effector role was investigated. Recently, bacterial reductase has been found to affect the structure and function of P450cam. This thesis shows that the presence of CPR accelerated the substrate-binding rate of aromatase. ITC experiments show that CPR binds the substrate-free form of aromatase with a lower dissociation constant compared to that of the substrate-bound form of the enzyme. These results reveal a new effector role of reductase. Such a role seems to have appeared during evolution. Indeed, sequence alignments and structural analysis showed that the surface of aromatase contacting CPR had been optimized in the process of evolution, which introduced new residues favouring the interaction with the redox partner. The sequence and structural comparison between 365 aromatase sequences from different species, mainly vertebrates, also showed the high level of conservation of residues involved in catalysis.

In the second part of the thesis, the research was focused on the study of the molecular bases for the involvement of human aromatase in various pathologies.

Firstly, the effect of two single nucleotide polymorphisms associated with an altered risk for estrogen-dependent pathologies was investigated. The two polymorphic variants (R264h and R264C) were studied by FTIR and fluorescence

spectroscopy that showed that the two mutations affect the flexibility of the enzyme required to bind the substrate.

Secondly, the possible effect of some pesticides on aromatase activity was studied. It is found that glyphosate inhibits aromatase activity in a non-competitive way. Computational simulations show the presence of a possible allosteric site for glyphosate binding that affects the enzyme activity.

Taken together, the results presented in this thesis shed lights on new aspects of the catalytic mechanism of human aromatase, ranging from the role played by few key residues to the modulation of activity played by its redox partner CPR. Moreover, it was shown how single mutations and exogenous molecules could alter the enzyme functionality that is important to maintain the correct levels of estrogens and prevent estrogen-related pathologies.

INDEX

Chapter 1

General introduction

1.1 Cytochromes P450

Cytochrome P450 superfamily (P450s, or CYPs) consists in heme thiolate enzymes widely distributed in the biosphere,[1] involved in many important biotransformations, especially drug metabolism.[2,3] These enzymes were first isolated and identified in the early 1950s.[4,5] The name "P450" comes from the electronic absorption spectrum, which appears after the reduction of heme in the active site of the enzyme, followed by the binding of carbon monoxide (CO) (Figure 1).[5,6] The absorption spectrum was unique compared with other cytochromes because its maximum absorption peak experienced a bathochromic shift (red-shift) from 420 nm to 450 nm, which did not appear in other heme proteins studied at that time.[6,7]

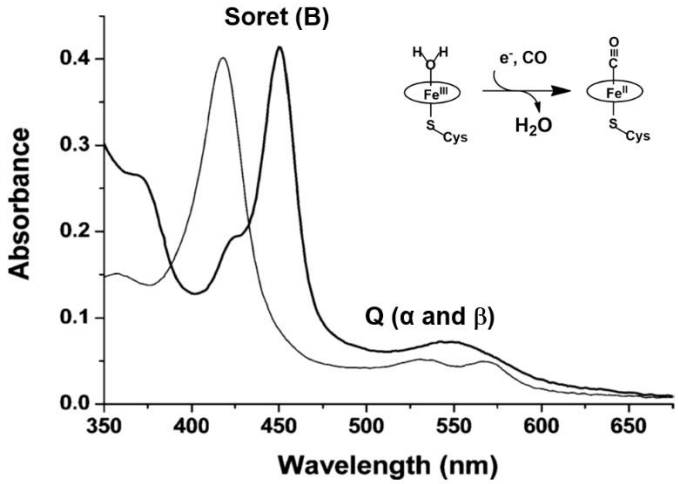

Figure 1 CO-binding spectra of P450 enzyme. thin solid line, low-spin ferric resting sate; thick solid line, reduced CO-bound state.[8]

Over the past several decades, P450 chemistry has gained a broad mechanistic understanding. P450 enzymes show a remarkable diversity of oxidation reactions by using the same active site geometry. In addition to hydroxylation or epoxidation of their substrates, they can also carry out heteroatom oxygenation, dealkylation, aromatization, and other reactions.[9,10] The diversity of P450 catalytic reactions is consistent with its presence in every major branch of the phylogenetic tree.[1,11] At present, the number of P450 enzymes is estimated to be more than 300,000 and P450 from different sources are found continuously.[12]

Although cytochrome P450 is responsible for a variety of different oxidation, the general catalytic reactions can be summarized as the following simplified reactions of methylene hydroxylation:

$$RH + O_2 + NAD(P)H \longrightarrow ROH + H_2O + NAD(P)^+$$

, where RH and ROH represent the substrate and the hydroxylated product respectively.

1.1.1 Catalytic mechanism of P450s

The typical P450 reaction cycle shown in Figure 2. It starts from the resting state of the enzyme, that is, the ferric low-spin state (S = 1/2) [1], which is caused by a coordinated water molecular as the sixth axial ligand.[13] The water is a weak ligand. When the substrate is bound, the water is often perturbed and easily released. The detachment of the water molecule from the heme iron transforms the enzyme into five coordinated high-spin ferric (S= 5/2) state [2], which can be easily detected by many spectroscopic techniques.[14–16] As shown in Figure 1, the absorption spectrum of cytochrome P450 has common spectral characteristics, which is composed of two major bands: Soret or B band (~ 400 nm) and Q band (~ 550 nm), usually split into α (~ 535 nm) and β (~ 570 nm) bands.[17,18] These special bands are produced by strong π - π * transitions affected by the heme state, such as the oxidation state of heme and the addition of coordination ligands in the axial position of heme. In general, the binding of substrates to enzymes replaces the water molecule, showing the maximum absorption peak (Soret band) shifts from 417-419 nm to 390-394 nm.[18] However, However, when the ligands are unnatural substrates or inhibitors, the maximum Soret peak is different.[19] In these cases, heme is six coordinated, and the maximum absorption peak is at 422-426 nm.[20]

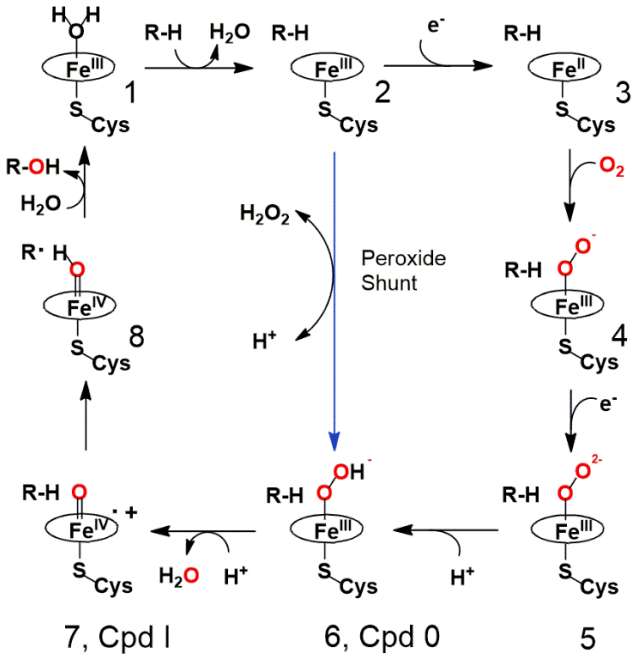

Figure 2 P450 catalytic cycle.[21]

The substrate-binding causes a change of the state of the heme change from low to high spin, which effectively increases the complex's redox potential and is easily reduced by NAD(P)H.[22,23] Although the electrons ultimately come from NAD(P)H, they need to be delivered by the redox partner of P450 in most cases. After the first electron transfer, a change of oxidation state of the ion from ferric to ferrous state [3], and the iron is ready to binding with oxygen form the environment. When the molecular oxygen binds to the reduced iron, the oxy-ferrous complex [4] is produced.[24] The oxy-

ferrous complex receives another electron from the redox partner and is reduced to ferric peroxide [5]. Then, the ferric peroxide is protonated at the distal oxygen to form the ferric hydroperoxide complex, known as “compound 0” [6]. In the second protonation step, compound 0 receives another proton and cleaves the O-O bond to generate a high-valent iron-oxo species, termed as compound I [7].[25–32] In the first step of protonation, if the proximal oxygen is protonated, it will lead to “uncoupling” and produce hydrogen peroxide. The compound I is a highly oxidizing species, which can directly extract electrons and protons from the C-H bond of the substrate, leading to the formation of a protonated compound II species [8].[33,34] At the same time, the hydroxylation product is formed by the rapid recombination of OH and the substrate radical. The hydroxylation product leaves the active site, and a new water molecule binds in the vacant coordination site, regenerates a resting ferric enzyme.

1.1.2 Classification of CYPs

Cytochrome P450s are monooxygenases, that receive electrons from a redox partner to enable to catalyze various reactions. In order to make it easier to discuss the diversity of cytochrome P450, they are classified according to their electron donors or “redox partners”.[35,36] To this date, P450s have been be classified into ten categories (Figure 3).[36] Class I and class II account for almost 90% of the known P450 enzymes.[35] The main focus of this work is on class II system.

The class I P450s usually are present in bacteria or are bound to the mitochondrial membrane of eukaryotes. This system consists of three proteins: FAD containing reductase, Fe_2S_2-containing redoxin and P450. During the catalytic reaction, FAD containing reductase binds to NADH, and the electrons of NADH are transferred from reductase to redoxin, and then to the P450 heme.[35,36]

The Class II P450s mainly come from eukaryotes. They are usually bound to the endoplasmic reticulum and contain two proteins, cytochrome P450 and NADPH cytochrome P450 reductase (CPR). CPR includes both FAD and FMN groups. In this system, electrons form NAPDH are transferred from FAD to FMN and then to P450 in CPR.[35] From a single species point of view, the number of P450 in a eukaryote is far more than that in a prokaryote.

The Class III system was found in 2002, which is very similar to the class I system.[37] The difference is that in this system, the second mediator protein is considered to be a flavodoxin, so electrons are transferred through the redox centers FAD and FMN.

Class IV P450 system is mainly composed of thermophilic P450, such as CYP119.[38,39] In this system, P450s could not obtain reduction equivalents from flavoprotein, but from putidaredoxin and putidaredoxin reductase.[40]

The Class V system consists of two independent proteins: a putative NAD(P)H-dependent reductase and a cytochrome P450 ferredoxin fusion protein, which is different from the classical three-component system.[41]

Class VI system is similar to class V system, in which cytochrome P450 and

flavodoxin form a fusion protein.[42]

In class VII system, the C-terminal of cytochrome P450 is fused with the reductase domain, but this reductase is usually independent of the P450 system.[43]

In class VIII system, P450s fuse with eukaryotic like flavin reductase via a polypeptide chain, so they are catalytically self-sufficiency.[44]

The class IX system is a special P450 system that only contains nitric oxide reductase(P450nor). P450nor uses NADH to catalyze the conversion of two molecules of nitric oxide to nitrous oxide.[45]

P450s from class X systems can catalyze substrate conversion using independent intramolecular transfer systems, such as CYP74A, CYP74B/C and CYP74D.[46–48]

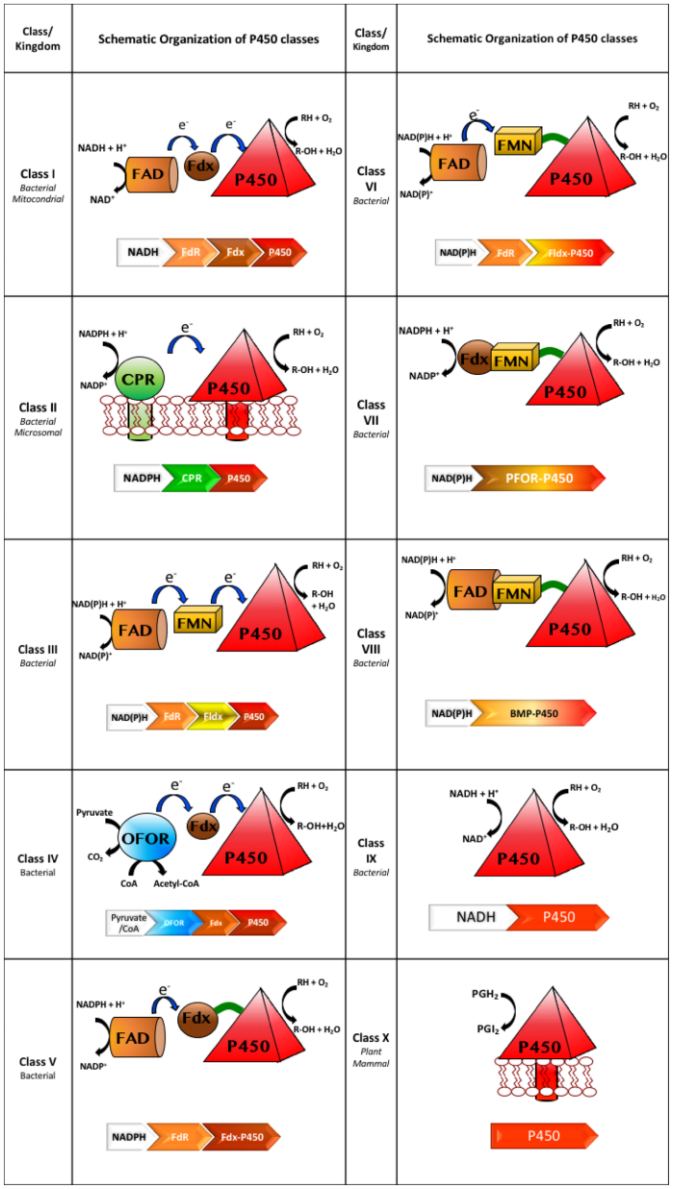

Figure 3 Schematic representation of the ten cytochromes P450 systems.[36]

1.1.3 Human cytochromes P450

There are 18 cytochrome P450 families in mammals, and 41 protein coding subfamilies in the human genome encode 57 genes.[49] According to the substrates and functions, they can be further classified, as shown in Table 1.[49,50] It should also be noted that this grouping is relatively arbitrary, and it should be considered that some P450s can be placed under other categories. For example, human P450 3A4 can not only metabolize xenobiotics but also play a role in steroid metabolism.[51–53]

Table 1 Classification of human P450s based on major substrate class.[49,50]

Sterols	Xenobiotics	Fatty acids	Eicosanoids	Vitamins	Unknown
1B1	1A1	2J2	4F2	2R1	2A7
7A1	1A2	2U1	4F3	24A1	2S1
7B1	2A6	4A11	4F8	26A1	2W1
8B1	2A13	4B1	5A1	26B1	4A22
11A1	2B6	4F11	8A1	26C1	4F22
11B1	2C8	4F12		27B1	4X1
11B2	2C9	4V2		27C1	4Z1
17A1	2C18				20A1
19A1	2C19				
21A2	2D6				
27A1	2E1				
39A1	2F1				
46A1	3A4				
51A1	3A5				
	3A7				
	3A43				

These enzymes have important biological functions in the human body, and are involved in catalyzing important physiological reactions, such as sterols and vitamins metabolism (Table 1). Like other genes and enzymes related to key functions of life, human P450s are associated with some diseases, and some diseases related to human p450 gene defects have been found in clinic.[49]

Steroid hormones are essential for life and reproduction. P450s play indispensable roles in steroidogenesis. Figure 4 shows the P450s involved in steroid biosynthesis pathway and their functions.[54] It involves three cytochrome P450 enzymes, CYP11A1, CYP17A1 and CYP19A1.

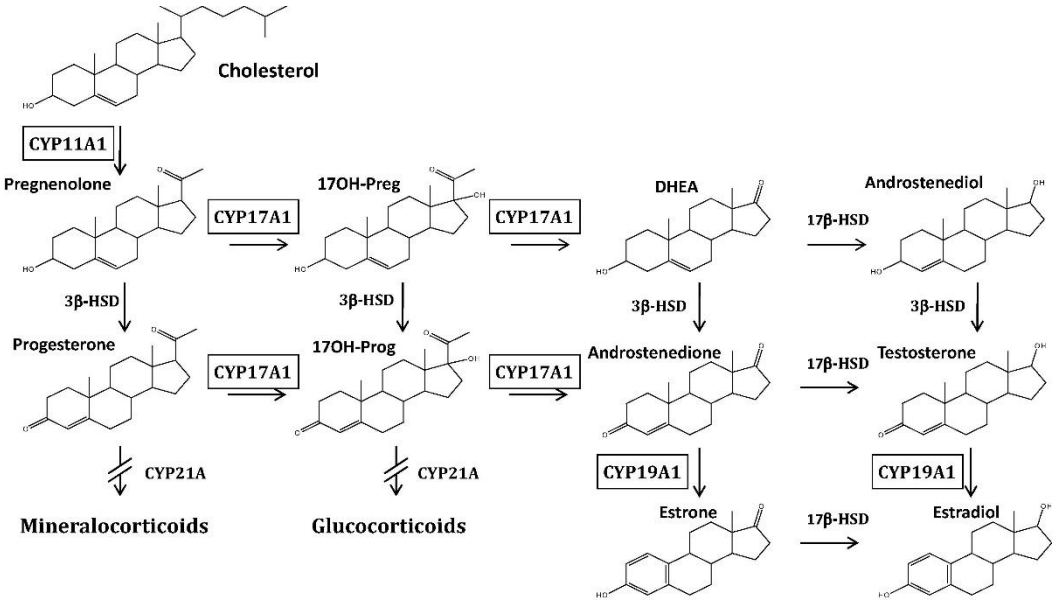

Figure 4 The roles of human P450s in steroidogenesis.[54]

1.2 Human aromatase

This thesis focuses on CYP19A1, also known as aromatase, that one of the human steroidogenic P450s, important for estrogen biosynthesis (Figure 4 and Figure 5).[55,56] It is a membrane-bound heme protein anchored to endoplasmic reticulum through a N-terminal helix. Aromatase is distributed in many tissues and organs, such as gonad, brain, bone, breast, adipose tissue, skin, adrenal gland, liver, placenta and so on.[57] Its expression and activity levels in these tissues and organs are different, and it also displays a gender specificity.

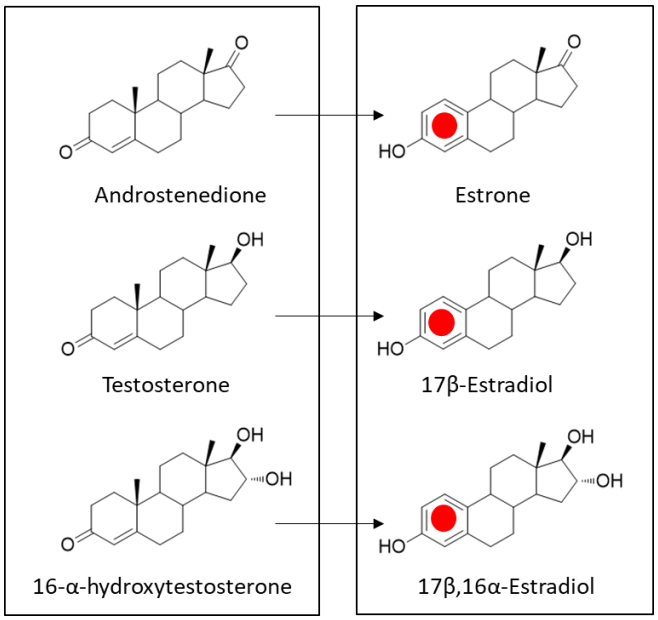

Figure 5 Aromatase catalyzed androgen substrates and corresponding estrogens.[56]

Abnormal expression or activity change of aromatase normally leads to disease. Aromatase inactivation mutations can lead to pseudo-hermaphroditism in female newborns and high stature in males due to epiphyseal closure failure and bone under mineralization.[58,59] Overactivation of aromatase leads to gynecomastia and infertility in males, and thelarche in females. Both sexes will experience adult height decline due to premature growth and early closure of epiphyseal plate.[60] In fact, the diseases caused by aromatase gene mutation are rare, and its abnormal expression has a more serious impact on human health, which may cause estrogen dependent breast cancer in postmenopausal women. The abnormal level of estrogen in postmenopausal women's breast is several times higher than that in premenopausal women, which can cause over activation of estrogen receptor (ER), and then lead to the growth and development of a tumor.

There are usually two ways to treat estrogen receptor positive or ER+ breast cancer. One is to prevent estrogen from activating its receptors. Tamoxifen has been widely used as an ER antagonist in clinic, but it can cause endometrial cancer, thromboembolism and other side effects [61,62] Another treatment strategy is to use inhibitors to inhibit aromatase activity, such as anastrozole. Although they have fewer side effects than tamoxifen, they can still cause heart disease and osteoporosis. Further understanding of the molecular mechanism of aromatase will contribute to the development of more specific inhibitors.

1.2.1 Protein structure

Compared with the soluble P450 in bacteria, P450s in mammals are membrane-associated. Generally, there is a 30-50 amino acid polypeptide chain at the N-terminal involved in membrane interaction. Aromatase consists of a heme group and a single peptide chain with 503 amino acid residues. Its N-terminal has a hydrophobic tail of

about 40 amino acids attached to the endoplasmic reticulum. In 2009, Ghosh and colleagues obtained the X-ray crystal structure of human placental aromatase in complex with androstenedione, which showed typical P450 folding.[63] However, the purification of human placental aromatase is difficult and expensive. Our group has developed a powerful recombinant bacterial system, replacing the N-terminal amino acids with hydrophilic and positively charged amino acids to increase its solubility and stability; adding 4x His-tag to the C-terminal to purify it by affinity chromatography.[64,65] We produced high yields of pure proteins through this method and obtained the crystal structure of recombinant human aromatase.[64,65] Its activity and crystal structure were found to be consistent with these of human placental aromatase.

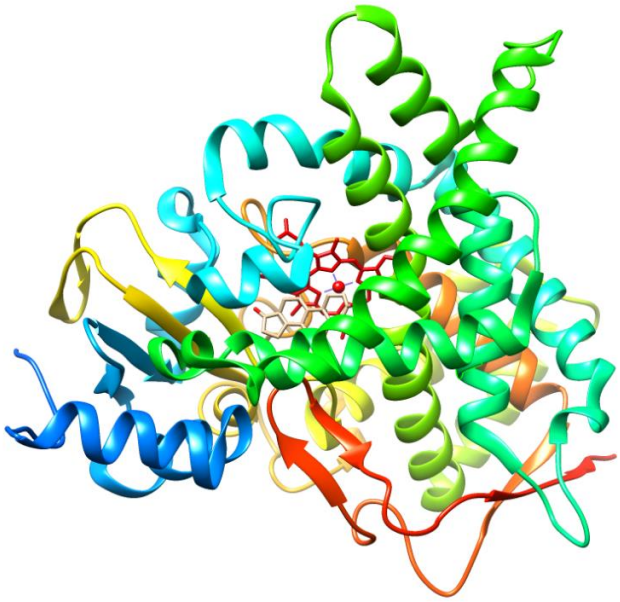

Figure 6 Crystal structure of human aromatase in complex with androstenedione. PDB ID: 3S79. This picture was realized by using UCSF Chimera.

Human aromatase retains the characteristic P450 fold with 12 α-helices (A-L) and 10 β-chains (1-10) (Figure 6).[63] Compared with other P450s, it has some differences in structure. The most notable one is that the unique residue in aromatase is Pro-308, which can cause I-helix distortion and is considered to create space for the substrate in the active site.[63,66] The substrate-binding pocket of aromatase is much smaller, only 400 $Å^3$, while other P450 such as 3A4 and 2D6 are 530 $Å^3$. Besides, the entrance diameter of the binding site is 3.24 Å. It is postulated that it is difficult for a bulkier compound to enter the active site, which requires aromatase to undergo conformational changes to allow the compound to enter. Recent studies have confirmed that some conformational changes occur at the entrance of the substrate channel.[67,68] In P450s, F and G helix can control the entry of substrate, which determines the “open” or “closed” state of the enzyme.[69,70]

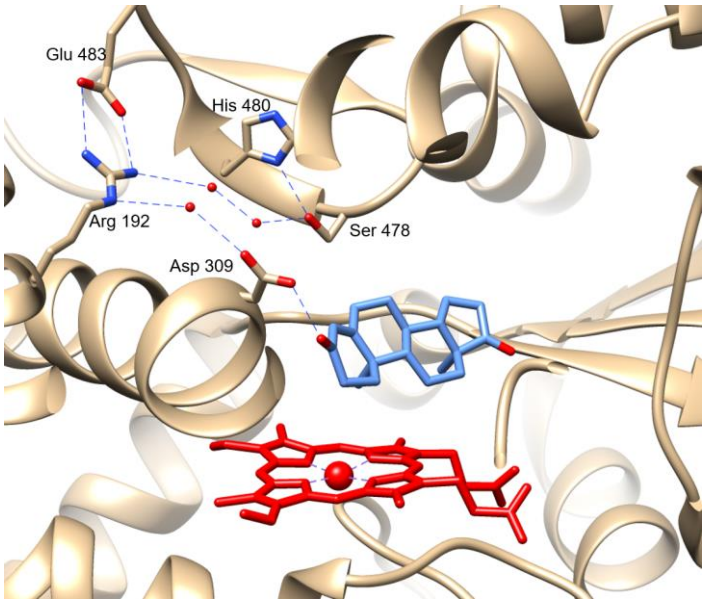

Figure 7 Active site of human aromatase. The network of hydrogen bonds from Ser-478 to His-480 to Arg-192 to Asp-309 has been proposed as crucial for catalysis as a proton donor network.

Near the aromatase substrate channel entrance, there are two amino acids, Arg-192 and Glu-483, which form a salt bridge and are thought to regulate the molecular passage through the active site (Figure 7). Apart from creating a salt bridge with Glu-483, Arg-192 guanidine group is also connected with Asp-309 at the catalytic center by hydrogen bond via a water molecule. The side chain of Asp-309 forms a hydrogen bond with the 3-keto group of androstenedione. In addition, Arg-192 forms two weak hydrogen bonds with Ser-478 through two water molecules. Ser-478 and His-380 also interact through a hydrogen bond. The hydrogen bond network composed of these amino acids and water molecules and the salt bridge play a key role in catalysis and are considered a proton donor network to Arg-309 active site. [63]

1.2.2 Aromatase interaction with its reduction partner

As mentioned before, cytochrome P450 catalyzed reactions require a reductase partner to provide electrons. In aromatase, two electrons transfer are provided by the same reductase, namely NADPH cytochrome P450 reductase (CPR).[71] CPR is also a membrane protein, which is anchored to the out (cytoplasmic) side of the endoplasmic reticulum through its N-terminal. CPR consists of three domains: FMN domain, linker domain and FAD domain.[71,72] CPR has absorption peaks at 370 nm and 450 nm as all flavin-containing proteins.

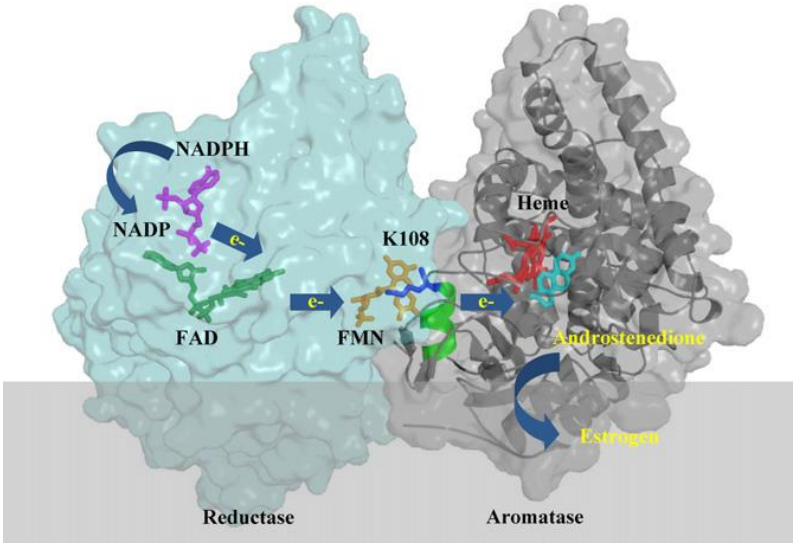

Figure 8 Schematic diagram of CPR-aromatase complex model.[73]

The interaction between CPR and aromatase is predicted to be mainly guided by electrostatic interactions[74,75]. On CPR, the surface of the FMN domain is composed of many carboxylic acid groups, including aspartic acid and glutamic acid side chains, forming a negatively charged surface[74]. However, there are many basic positively charged residues on the near-surface of aromatase. Therefore, these residues on the surface of aromatase form ion pairs with acidic negatively charged residues present on the surface of CPR.[73,74,76,77] This kind of charge interaction has been confirmed by theoretical calculation and experiment.[78,79] The aromatase CPR complex model shows that Lys-108, which is located in B' helix of aromatase, is inserted into the cleft between FMN and FAD domain and interacts with Glu-115/Asp-147 residues of CPR (Figure 8).[73,74] During the synthesis of estrogen, NADPH binds to CPR, and the electrons from NADPH are transferred from FAD to FMN, and finally to the heme of aromatase (Figure 8). Recently, some studies on bacterial P450 have shown that reductase plays an essential role in the structure and function of P450.[80–82] For human P450, whether CPR has a similar function is an important problem to be solved.

1.2.3 Catalytic mechanism of aromatase reaction

Aromatase can catalyze the conversion of androgen (androstenedione, testosterone and 16α-hydroxytestosterone) to estrogen (estrone, 17β-estradiol and 17β,16α-estriol respectively) through a three-step sequential reaction, which consumes three moles of oxygen and three moles of NADPH (Figure 9).[56,83]

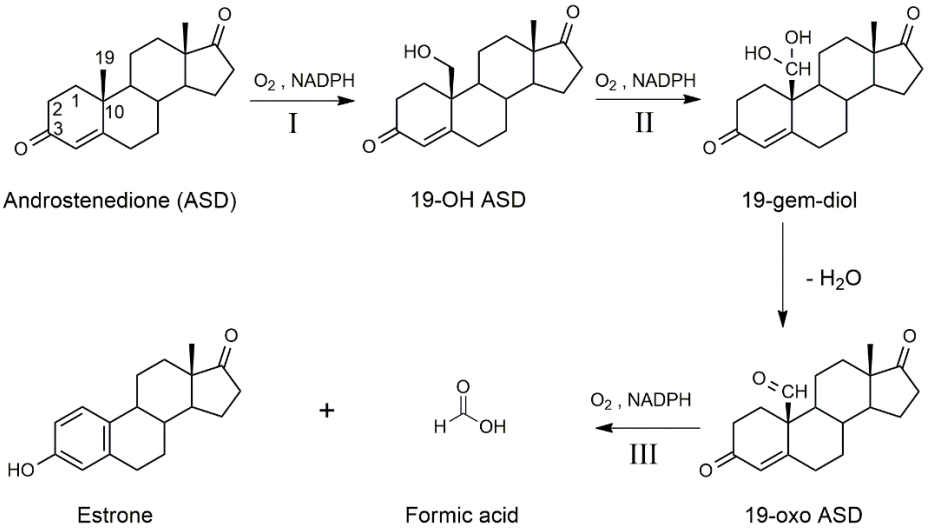

Figure 9 The three-step reactions performed by aromatase

The catalytic action starts from the C19 hydroxylation of androstenedione (ASD) to obtain 19-OH ASD [I], and then hydroxylates the same carbon to form 19-*gem*-diol ASD [II]. The *gem*-diol intermediate is dehydrated to form 19-oxo ASD. In the third step, the C-C bond between C19 and C10 of 19-oxo ASD was broken, the C19 carboxyl group was separated as formic acid, and the A-ring of steroid molecule was aromatized.[83]

There are two hypotheses about the last step of catalysis: one is that the ferric peroxide (5, Figure 2) acts as an active iron species to attack carbonyl group;[84–88] the other is that compound I (7, Figure 2) is still the reactive intermediate. The third step catalytic reaction mechanism has been controversial for a long time because there is much conflicting evidence, such as deacetylation mimicked by a peroxo ferric porphyrin complex,[89] C-C cleavage catalyzed by ferric peroxide species in CYP17A1,[90,91] and some reactions catalyzed by nitric oxide synthase[92]. However, in recent studies, the mechanism of compound I is supported by kinetic solvent isotope effect, resonance Raman spectroscopy and ^{18}O isotope labelling.[93–95] The essential difference between these two hypotheses is whether it needs the proton transport network in protein,[23,80,96,97] because the theory of ferric peroxide is to extract hydrogen from the substrate.[98]

In this thesis, the catalytic mechanism of recombinant aromatase was studied by various biochemical and biophysical techniques, including the catalytic active intermediate of aromatase, proton transfer network and the interaction between aromatase and reductase. In addition, the molecular basis of aromatase involved in various pathological processes was also studied.

1.3 References

[1] Nelson, D. R. A World of Cytochrome P450s. *Philos. Trans. R. Soc. Lond. B. Biol. Sci.* **2013**, *368* (1612), 20120430. https://doi.org/10.1098/rstb.2012.0430.

[2] Ortiz de Montellano, P.R. *Cytochrome P450: Structure, Mechanism, and Biochemistry*, 3rd ed.; Ortiz de Montellano, P.R., Ed.; Kluwer Academic/Plenum Publishers: New York, NY, USA, **2005**. https://doi.org/10.1007/b139087.

[3] Poulos, T. L. Heme Enzyme Structure and Function. *Chem. Rev.* **2014**, *114* (7), 3919–3962. https://doi.org/10.1021/cr400415k.

[4] Brodie, B. B.; Axelrod, J.; Cooper, J. R.; Gaudette, L.; Du, B. N. L.; Mitoma, C.; Udenfriend, S. Detoxication of Drugs and Other Foreign Compounds by Liver Microsomes. *Science* **1955**, *121* (3147), 603–604. https://doi.org/10.1126/science.121.3147.603.

[5] Klingenberg, M. Pigments of Rat Liver Microsomes. *Arch. Biochem. Biophys.* **1958**, *75* (2), 376–386. https://doi.org/10.1016/0003-9861(58)90436-3.

[6] Omura, T.; Sato, R. A New Cytochrome in Liver Microsomes. *J. Biol. Chem.* **1962**, *237*, 1375–1376. PMID: 14482007

[7] Omura, T.; Sato, R. The Carbon Monoxide-Binding Pigment of Liver Microsomes. II. Solubilization, Purification, and Properties. *J. Biol. Chem.* **1964**, *239* (7), 2379–2385. https://doi.org/10.1016/S0021-9258(20)82245-5.

[8] Munro, A. W.; Girvan, H. M.; McLean, K. J. Variations on a (t)Heme—Novel Mechanisms, Redox Partners and Catalytic Functions in the Cytochrome P450 Superfamily. *Nat. Prod. Rep.* **2007**, *24* (3), 585–609. https://doi.org/10.1039/B604190F.

[9] Werck-Reichhart, D.; Feyereisen, R. Cytochromes P450: A Success Story. *Genome Biol.* **2000**, *1* (6), reviews3003.1. https://doi.org/10.1186/gb-2000-1-6-reviews3003.

[10] Guengerich, F. Uncommon P450-Catalyzed Reactions. *Curr. Drug Metab.* **2001**, *2* (2), 93–115. https://doi.org/10.2174/1389200013338694.

[11] Nelson, D. R. The Cytochrome P450 Homepage. *Hum. Genomics.* **2009**, *4* (1), 59–65. https://doi.org/10.1186/1479-7364-4-1-59.

[12] Nelson, D. R. Cytochrome P450 Diversity in the Tree of Life. *Biochim. Biophys. Acta.* **2018**, *1866* (1), 141–154. https://doi.org/10.1016/j.bbapap.2017.05.003.

[13] Sharrock, M.; Münck, E.; Debrunner, P. G.; Marshall, V.; Lipscomb, J. D.; Gunsalus, I. C. Mössbauer Studies of Cytochrome P-450 Cam. *Biochemistry* **1973**, *12* (2), 258–265. https://doi.org/10.1021/bi00726a013.

[14] Omura, T.; Sato, R. The Carbon Monoxide-binding Pigment of Liver Microsomes. II. Evidence Its Hemoprotein Nature. *J. Biol. Chem.* **1964**, *239*, 2370–2378.

PMID: 14209972

[15] Tsai, R.; Yu, C. A.; Gunsalus, I. C.; Peisach, J.; Blumberg, W.; Orme-Johnson, W. H.; Beinert, H. Spin-state Changes in Cytochrome P-450cam on Binding of Specific Sustrates. *PNAS* **1970**, *66* (4), 1157–1163. https://doi.org/10.1073/pnas.66.4.1157.

[16] Sharrock, M.; Debrunner, P. G.; Schulz, C.; Lipscomb, J. D.; Marshall, V.; Gunsalus, I. C. Cytochrome P450cam and Its Complexes. Mössbauer Parameters of the Heme Iron. *Biochim. Biophys. Acta.* **1976**, *420* (1), 8–26. https://doi.org/10.1016/0005-2795(76)90340-8.

[17] Gouterman, M. Spectra of Porphyrins. *J. Mol. Spectrosc.* **1961**, *6*, 138–163. https://doi.org/10.1016/0022-2852(61)90236-3.

[18] Danielson, P. B. The Cytochrome P450 Superfamily: Biochemistry, Evolution and Drug Metabolism in Humans. *Curr Drug Metab* **2002**, *3* (6), 561–597. https://doi.org/10.2174/1389200023337054.

[19] Conner, K. P.; Vennam, P.; Woods, C. M.; Krzyaniak, M. D.; Bowman, M. K.; Atkins, W. M. 1,2,3-Triazole-Heme Interactions in Cytochrome P450: Functionally Competent Triazole-Water-Heme Complexes. *Biochemistry* **2012**, *51* (32), 6441–6457. https://doi.org/10.1021/bi300744z.

[20] Schenkman, J. B.; Sligar, S. G.; Cinti, D. L. Substrate Interaction with Cytochrome P-450. *Pharmacol. Ther.* **1981**, *12* (1), 43–71. https://doi.org/10.1016/0163-7258(81)90075-9.

[21] Gilardi, G.; Di Nardo, G. Heme Iron Centers in Cytochrome P450: Structure and Catalytic Activity. *Rend. Fis. Acc. Lincei* **2017**, *28* (S1), 159–167. https://doi.org/10.1007/s12210-016-0565-z.

[22] Lipscomb, J. D. Electron Paramagnetic Resonance Detectable States of Cytochrome P-450cam. *Biochemistry* **1980**, *19* (15), 3590–3599. https://doi.org/10.1021/bi00556a027.

[23] Denisov, I. G.; Makris, T. M.; Sligar, S. G.; Schlichting, I. Structure and Chemistry of Cytochrome P450. *Chem. Rev.* **2005**, *105* (6), 2253–2278. https://doi.org/10.1021/cr0307143.

[24] Momenteau, M.; Reed, C. A. Synthetic Heme-Dioxygen Complexes. *Chem. Rev.* **1994**, *94* (3), 659–698. https://doi.org/10.1021/cr00027a006.

[25] Dunford, H. B.; Stillman, J. S. On the Function and Mechanism of Action of Peroxidases. *Coord. Chem. Rev.* **1976**, *19* (3), 187–251. https://doi.org/10.1016/S0010-8545(00)80316-1.

[26] Green, M. T. Evidence for Sulfur-Based Radicals in Thiolate Compound I Intermediates. *J. Am. Chem. Soc.* **1999**, *121* (34), 7939–7940. https://doi.org/10.1021/ja991541v.

[27] Green, M. T. CH Bond Activation in Heme Proteins: The Role of Thiolate Ligation in Cytochrome P450. *Curr. Opin. Chem. Biol.* **2009**, *13* (1), 84–88. https://doi.org/10.1016/j.cbpa.2009.02.028.

[28] Stone, K. L.; Behan, R. K.; Green, M. T. X-Ray Absorption Spectroscopy of Chloroperoxidase Compound I: Insight into the Reactive Intermediate of P450 Chemistry. *PNAS* **2005**, *102* (46), 16563–16565. https://doi.org/10.1073/pnas.0507069102.

[29] Rittle, J.; Green, M. T. Cytochrome P450 Compound I: Capture, Characterization, and C-H Bond Activation Kinetics. *Science* **2010**, *330* (6006), 933–937. https://doi.org/10.1126/science.1193478.

[30] Rittle, J.; Younker, J. M.; Green, M. T. Cytochrome P450: The Active Oxidant and Its Spectrum. *Inorg. Chem.* **2010**, *49* (8), 3610–3617. https://doi.org/10.1021/ic902062d.

[31] Krest, C. M.; Onderko, E. L.; Yosca, T. H.; Calixto, J. C.; Karp, R. F.; Livada, J.; Rittle, J.; Green, M. T. Reactive Intermediates in Cytochrome P450 Catalysis. *J. Biol. Chem.***2013**, *288* (24), 17074–17081. https://doi.org/10.1074/jbc.R113.473108.

[32] Krest, C. M.; Silakov, A.; Rittle, J.; Yosca, T. H.; Onderko, E. L.; Calixto, J. C.; Green, M. T. Significantly Shorter Fe-S Bond in Cytochrome P450-I Is Consistent with Greater Reactivity Relative to Chloroperoxidase. *Nat. Chem.* **2015**, *7* (9), 696–702. https://doi.org/10.1038/nchem.2306.

[33] Davydov, R.; Makris, T. M.; Kofman, V.; Werst, D. E.; Sligar, S. G.; Hoffman, B. M. Hydroxylation of Camphor by Reduced Oxy-Cytochrome P450cam: Mechanistic Implications of EPR and ENDOR Studies of Catalytic Intermediates in Native and Mutant Enzymes. *J. Am. Chem. Soc.* **2001**, *123* (7), 1403–1415. https://doi.org/10.1021/ja003583l.

[34] Groves, J. T. High-Valent Iron in Chemical and Biological Oxidations. *J. Inorg. Biochem.* **2006**, *100* (4), 434–447. https://doi.org/10.1016/j.jinorgbio.2006.01.012.

[35] Hannemann, F.; Bichet, A.; Ewen, K. M.; Bernhardt, R. Cytochrome P450 Systems—Biological Variations of Electron Transport Chains. *Biochim. Biophys. Acta.* **2007**, *1770* (3), 330–344. https://doi.org/10.1016/j.bbagen.2006.07.017.

[36] (36) Ciaramella, A.; Minerdi, D.; Gilardi, G. Catalytically Self-Sufficient Cytochromes P450 for Green Production of Fine Chemicals. *Rend. Fis. Acc. Lincei* **2017**, *28* (S1), 169–181. https://doi.org/10.1007/s12210-016-0581-z.

[37] Hawkes, D. B.; Adams, G. W.; Burlingame, A. L.; Ortiz de Montellano, P. R.; De Voss, J. J. Cytochrome P450cin (CYP176A), Isolation, Expression, and Characterization. *J. Biol. Chem.* **2002**, *277* (31), 27725–27732. https://doi.org/10.1074/jbc.M203382200.

[38] Wright, R. L.; Harris, K.; Solow, B.; White, R. H.; Kennelly, P. J. Cloning of a Potential Cytochrome P450 from the Archaeon Sulfolobus Solfataricus. *FEBS Lett.* **1996**, *384* (3), 235–239. https://doi.org/10.1016/0014-5793(96)00322-5.

[39] Oku, Y.; Ohtaki, A.; Kamitori, S.; Nakamura, N.; Yohda, M.; Ohno, H.; Kawarabayasi, Y. Structure and Direct Electrochemistry of Cytochrome P450 from the Thermoacidophilic Crenarchaeon, Sulfolobus Tokodaii Strain 7. *J. Inorg. Biochem.* **2004**, *98* (7), 1194–1199. https://doi.org/10.1016/j.jinorgbio.2004.05.002.

[40] Puchkaev, A. V. The Sulfolobus Solfataricus Electron Donor Partners of Thermophilic CYP119: An Unusual Non-NAD(P)H-Dependent Cytochrome P450 System. *Arch. Biochem. Biophys.* **2005**, *34*(1), 169-77. https://doi.org/doi: 10.1016 / j.abb.2004.10.022.

[41] Jackson, C. J.; Lamb, D. C.; Marczylo, T. H.; Warrilow, A. G. S.; Manning, N. J.; Lowe, D. J.; Kelly, D. E.; Kelly, S. L. A Novel Sterol 14 alpha-Demethylase/Ferredoxin Fusion Protein (MCCYP51FX) from Methylococcus Capsulatus Represents a New Class of the Cytochrome P450 Superfamily. *J. Biol. Chem.* **2002**, *277*(49), 46959-65. https://doi.org/10.1074/jbc.M203523200.

[42] Rylott, E. L.; Jackson, R. G.; Edwards, J.; Womack, G. L.; Seth-Smith, H. M. B.; Rathbone, D. A.; Strand, S. E.; Bruce, N. C. An Explosive-Degrading Cytochrome P450 Activity and Its Targeted Application for the Phytoremediation of RDX. *Nat. Biotechnol.* **2006**, *24* (2), 216–219. https://doi.org/10.1038/nbt1184.

[43] Roberts, G. A.; Grogan, G.; Greter, A.; Flitsch, S. L.; Turner, N. J. Identification of a New Class of Cytochrome P450 from a Rhodococcus Sp. *J. Bacteriol.* **2002**, *184* (14), 3898–3908. https://doi.org/10.1128/jb.184.14.3898-3908.2002.

[44] Warman, A. J.; Roitel, O.; Neeli, R.; Girvan, H. M.; Seward, H. E.; Murray, S. A.; McLean, K. J.; Joyce, M. G.; Toogood, H.; Holt, R. A.; Leys, D.; Scrutton, N. S.; Munro, A. W. Flavocytochrome P450 BM3: An Update on Structure and Mechanism of a Biotechnologically Important Enzyme. *Biochem. Soc. Trans.* **2005**, *33* (4), 747–753. https://doi.org/10.1042/BST0330747.

[45] (45) Nakahara, K. Cytochrome P-450 55A1 (P-450dNIR) Acts as Nitric Oxide Reductase Employing NADH as the Direct Electron Donor. *J. Biol. Chem.* **1993**, *268* (11), 8350–8355. PMID: 8463342.

[46] Froehlich, J. E.; Itoh, A.; Howe, G. A. Tomato Allene Oxide Synthase and Fatty Acid Hydroperoxide Lyase, Two Cytochrome P450s Involved in Oxylipin Metabolism, Are Targeted to Different Membranes of Chloroplast Envelope. *Plant Physiol.* **2001**, *125* (1), 306–317. https://doi.org/10.1104/pp.125.1.306.

[47] Lau, S. M. C.; Harder, P. A.; O'Keefe, D. P. Low Carbon Monoxide Affinity Allene Oxide Synthase Is the Predominant Cytochrome P450 in Many Plant Tissues. *Biochemistry* **1993**, *32* (8), 1945–1950. https://doi.org/10.1021/bi00059a010.

[48] Y, S.; K, M.; T, K.; A, H. Fatty Acid Hydroperoxide Lyase Is a Heme Protein. *Biochem Biophys Res Commun* **1995**, *207* (1), 438–443. https://doi.org/10.1006/bbrc.1995.1207.

[49] Nebert, D. W.; Wikvall, K.; Miller, W. L. Human Cytochromes P450 in Health and Disease. *Philos. Trans. R Soc. Lond. B Biol. Sci.* **2013**, *368* (1612), 20120431. https://doi.org/10.1098 / rstb.2012.0431

[50] Guengerich, F. P.; Wu, Z.-L.; Bartleson, C. J. Function of Human Cytochrome P450s: Characterization of the Orphans. *Biochem. Biophys. Res. Commun.* **2005**, *338* (1), 465–469. https://doi.org/10.1016/j.bbrc.2005.08.079.

[51] (51) Kenworthy, K. E.; Bloomer, J. C.; Clarke, S. E.; Houston, J. B. CYP3A4 Drug Interactions: Correlation of 10 in Vitro Probe Substrates. *Br. J. Clin. Pharmacol.* **1999**, *48* (5), 716–727. https://doi.org/10.1046/j.1365-2125.1999.00073.x.

[52] Krauser, J. A.; Voehler, M.; Tseng, L.-H.; Schefer, A. B.; Godejohann, M.; Guengerich, F. P. Testosterone 1 Beta-Hydroxylation by Human Cytochrome P450 3A4. *Eur. J. Biochem.* **2004**, *271* (19), 3962–3969. https://doi.org/10.1111/j.1432-1033.2004.04339.x.

[53] Cheng, Q.; Sohl, C. D.; Yoshimoto, F. K.; Guengerich, F. P. Oxidation of Dihydrotestosterone by Human Cytochromes P450 19A1 and 3A4. *J. Biol. Chem.* **2012**, *287* (35), 29554–29567. https://doi.org/10.1074/jbc.M112.390047.

[54] Goldstone, J. V. Genetic and Structural Analyses of Cytochrome P450 Hydroxylases in Sex Hormone Biosynthesis: Sequential Origin and Subsequent Coevolution. *Mol. Phylogenet. Evol.* **2016**, 12.

[55] Thompson, E. A.; Siiteri, P. K. The Involvement of Human Placental Microsomal Cytochrome P-450 in Aromatization. *J. Biol. Chem.* **1974**, *249* (17), 5373–5378.

[56] Di Nardo, G.; Gilardi, G. Human Aromatase: Perspectives in Biochemistry and Biotechnology. *Biotechnol. Appl. Biochem.* **2013**, *60* (1), 92–101. https://doi.org/10.1002/bab.1088.

[57] Simpson, E. R.; Mahendroo, M. S.; Means, G. D.; Kilgore, M. W.; Hinshelwood, M. M.; Graham-Lorence, S.; Amarneh, B.; Ito, Y.; Fisher, C. R.; Michael, M. D.; Mendelson, C. R.; Bulun, S. E. Aromatase Cytochrome P450, The Enzyme Responsible for Estrogen Biosynthesis. *Endocr. Rev.* **1994**, *15* (3), 342–355. https://doi.org/10.1210/edrv-15-3-342.

[58] Simpson, E. R. Genetic Mutations Resulting in Loss of Aromatase Activity in Humans and Mice. *J. Soc. Gynecol. Investig.* **2000**, *7* (1 Suppl), S18-21.

[59] Jones, M. E. E.; Boon, W. C.; McInnes, K.; Maffei, L.; Carani, C.; Simpson, E. R. Recognizing Rare Disorders: Aromatase Deficiency. *Nat. Clin. Pract. Endocrinol. Metab.* **2007**, *3* (5), 414–421. https://doi.org/10.1038/ncpendmet0477.

[60] Shozu, M.; Sebastian, S.; Takayama, K.; Hsu, W.-T.; Schultz, R. A.; Neely, K.;

Bryant, M.; Bulun, S. E. Estrogen Excess Associated with Novel Gain-of-Function Mutations Affecting the Aromatase Gene. *N. Engl. J. Med.* **2003**, *348* (19), 1855–1865. https://doi.org/10.1056/NEJMoa021559.

[61] Love, R. R.; Barden, H. S.; Mazess, R. B.; Epstein, S.; Chappell, R. J. Effect of Tamoxifen on Lumbar Spine Bone Mineral Density in Postmenopausal Women after 5 Years. *Arch. Intern. Med.* **1994**, *154* (22), 2585–2588.

[62] Cuzick, J.; Powles, T.; Veronesi, U.; Forbes, J.; Edwards, R.; Ashley, S.; Boyle, P. Overview of the Main Outcomes in Breast-Cancer Prevention Trials. *Lancet* **2003**, *361* (9354), 296–300. https://doi.org/10.1016/S0140-6736(03)12342-2.

[63] Ghosh, D.; Griswold, J.; Erman, M.; Pangborn, W. Structural Basis for Androgen Specificity and Oestrogen Synthesis in Human Aromatase. *Nature* **2009**, *457* (7226), 219–223. https://doi.org/10.1038/nature07614.

[64] Lo, J.; Di Nardo, G.; Griswold, J.; Egbuta, C.; Jiang, W.; Gilardi, G.; Ghosh, D. Structural Basis for the Functional Roles of Critical Residues in Human Cytochrome P450 Aromatase. *Biochemistry* **2013**, *52* (34), 5821–5829. https://doi.org/10.1021/bi400669h.

[65] Di Nardo, G.; Breitner, M.; Sadeghi, S. J.; Castrignanò, S.; Mei, G.; Venere, A. D.; Nicolai, E.; Allegra, P.; Gilardi, G. Dynamics and Flexibility of Human Aromatase Probed by FTIR and Time Resolved Fluorescence Spectroscopy. *PLOS ONE* **2013**, *8* (12), e82118. https://doi.org/10.1371/journal.pone.0082118.

[66] Ghosh, D.; Griswold, J.; Erman, M.; Pangborn, W. X-Ray Structure of Human Aromatase Reveals an Androgen-Specific Active Site. *J. Steroid Biochem. Mol. Biol.* **2010**, *118* (4–5), 197–202. https://doi.org/10.1016/j.jsbmb.2009.09.012.

[67] Ghosh, D.; Lo, J.; Morton, D.; Valette, D.; Xi, J.; Griswold, J.; Hubbell, S.; Egbuta, C.; Jiang, W.; An, J.; Davies, H. M. L. Novel Aromatase Inhibitors by Structure-Guided Design. *J. Med. Chem.* **2012**, *55* (19), 8464–8476. https://doi.org/10.1021/jm300930n.

[68] Di Nardo, G.; Cimicata, G.; Baravalle, R.; Dell'Angelo, V.; Ciaramella, A.; Catucci, G.; Ugliengo, P.; Gilardi, G. Working at the Membrane Interface: Ligand-Induced Changes in Dynamic Conformation and Oligomeric Structure in Human Aromatase. *Biotechnol. Appl. Biochem.* **2018**, *65* (1), 46–53. https://doi.org/10.1002/bab.1613.

[69] Hays, A.-M. A.; Dunn, A. R.; Chiu, R.; Gray, H. B.; Stout, C. D.; Goodin, D. B. Conformational States of Cytochrome P450cam Revealed by Trapping of Synthetic Molecular Wires. *J. Mol. Biol.* **2004**, *344* (2), 455–469. https://doi.org/10.1016/j.jmb.2004.09.046.

[70] Lee, Y.-T.; Wilson, R. F.; Rupniewski, I.; Goodin, D. B. P450cam Visits an Open Conformation in the Absence of Substrate. *Biochemistry* **2010**, *49* (16), 3412–3419. https://doi.org/10.1021/bi100183g.

[71] Iyanagi, T. Structure and Function of NADPH-Cytochrome P450 Reductase and Nitric Oxide Synthase Reductase Domain. *Biochem. Biophys. Res. Commun.* **2005**, *338* (1), 520–528. https://doi.org/10.1016/j.bbrc.2005.08.043.

[72] Wang, M.; Roberts, D. L.; Paschke, R.; Shea, T. M.; Masters, B. S. S.; Kim, J.-J. P. Three-Dimensional Structure of NADPH–Cytochrome P450 Reductase: Prototype for FMN- and FAD-Containing Enzymes. *PNAS* **1997**, *94* (16), 8411–8416. https://doi.org/10.1073/pnas.94.16.8411.

[73] Hong, Y.; Rashid, R.; Chen, S. Binding Features of Steroidal and Nonsteroidal Inhibitors. *Steroids* **2011**, *76* (8), 802–806. https://doi.org/10.1016/j.steroids.2011.02.037.

[74] Hong, Y.; Li, H.; Yuan, Y.-C.; Chen, S. Sequence-Function Correlation of Aromatase and Its Interaction with Reductase. *J. Steroid. Biochem. Mol. Biol.* **2010**, *118* (4–5), 203–206. https://doi.org/10.1016/j.jsbmb.2009.11.010.

[75] Hlavica, P. Mechanistic Basis of Electron Transfer to Cytochromes P450 by Natural Redox Partners and Artificial Donor Constructs. *Adv. Exp. Med. Biol.* **2015**, *851*, 247–297. https://doi.org/10.1007/978-3-319-16009-2_10.

[76] Bernhardt, R.; Pommerening, K.; Ruckpaul, K. Modification of Carboxyl Groups on NADPH-Cytochrome P-450 Reductase Involved in Binding of Cytochromes C and P-450 LM2. *Biochem. Int.* **1987**, *14* (5), 823–832.

[77] Nadler, S. G.; Strobel, H. W. Role of Electrostatic Interactions in the Reaction of NADPH-Cytochrome P-450 Reductase with Cytochromes P-450. *Arch. Biochem. Biophys.* **1988**, *261* (2), 418–429. https://doi.org/10.1016/0003-9861(88)90358-X.

[78] Bernhardt, R.; Kraft, R.; Otto, A.; Ruckpaul, K. Electrostatic Interactions between Cytochrome P-450 LM2 and NADPH-Cytochrome P-450 Reductase. *Biomed. Biochim. Acta.* **1988**, *47* (7), 581–592.

[79] Shimizu, T.; Tateishi, T.; Hatano, M.; Fujii-Kuriyama, Y. Probing the Role of Lysines and Arginines in the Catalytic Function of Cytochrome P450d by Site-Directed Mutagenesis. Interaction with NADPH-Cytochrome P450 Reductase. *J. Biol. Chem.* **1991**, *266* (6), 3372–3375.

[80] Tripathi, S.; Li, H.; Poulos, T. L. Structural Basis for Effector Control and Redox Partner Recognition in Cytochrome P450. *Science* **2013**, *340* (6137), 1227–1230. https://doi.org/10.1126/science.1235797.

[81] Hollingsworth, S. A.; Batabyal, D.; Nguyen, B. D.; Poulos, T. L. Conformational Selectivity in Cytochrome P450 Redox Partner Interactions. *PNAS* **2016**, *113* (31), 8723–8728. https://doi.org/10.1073/pnas.1606474113.

[82] Zhang, W.; Liu, Y.; Yan, J.; Cao, S.; Bai, F.; Yang, Y.; Huang, S.; Yao, L.; Anzai, Y.; Kato, F.; Podust, L. M.; Sherman, D. H.; Li, S. New Reactions and Products Resulting from Alternative Interactions between the P450 Enzyme and Redox

Partners. *J. Am. Chem. Soc.* **2014**, *136* (9), 3640–3646. https://doi.org/10.1021/ja4130302.

[83] Akhtar, M.; Wright, J. N.; Lee-Robichaud, P. A Review of Mechanistic Studies on Aromatase (CYP19) and 17α-Hydroxylase-17,20-Lyase (CYP17). *J. Steroid Biochem. Mol. Biol.* **2011**, *125* (1–2), 2–12. https://doi.org/10.1016/j.jsbmb.2010.11.003.

[84] Akhtar, M.; Calder, M. R.; Corina, D. L.; Wright, J. N. Mechanistic Studies on C-19 Demethylation in Oestrogen Biosynthesis. *Biochem. J* **1982**, *201* (3), 569–580.

[85] Akhtar, M.; Corina, D.; Miller, S.; Shyadehi, A. Z.; Wright, J. N. Mechanism of the Acyl-Carbon Cleavage and Related Reactions Catalyzed by Multifunctional P-450s: Studies on Cytochrome P-45017.Alpha. *Biochemistry* **1994**, *33* (14), 4410–4418. https://doi.org/10.1021/bi00180a039.

[86] Caspi, Eliahu.; Arunachalam, Thangavel.; Nelson, P. A. Biosynthesis of Estrogens: Aromatization of (19R)-, (19S)-, and (19RS)-[19-3H,2H,1H]-3.Beta.-Hydroxyandrost-5-En-17-Ones by Human Placental Aromatase. *J. Am. Chem. Soc.* **1986**, *108* (8), 1847–1852. https://doi.org/10.1021/ja00268a023.

[87] Shyadehi, A. Z.; Lamb, D. C.; Kelly, S. L.; Kelly, D. E.; Schunck, W. H.; Wright, J. N.; Corina, D.; Akhtar, M. The Mechanism of the Acyl-Carbon Bond Cleavage Reaction Catalyzed by Recombinant Sterol 14 Alpha-Demethylase of Candida Albicans (Other Names Are: Lanosterol 14 Alpha-Demethylase, P-45014DM, and CYP51). *J. Biol. Chem.* **1996**, *271* (21), 12445–12450. https://doi.org/10.1074/jbc.271.21.12445.

[88] Akhtar, M.; Corina, D.; Pratt, J.; Smith, T. Studies on the Removal of C-19 in Oesterogen Biosynthesis Using 18O2. *J. Chem. Soc., Chem. Commun.* **1976**, No. 21, 854–856. https://doi.org/10.1039/C39760000854.

[89] Wertz, D. L.; Sisemore, M. F.; Selke, M.; Driscoll, J.; Valentine, J. S. Mimicking Cytochrome P-450 2B4 and Aromatase: Aromatization of a Substrate Analogue by a Peroxo Fe(III) Porphyrin Complex. *J. Am. Chem. Soc.* **1998**, *120* (21), 5331–5332. https://doi.org/10.1021/ja980395a.

[90] Gregory, M. C.; Denisov, I. G.; Grinkova, Y. V.; Khatri, Y.; Sligar, S. G. Kinetic Solvent Isotope Effect in Human P450 CYP17A1-Mediated Androgen Formation: Evidence for a Reactive Peroxoanion Intermediate. *J. Am. Chem. Soc.* **2013**, *135* (44), 16245–16247. https://doi.org/10.1021/ja4086403.

[91] Mak, P. J.; Duggal, R.; Denisov, I. G.; Gregory, M. C.; Sligar, S. G.; Kincaid, J. R. Human Cytochrome CYP17A1: The Structural Basis for Compromised Lyase Activity with 17-Hydroxyprogesterone. *J. Am. Chem. Soc.* **2018**, *140* (23), 7324–7331. https://doi.org/10.1021/jacs.8b03901.

[92] Li, D.; Kabir, M.; Stuehr, D. J.; Rousseau, D. L.; Yeh, S.-R. Substrate- and Isoform-

Specific Dioxygen Complexes of Nitric Oxide Synthase. *J. Am. Chem. Soc.* **2007**, *129* (21), 6943–6951. https://doi.org/10.1021/ja070683j.

[93] Khatri, Y.; Luthra, A.; Duggal, R.; Sligar, S. G. Kinetic Solvent Isotope Effect in Steady-State Turnover by CYP19A1 Suggests Involvement of Compound 1 for Both Hydroxylation and Aromatization Steps. *FEBS Lett.* **2014**, *588* (17), 3117–3122. https://doi.org/10.1016/j.febslet.2014.06.050.

[94] Mak, P. J.; Luthra, A.; Sligar, S. G.; Kincaid, J. R. Resonance Raman Spectroscopy of the Oxygenated Intermediates of Human CYP19A1 Implicates a Compound I Intermediate in the Final Lyase Step. *J. Am. Chem. Soc.* **2014**, *136* (13), 4825–4828. https://doi.org/10.1021/ja500054c.

[95] Yoshimoto, F. K.; Guengerich, F. P. Mechanism of the Third Oxidative Step in the Conversion of Androgens to Estrogens by Cytochrome P450 19A1 Steroid Aromatase. *J. Am. Chem. Soc.* **2014**, *136* (42), 15016–15025. https://doi.org/10.1021/ja508185d.

[96] Vidakovic, M.; Sligar, S. G.; Li, H.; Poulos, T. L. Understanding the Role of the Essential Asp251 in Cytochrome P450cam Using Site-Directed Mutagenesis, Crystallography, and Kinetic Solvent Isotope Effect. *Biochemistry* **1998**, *37* (26), 9211–9219. https://doi.org/10.1021/bi980189f.

[97] Follmer, A. H.; Tripathi, S.; Poulos, T. L. Ligand and Redox Partner Binding Generates a New Conformational State in Cytochrome P450cam (CYP101A1). *J. Am. Chem. Soc.* **2019**, *141* (6), 2678–2683. https://doi.org/10.1021/jacs.8b13079.

[98] Mak, P. J.; Gregory, M. C.; Denisov, I. G.; Sligar, S. G.; Kincaid, J. R. Unveiling the Crucial Intermediates in Androgen Production. *PNAS* **2015**, *112* (52), 15856–15861. https://doi.org/10.1073/pnas.1519376113.

Chapter 2

Compound I in human aromatase: capture, characterization and involvement in aromatization reaction

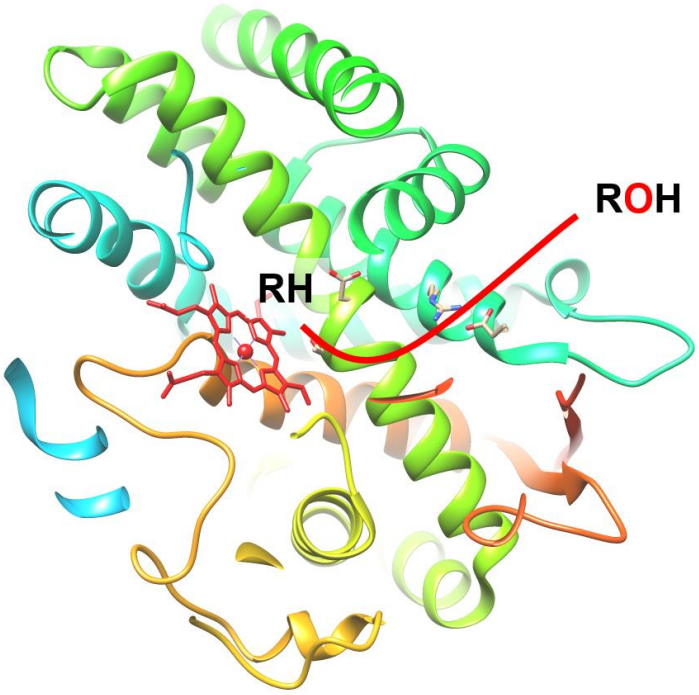

2.1 Abstract

Human aromatase (CYP19A1) is the cytochrome P450 that catalyzes the conversion of androgens into estrogens in a three steps reaction, which is essential to maintain the sex steroid hormones balance. Here we report the spectroscopic capture and characterization of its compound I (Cpd I), the main reactive species in cytochromes P450 responsible for the activation of C-H bonds. Aromatase and *meta*-chloroperoxybenzoic acid (*m*-CPBA) were rapidly mixed using the stopped-flow technique and the typical spectroscopic transitions indicating the formation of Cpd I were identified. Moreover, it was possible to obtain the estrogen product from the same reaction mixture, demonstrating the involvement of Cpd I in the aromatization reaction. Site-directed mutagenesis was applied to target the acid-alcohol pair (D309 and T310) and an arginine residue predicted to be part of the proton relay pathway (R192). The absence of Cpd I formation and the 88% loss of activity of the mutant D309N, together with the absence of pH dependence in the catalytic reaction, indicate that D309 is crucial for proton delivery. Since this residue is known to donate a proton to the substrate for aromatization, it has a double role in human aromatase. Also, the mutant R192Q showed a different pH dependence of its 82% reduced catalytic activity and no Cpd I was detected, indicating its involvement in the proton relay network. Cpd I was captured only for the T310A mutant that showed a 2.9- and 4.4-fold faster rate of formation and decay, respectively, when compared to the wide type enzyme. However, its activity was lower and a larger amount of H_2O_2 was produced during the catalytic process, indicating that T310 has an essential role in proton gating and Cpd 0 and Cpd I stabilization. The data presented provide a direct demonstration of Cpd I involvement in androgen aromatization reaction and add new evidence on the role of threonine belonging to the conserved “acid-alcohol” pair in human aromatase.

2.2 Introduction

Cytochromes P450 (P450s or CYP) are heme-thiolate monooxygenases widely distributed in nature and catalyze various oxidation reactions, including hydroxylation, epoxidation and heteroatom oxidation,[1–3] thus having some important physiological functions, such as steroids hormone biosynthesis, drug metabolism and xenobiotics detoxification.[4–6]

Among them, aromatase (CYP19A1) is a well-conserved among all vertebrates,[7] where it is responsible for the transformation of androgens into estrogens, thus playing a crucial role in regulating human sex steroids balance.[8–11] This enzyme has received considerable attention for a long time because it can be an effective target for estrogen-dependent cancer therapy.[12–15] From the catalytic reaction perspective, aromatase is very intriguing as it is one of the few enzymes that can generate aromatic rings. The reaction requires three sequential steps where the 19-methyl group of the androgen is first hydroxylated at C19, then again hydroxylated to produce a 19-gem-diol intermediate that spontaneously dehydrates to form an aldehyde.[16,17] In the third step, oxidative cleavage occurs on the carbon bond between C19 and C10, which results in the release of C19 as formic acid, accompanied by the A ring aromatization

of the steroid (Figure 1A).[18,19]

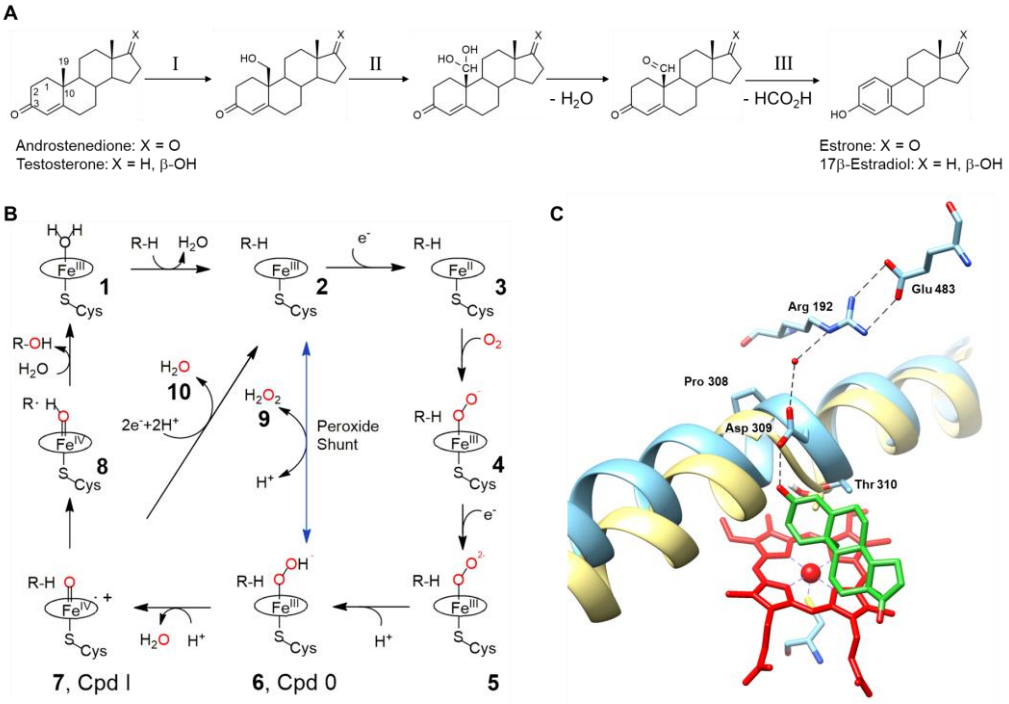

Figure 1. Reaction and catalytic mechanism of human aromatase. A) The three-step reaction catalyzed by aromatase allowing the conversion of androgens into estrogens. B) Catalytic cycle of cytochromes P450 and the uncoupling pathways. The peroxide shunt pathway can generate directly Cpd 0 and Cpd I. C) Active site of human aromatase (blue, PDB ID 3S79) with the predicted proton relay network. The helix I is superimposed to the corresponding one in cytochrome P450cam (yellow, PDB ID 5CP4) to show the distortion in human aromatase due to the presence of Pro308. The Heme is shown in red and the substrate androstenedione in green. Dashed black lines represent the predicted proton relay network.

A close look at the general P450 catalytic cycle shows that there are two protonation steps in the formation of Compound I (Cpd I) (Figure 1B): in the first, the peroxo ferric intermediate is protonated at the distal oxygen to form the hydroperoxo-ferric complex, also known as Cpd 0 (Figure 1B, 6); in the second protonation step, the Cpd 0 receives another proton and the following cleavage of the O-O bond forms Cpd I (Figure 1, 7).[20] After the first step of protonation, if the coordinated peroxide dissociates, it will lead to "uncoupling" and produce hydrogen peroxide (Figure 1B, 9). After the second protonation step, another uncoupling reaction can take place from Cpd I producing a water molecule (Figure 1B, 10).

By analogy and comparison with other P450 catalyzed reactions, it is widely accepted that the first and second oxidation steps catalyzed by aromatase are classic hydroxylation mediated by the active iron species Cpd I (Figure 1B, 7).[21–23] However, the presence of the intermediate involved in the third step has been controversial for many years and only recent experimental results suggested that the last step is still mediated by Cpd I.[24–26]

It is known that the well-conserved acid-alcohol pair in cytochromes P450, located on helix I, is involved in oxygen activation to produce Cpd I.[20,27] In particular, the acidic residue is part of the proton relay network. Indeed, mutation of this residue in different cytochromes P450, including aromatase, led to a significant reduction of NAD(P)H oxidation rate and of enzyme activity that is almost completely lost in the bacterial cytochrome P450cam D251N mutant.[28–32]

The role of threonine is more intriguing because its mutation into an alanine has a different effect on various P450 enzymes. In P450cam, the mutant shows a small reduction in NADH consumption but the enzyme becomes 95% uncoupled.[33,34] The crystal structure of the mutant suggested a role of this residue as a hydrogen bond acceptor for Cpd 0 with a consequent stabilization of this intermediate that promotes the second proton transfer to form Cpd I.[35] However, the mutation of the Thr belonging to the acid-alcohol pair in other P450 enzymes has shown that this residue is important but not essential for catalysis.[36] Moreover, in cytochrome P450 BM3, the activity of the mutant T268A was shown to depend on the substrate used, and for some substrates, it was possible to obtain the same activity as the wild type protein.[37]

More recently, the T252A mutant of the bacterial CYP199A4, showed a reduction of the activity and coupling efficiency not as dramatic as in P450cam.[36] For P450cam, CYP199A4 and P450 BM3, the availability of the crystal structures of the wild-type proteins and their Thr mutants, have shown significant differences providing the structural basis for the different effect of Thr mutation. In P450cam, the crystal structure of wide type (WT) and T252A mutants in complex with dioxygen is also available and shows that, upon oxygen binding, there is a change in helix I conformation and a flip of the aspartic acid residue by 90 ° (D251) that allows access into the active site of two water molecules, that take part to a hydrogen bond network proposed to enable proton delivery.[35,38] An enlargement of the oxygen-binding groove is also present in the structure of P450cam T252A mutant compared to that of WT.[39] In CYP199A4 and P450 BM3, such structural changes on helix I that modify the oxygen binding groove are not as large as in P450cam in the corresponding threonine mutants.[36,40] In these enzymes, the most significant differences compared to P450cam were found to be a presence of a second Thr residue that contributes to the hydrogen bonding network and the lack of a salt bridge between the acidic residue of the acid-alcohol pair and a positively charged one.[36]

In aromatase, an overall different situation is present. The crystal structure in complex with the substrate showed that the aspartate belonging to the acid-alcohol pair (D309) is not involved in a salt bridge as in P450cam and it forms a hydrogen bond with the 3-keto group of the substrate androstenedione (ASD) that is predicted to accept the proton from D309 for substrate aromatization.[41–43] Moreover, D309 is connected through a water molecule to an arginine residue (R192) that forms a salt bridge with E483 (Figure 1C).[41,44] Thus, D309 and R192, together with a water molecule, are predicted to form the proton relay network.[41,44] Indeed, their mutation in non-protonable residues resulted in a significant decrease in activity.[32] Furthermore, instead of a second threonine after T310 belonging to the acid-alcohol pair as found

in CYP199A4 and P450 BM3, there is a methionine residue (valine in P450cam). This leads to important questions are whether D309 in aromatase plays a double role (proton delivery for oxygen activation and proton delivery to the substrate) and whether the threonine residue is essential for catalysis and what is its role in aromatase.

Here, we report the capture and characterization of Cpd I in human aromatase and we provide further evidence for its involvement in the last aromatization step of reaction. Moreover, we investigate by site directed mutagenesis the role and involvement of D309, T310 and R192 in Cpd I formation and catalysis. Since the acid-alcohol pair is a well-conserved motif in cytochromes P450, with some exception represented for example by P450 acting as peroxygenases,[45] P450cin[28] and P450eryF[46], the data obtained in aromatase show significant differences with the other bacterial cytochrome P450 enzymes characterized, providing new insights in P450 mechanism of oxygen activation.

2.3 Results and discussion

2.3.1 Compound I in aromatase: capture and characterization

The principal reactive intermediate involved in catalysis in cytochromes P450 (Cpd I) has been spectroscopically captured and characterized in different P450 enzymes, mainly from bacteria[23,47–50] and the mammalian rabbit P450 2B4.[51] This has been achieved through the peroxide shunt obtained by mixing the enzyme with oxidizing agents such as *meta*-chloroperoxybenzoic acid (*m*-CPBA) and transiently detecting its absorbance spectrum by stopped-flow techniques. The same approach has been used in this work for human aromatase, and the results are shown in Figure 2A. This shows the spectral changes obtained upon mixing 7 µM of recombinant human aromatase (Aro) with 200 µM of *m*-CPBA in 0.8 s at 4 °C. A rapid decrease in the Soret region at 418 nm and a concurrent increase of absorption at 380 nm was observed. Moreover, the two bands at 537 and 570 nm decreased and a band at 610 nm appeared. We did not detect the band at 690 nm previously observed with the lowest absorption in CYP119 due to the lower yield of Cpd I formation in Aro. However, the spectral changes observed and presence of five isosbestic points at 353, 399, 435, 523 and 582 nm indicate the presence of two species, the ferric enzyme and its Cpd I.[23]

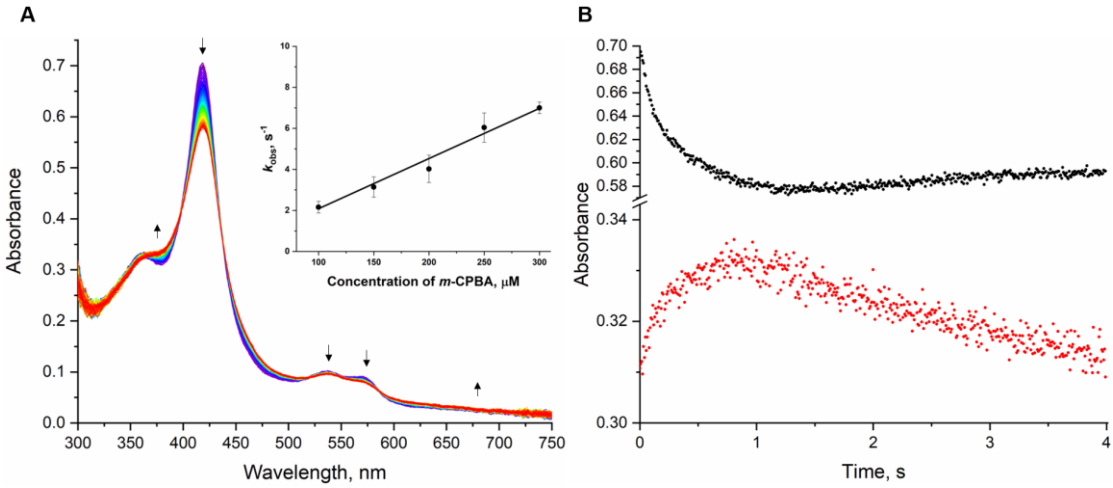

Figure 2. Cpd I formation in Aro. (A) UV/Visible spectral changes in 0.8 s after mixing of 7 µM aromatase (final concentration) with 200 µM *m*-CPBA (final concentration) in 100 mM potassium phosphate buffer, 10 % glycerol, pH 7.5, at 4 °C. Inset: plot of observed rate constants (k_{obs}) for Cpd I formation against various concentrations of *m*-CPBA at pH 7.5 and 4 °C. (B) Kinetic traces of reaction between aromatase and *m*-CPBA at 418 nm (black) and 380 nm (red) in 4.0 s.

Cpd I was found to form in 0.8 seconds and to decay in 4 seconds, as shown by the kinetic traces of the reaction between aromatase and *m*-CPBA at 380 and 418 nm (Figure 2B). A first exponential increase at 380 nm, followed by a linear decrease reflects the formation and decomposition of Cpd I,[48,52] respectively, that can be described by eq. 1:

$$\text{Aromatase (ferric)} + m\text{-CPBA} \xrightarrow{k_1} \text{Aromatase-Compound I} \xrightarrow{k_2} \text{Aromatase (ferric)} \quad \text{(eq. 1)}$$

where k_1 and k_2 are formation and decomposition rate constants, respectively. The absorbance at 418 nm showed an opposite trend as a function of time. In order to estimate the observed rate constant (k_{obs}), different amounts of *m*-CPBA were tested and different k_1 values were obtained and plotted as a function of *m*-CPBA concentration (inset in Figure 2A). A linear trend was obtained and the slope of linear fitting provided a second-order rate constant of 0.25 (± 0.01) × 10^5 $M^{-1}s^{-1}$. The decomposition of Cpd I followed a first-order kinetic process and was independent of the concentration of *m*-CPBA.[48] The k_2 can be obtained directly by exponential equation fitting, which is 0.16 (± 0.01) s^{-1}.

In order to confirm the capture of the reactive species Cpd I in Aro, the same experiment was performed with the enzyme in the presence of the substrate. Since the last step of aromatase reaction has been the focus of many studies aimed at elucidating which reactive species (Cpd 0 *versus* Cpd I) is involved in this crucial aromatization reaction, we investigated this step using the intermediate 19-oxoandrostenedione (19-oxo ASD) as substrate. Figure 3A shows the spectral transitions observed by mixing Aro in complex with 19-oxo ASD and *m*-CPBA in 5 seconds. A red-shift was observed for the Soret peak, with a decrease of the band at 394 nm, typical of the high spin state of Aro in complex with the substrate, and an

increase at 418 nm, typical of the low spin substrate-free Aro (inset Figure 3A). These data are interpreted with substrate turnover and release of the product. The spectrum did not shift completely here, which is consistent with an insufficient Cpd I amount for the total conversion of the substrate. Moreover, the kinetic traces at 418 nm and 394 nm showed that the spectral changes occur within 4 seconds that is the timescale where Cpd I formation and decay were previously found (Figure 3B).

In order to give further evidence for Cpd I formation and for its involvement in the aromatization reaction, different reactions were set up by adding the substrate 19-oxo ASD after 1 second from the addition of *m*-CPBA. The reactions were then pooled together in order to check the presence of estrone that was detected by HPLC (Figure 3C). Although the production is very low consistently with the low yield of Cpd I previously observed, this result also supports Cpd I as the third step active species. The results add direct evidence that this intermediate mediates the aromatization process. Several studies suggested that the ferric-peroxyanion gives a nucleophilic attack of the, Fe(III)–O–O^-, on the acyl carbon to furnish a tetrahedral intermediate which fragments, leading to acyl–carbon cleavage.[53] However, activity assays in the presence of $^{18}O_2$ in combination with high resolution mass spectrometry, resonance Raman spectroscopy studies and the evaluation of solvent isotope effect in steady-state turnover of aromatase, suggested that Cpd I is the active iron species rather than ferric peroxide.[24–26]

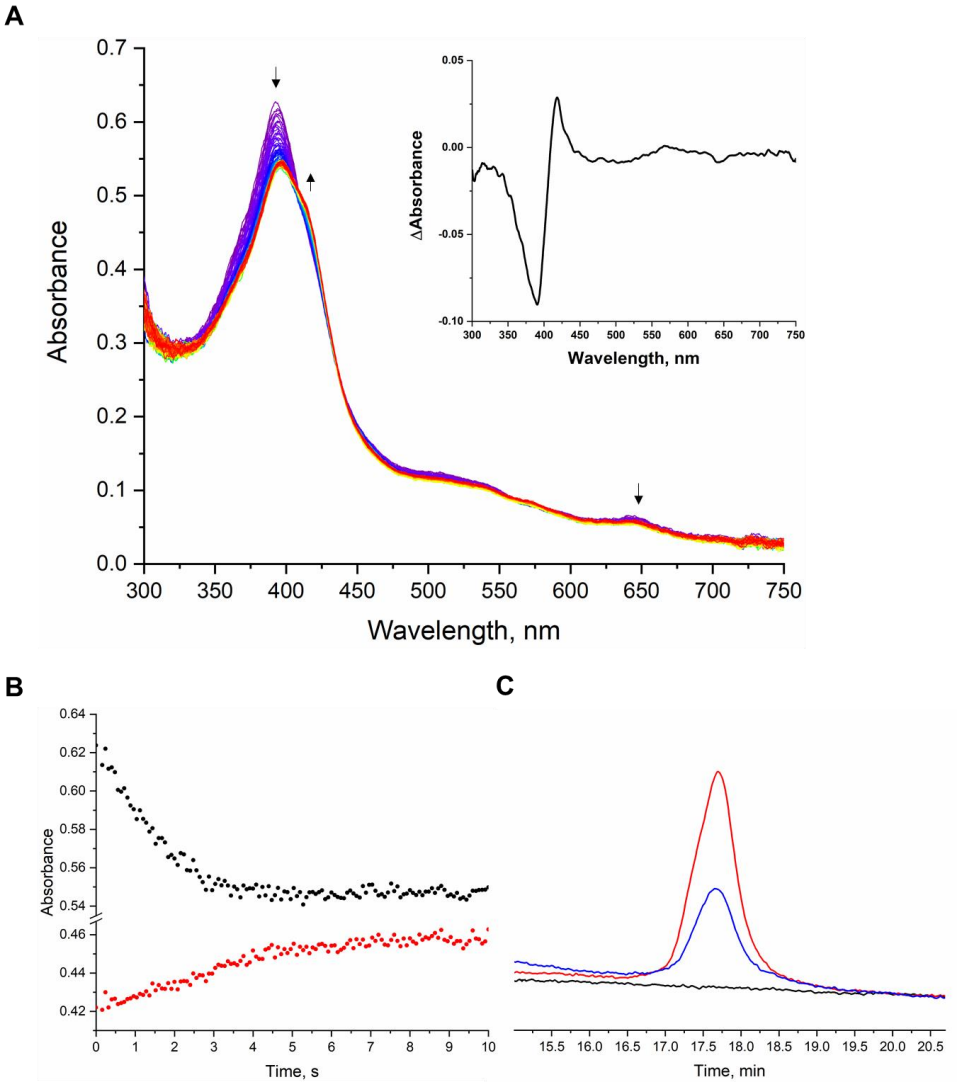

Figure 3 Cpd I formation in human aromatase in complex with 19-oxo ASD (A) Spectral changes obtained after mixing Aro (7 µM final concentration) with *m*-CPBA (200 µM final concentration) in 10 s in 100 mM potassium phosphate buffer, 200 µM 19-oxo ASD, 10% glycerol, pH 7.5, at 4 °C. Inset: Difference spectrum obtained by subtracting the spectrum at 0 s from the spectrum at 10 s. (B) Kinetic traces at 394 nm (black) and 418 nm (red) extrapolated from panel A. (C) HPLC traces showed the *m*-CPBA-driven formation of estrone product. The analyses were performed at a flow rate of 0.5 mL/min of water/acetonitrile (50/50, v/v). The detection wavelength was 280 nm. The red line corresponds to the HPLC trace of estrone standard, the blue line is the chromatographic profile obtained from the reaction mixture, and the black line is the trace from the control. The reaction mixture contained 7 µM of Aro, 200 µM *m*-CPBA, 200 µM 19-oxo ASD in 100 mM potassium phosphate buffer (10% glycerol) at pH 7.5 and 4 °C. The control reaction contained heat-inactivated Aro.

2.3.2 Role of D309, T310 and R192 in Cpd I formation.

The role of the amino acids of the acid-alcohol pair (D309 and T310) and R192 in Cpd I formation was investigated by site directed mutagenesis. To this end, the

mutants were expressed and purified in the absence of substrates or inhibitors. The UV-Vis spectrum of the D309N mutant in the resting state showed a maximum absorption peak at 423 nm and a small shoulder peak near 394 nm (Figure 4B), indicating that the mutant is partially in a high spin state even in the absence of any ligand. When it was mixed with *m*-CPBA, the absorption at 423 nm showed an increase followed by a full decrease within 4 s. The same phenomenon occurred at 540 and 570 nm. However, the absorption at 394 nm decreased continuously, and the same behavior was observed near the peak at 640 nm. The intermediate formed by D309N is difficult to be considered as Cpd I. The mutant was then co-purified with the substrate ASD and showed the same maximum absorption at 394 nm as Aro in complex with the substrate. When D309N in complex with the substrate androstenedione was mixed with *m*-CPBA, no spin shift was observed, even if the peroxide concentration was increased or the reaction time was prolonged (Figure 4C). Such a shift from 394 nm to 418 nm was previously observed in the wide type protein, indicating the progress of the catalytic oxidation of the substrate (Figure 3A). These data are consistent with the activity reported for D309N mutant that is decreased by 98% compared to WT.[32]

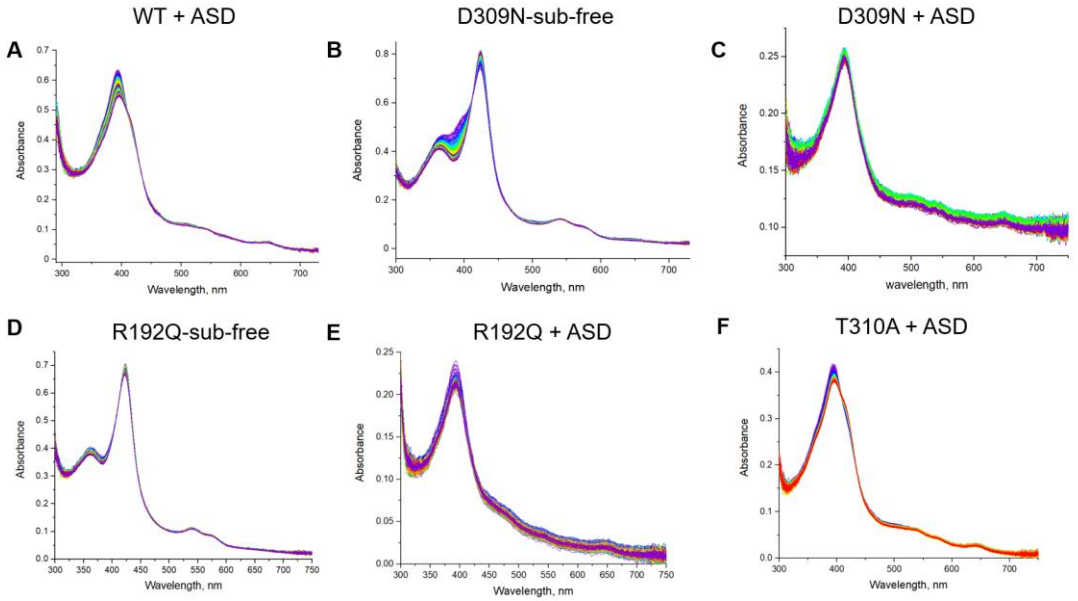

Figure 4 *m*-CPBA reacted with wild type and mutants in the presence or absence of substrate. (A) Substrate-bound high-spin ferric WT. Scanning time, 4 s; (B) Substrate-free low-spin ferric D309N. Scanning time, 40 s (C) Substrate-bound high-spin ferric D309N. Scanning time, 400 s; (D) Substrate-free low-spin ferric R192Q. Scanning time, 40 s (E) Substrate-bound low-spin ferric R192Q. Scanning time, 800s. (F) Substrate-bound high-spin ferric T310A. Scanning time, 40 s. Reaction condition: enzyme was mixed 1:1 (v/v) with 25 eq mol of *m*-CPBA in 100 mM potassium phosphate buffer, 10% glycerol, pH 7.5, at 4 °C. In the presence of substrate: 100 µM of ASD was added into the buffer.

The spectra of R192Q reacting with *m*-CPBA only decreased in the Soret region and did not show a characteristic spectrum similar to Cpd I (Figure 4C). In addition, no

red-shift was observed in the reaction with the substrate-bound R192Q (Figure 4D). The replacement of Arg192 with Gln significantly affects the formation of Cpd I, consistent with the 88% reduced activity of this mutant compared to WT.[32]

There are several possibilities to explain why Cpd I was not detected in mutants D309N and R192Q. These two residues are located in the proton delivery network. The mutation of these two sites interferes with the proton transfer pathway and make protons unable to be transferred. Another possible reason is that the mutations change the structure near the heme pocket, and changes the distribution of water molecules, which may reduce the availability of protons required for heterolysis and formation of Cpd I, limiting or preventing its formation in the mutants.

The mutant T310A was then tested for Cpd I formation and Figure 5A shows the spectral changes obtained by mixing the protein with *m*-CPBA at pH 7.5, 4 ºC. The spectral transitions observed are similar to those of the WT. Interestingly, the formation and decomposition rates of Cpd I in T310A were faster than those of the WT. The absorbance at 380 nm increased more rapidly, reached the maximum in ~ 0.4 s and then decreased (Figure 5B). By plotting the k_{obs} versus *m*-CPBA concentration, the k_1 of T310A was found to be $0.72 \pm 0.03 \times 10^5$ $M^{-1}s^{-1}$, which is 2.9 times higher than that of the WT. (Figure 5C). However, the yield of Cpd I of T310A appears to be the same as the WT (Figure 5B). The increased reactivity to *m*-CPBA may be slightly affected by the increased hydrophobicity near the heme pocket, which makes the binding of *m*-CPBA more effective. [54] Also the decomposition rate constant (k_2) increased in the mutant, which is 4.4 times higher than that of the WT ($k_2 = 0.71 \pm 0.06$ s^{-1} in T310A *versus* $k_2 = 0.16 \pm 0.01$ s^{-1} in the WT), indicating that the Cpd I is more unstable.

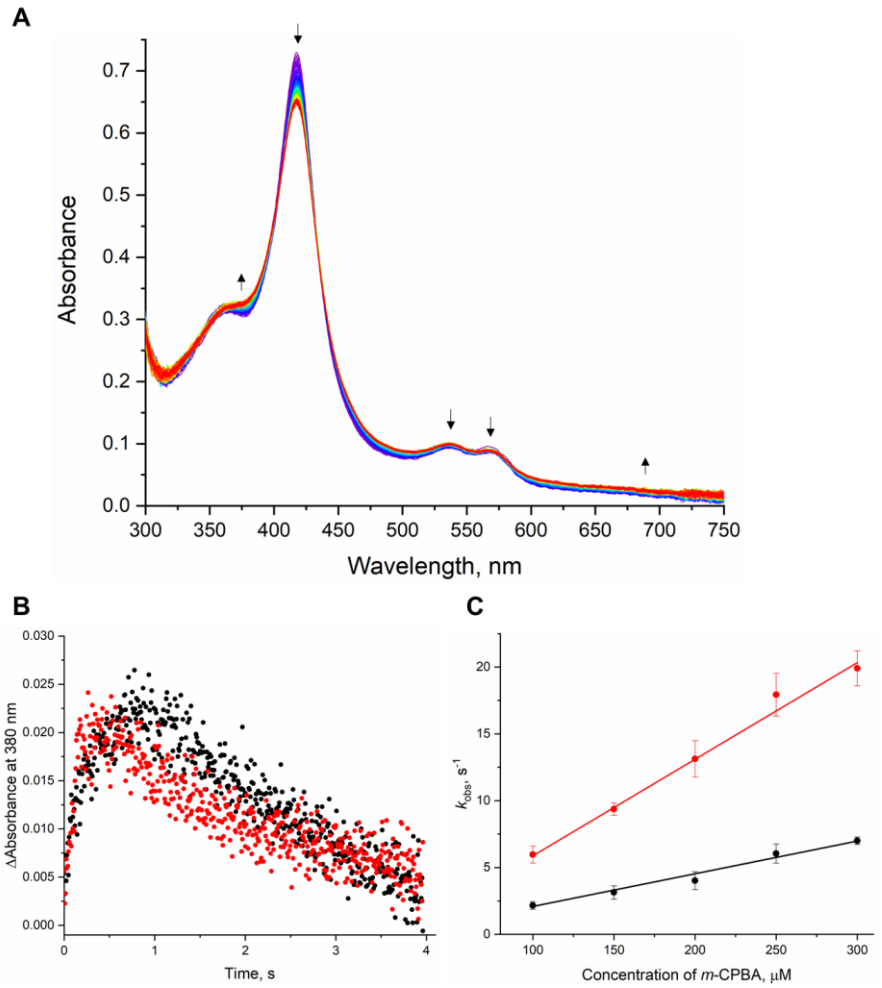

Figure 5. Cpd I formation in T310A. (A) UV/Visible spectral changes in 0.4 s after mixing T310A (7 μM final concentration) with *m*-CPBA (200 μM final concentration) in 100 mM potassium phosphate buffer, 10 % glycerol, pH 7.5, at 4 °C. (B) Kinetic traces at 380 nm of the WT (black) and T310A (red) in 4.0 s. (C) Plots of observed rate constant (k_{obs}) of Cpd I formation against various concentrations of *m*-CPBA at pH 7.5 and 4 °C. A linear fit was used to derive formation rate constants of k_1 = 0.25 (± 0.01) × 10^5 $M^{-1}s^{-1}$ for the WT (black) and k_1 = 0.72 (± 0.03) × 10^5 M^{-1} s^{-1} for T310A (red).

The higher rates of formation of Cpd I in T310A compared to the WT were confirmed at different pH values. Figure 6A and Figure 6B show the time course of formation of Cpd I at 380 nm at different pH. It should be taken into account that the pH dependence of the formation of Cpd I is affected by the pKa of *m*-CPBA being 7.4.[48] However, the formation rate decreased significantly from pH 6.5 to pH 8.5 in both enzymes and the plot of the decay rate k_2 (that is not affected by the pKa of *m*-CPBA as k_1) against pH shows that the decomposition rate of Cpd I in T310A is higher than that of the WT at any pH (Figure 6C), which means that the lifetime of T310A Cpd I is shorter.

It is also interesting to note that the amount of Cpd I was comparable between the WT and the T310A mutant, indicating that Thr310 is not directly involved in proton

relay. Instead, the data indicate T310 has a role in modulating the rate of formation and decay of Cpd I. It is known that the corresponding residue in cytochrome P450cam has a crucial role in dioxygen activation as it accepts a hydrogen bond from the hydroperoxy (Fe(III)-OOH) intermediate (Cpd 0) promoting the second protonation leading to Cpd I.[35] Our data show faster formation and decay rates for Cpd I suggesting that Thr also has a gating role for the second proton transfer as well as a stabilizing role for Cpd I. The implications of these finding for catalysis were investigated. In particular, we aimed at investigating how the different Cpd I formation and decay rates observed for the two mutants at different pH relate to product formation. Moreover, we characterized more in deep the activity of Aro and the three mutants in terms of reaction intermediates and product formed and coupling efficiency.

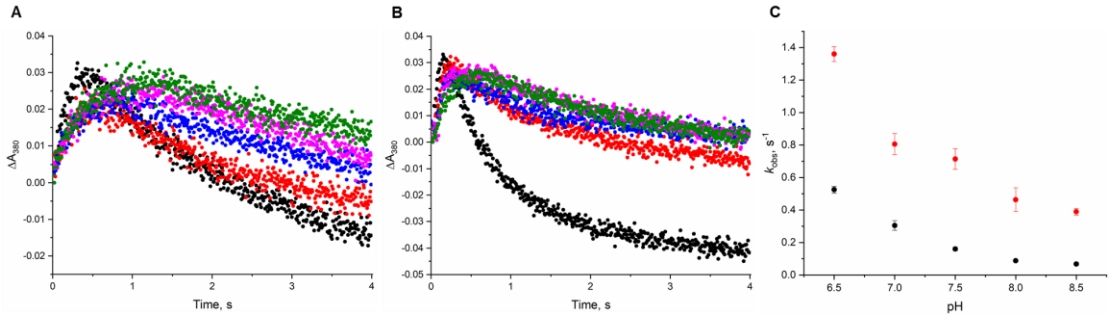

Figure 6. Effect of pH on Cpd I formation and decay. Kinetic traces at 380 nm of aromatase (A) WT and (B) T310A at different pH. (C) Plot of the k_2 obtained for WT (black circles) and T310A (red circles) as a function of pH.

2.3.3 Catalytic activity of Aro and mutants at different pH.

In order to study only the effect of pH in a simplified one-step reaction, only the third aromatization step was considered and 19-oxoASD was used as the starting substrate for this set of experiments.

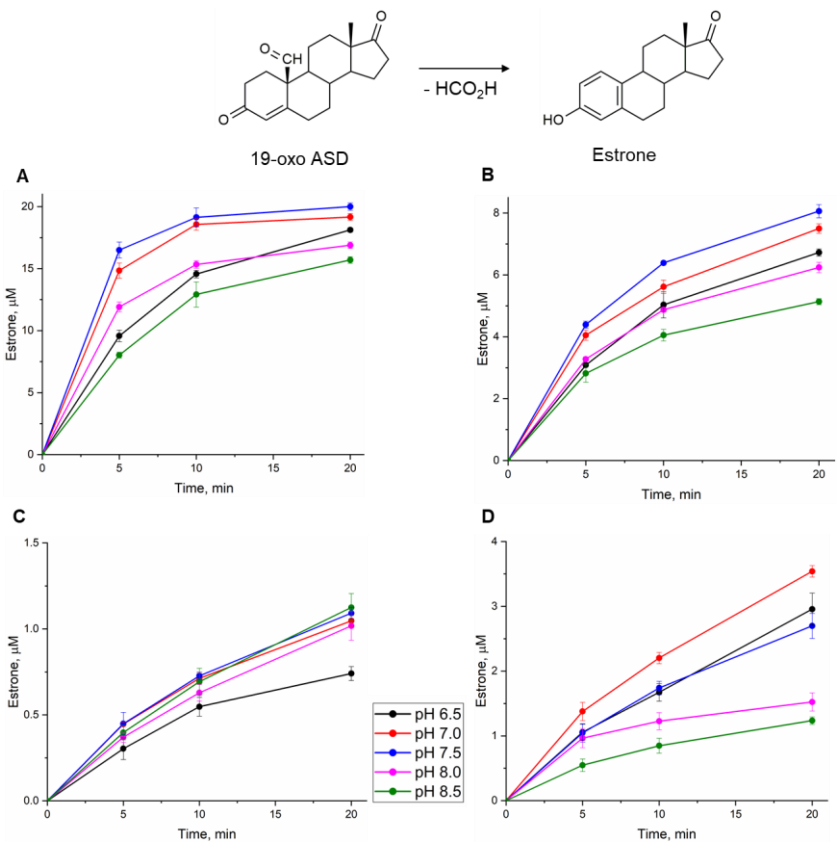

Figure 7. Effect of pH on catalytic activity of WT and its mutants. The activity as a function of time was measured for (A) WT, (B) T310A, (C) D309N and (D) R192Q. Reaction conditions: 0.5 µM enzyme, 0.5 µM CPR, 20 µM 19-oxo ASD, 0.5 mM NADPH in 100 mM potassium phosphate buffer, 10% glycerol, at 30 °C.

The estrone production was followed as a function of time and the results for the WT and the mutants are shown in Figure 7. As can be seen, the maximal activity in the WT is reached at pH 7.0-7.5 that is reasonable as it corresponds to the physiological pH (Figure 7A). It is interesting to note that the maximal activity was obtained at pH values that do not correspond to the lowest rate of decay of Cpd I, indicating that a higher stability of Cpd I (obtained at pH 8.0-8.5) does not necessarily imply a higher activity.

In T310A mutant, despite the faster rates of Cpd I formation and decay, the activity is reduced by 60% when compared to the WT at every pH value. Thus, a higher formation rate does not necessarily imply a higher activity. The optimal catalytic activity is achieved with intermediate formation and decay rates. Taken together, the data suggest that T310 controls the timing for proton delivery having a proton-gating role. Moreover, it stabilizes Cpd I optimizing the catalytic activity of human aromatase.

For what concern the pH dependence observed, the effect of pH on T310A was similar to that of the WT, with the maximal activity observed at pH 7.5 that is the physiological pH (Figure 7B). Moreover, the effect of pH on the catalytic reaction of T310A showed the same trend as that of the WT, suggesting that this residue is not

responsible for the pH dependence of the catalytic activity in human aromatase. Thus, we carried out the same set of experiments on the other two mutants that are predicted to be directly involved in the proton delivery network (Figure 7). In the mutant D309N, the mutation resulted in a dramatic loss of activity by 95% towards 19-oxoASD (Figure 7C), consistent with the previous lack of detection of Cpd I. Moreover, the effect of pH on D309N was lost as the production rate of D309N was almost pH-independent, consistent with our previous data reporting a pKa of 8.2 for D309 and a crucial role of this residue for catalysis.[32,42]

The mutant R192Q showed a 83% loss of activity compared to the WT. However, a pH dependence of the catalytic activity is present in this mutant and the effect of pH is different compared to WT. Indeed, the maximal activity for this mutant is observed at pH 7.0 (Figure 7D). These data, together with the lack of Cpd I detection previously obtained for this mutant, are consistent with an important role of R192 in proton transfer. The residual activity observed in D309N and R192Q mutants together with the different pH dependence of R192Q mutant can be explained the presence of possible alternative but poorly efficient proton transfer networks in human aromatase.

2.3.4 Catalytic rate and uncoupling in Aro WT and mutants.

To better understand the role of the three amino acids in proton transfer and catalysis, NADPH consumption, products formation and H_2O_2 production were measured. Two sets of experiments were carried out, the first one using androstenedione as the starting substrate to follow the three steps of reaction (Table 1), the second one using 19-oxoandrostenedione as the starting substrate to follow only the aromatization reaction (Table 1). In both cases, the mutants D309N and R192Q consumed a lower amount of NADPH and showed to produce a higher amount of H_2O_2 compared to WT, consistent with a slower electron-coupled proton transfer.[55] The residual activity and the H_2O_2 formed indicate that the mutants can still use alternative proton relay networks to deliver the first proton to produce Cpd 0. However, this reactive compound is poorly formed and active as oxidizing species in the three steps of reaction and it decays releasing hydrogen peroxide rather than forming the products increasing the uncoupling of the enzyme.

On the other hand, the amount of NADPH consumed by WT and T310A mutant is similar, even if the T310A mutant has a lower activity. This is due to an increased amount of H_2O_2 produced by the mutant that is 7-folds higher than the WT when androstenedione is used as substrate. This result is in line with the corresponding mutants in other P450 enzymes and indicates a lack of stabilization of Cpd 0 by the threonine residue belonging to the acid-alcohol pair. In the absence of the Thr residue, Cpd 0 is not stabilized by hydrogen bond and it is more easily released as hydrogen peroxide rather than producing Cpd I.[35]

Table 1. Rates of NADPH consumption, H_2O_2 production and product formation for Aro and the three mutants.

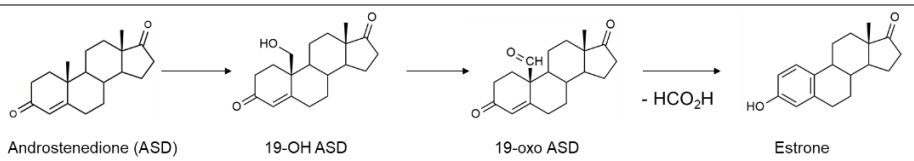

Androstenedione (ASD) | 19-OH ASD | 19-oxo ASD | Estrone

	NADPH consumption rate (min^{-1})	H_2O_2 (-SOD) (min^{-1})	H_2O_2 (+SOD) (min^{-1})	19-OH ASD (min^{-1})	19-oxo ASD (min^{-1})	Estrone (min^{-1})	Coupling (%)	H_2O_2/ NADPH (%)
WT	34.65 ± 0.52	2.20 ± 0.16	2.62 ± 0.07	0.48 ± 0.01	0.89 ± 0.02	2.31 ± 0.03	26.5	6.3
D309N	18.63 ± 1.41	3.76 ± 0.22	4.23 ± 0.38	0.06 ± 0.01	0.14 ± 0.01	0.43 ± 0.01	8.7	20.2
T310A	32.97 ± 0.16	14.16 ± 0.05	15.77 ± 1.32	0.64 ± 0.01	0.27 ± 0.02	0.42 ± 0.01	7.4	43.0
R192Q	20.36 ± 2.21	4.05 ± 0.15	4.99 ± 0.32	0.07 ± 0.01	0.23± 0.02	0.75 ± 0.01	13.7	19.9

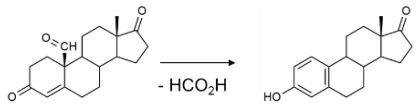

19-oxo ASD | Estrone

	NADPH (min^{-1})	H_2O_2 (-SOD) (min^{-1})	H_2O_2 (+SOD) (min^{-1})	Estrone (min^{-1})	Coupling (%)	H_2O_2/NADPH (%)
WT	25.07 ± 1.78	1.70 ± 0.27	2.39 ± 0.42	13.07 ± 0.12	52.1	6.8
D309N	18.37 ± 2.50	2.26 ± 0.06	3.11 ± 0.20	0.36 ± 0.01	2.0	12.3
T310A	24.01 ± 2.43	4.23 ± 0.26	5.42 ± 0.18	3.58 ± 0.04	14.9	17.6
R192Q	22.68 ± 2.23	2.52 ± 0.15	4.13 ± 0.52	1.06 ± 0.09	4.7	11.1

The loss in activity of T310A mutant is not as drastic as in P450cam. Indeed, the mutant shows a 36% residual activity toward androstenedione and a 27.5% residual activity for the aromatization reaction. In this mutant, the amount of Cpd I formed and the NADPH consumption rate are comparable to those of the WT, whereas the amount of H_2O_2 is higher. However, the amount of products and H_2O_2 formed do not correlate to the level of NADPH consumed indicating that the uncoupling pathway leading to water production from Cpd I is active in the WT and even more so in the T310A mutant. To test this hypothesis, the activity of the enzymes was also measured

in the presence of superoxide dismutase (SOD) to check the presence of superoxide anion, but a significant increase in the level of H_2O_2 was observed. These results indicate again that Thr310 has a stabilizing role not only for Cpd 0 but also for Cpd I.

Whether these findings are specific for aromatase is difficult to predict. Indeed, the crystal structure of the enzyme shows a unique proline residue (P308) just before the acidic-alcohol pair that kinks the helix I and allows the side chain of D309 to form a hydrogen bond with the substrate (Figure 1C). The oxygen-binding groove is different when compared to P450cam and the processing of the substrate through a three steps reaction most probably triggers some structural rearrangements involving the active site residues and water molecules. The other major difference is the involvement of the Asp residue in a hydrogen bond with the substrate that is essential for the correct positioning of the substrate in the active site that promotes the highly regioselective hydroxylation at C19. Computational studies have shown that the most energetically favored pathway for aromatase reaction involves substrate enolization as a consequence of proton donation from a water molecule through Asp309. A rotation of this residue induces a water mediated proton transfer leading to Cpd I.[43] Such a mechanism resembles in part what observed in P450cam, where a flip of the Asp residue allows the entry of water molecules and proton transfer.

In conclusion, the Cpd I was captured in a human cytochrome P450 that acts as the key player for estrogen production. Moreover, its involvement in the third step of reaction was directly demonstrated. By means of site directed mutagenesis, the alcohol-acid pair in human aromatase was shown to play a similar role than the one reported for the bacterial cytochrome P450cam. The aspartic acid residue is involved in proton delivery and its absence almost completely blocks the activity of the enzyme. However, this residue has a double role in aromatase since it is responsible also for proton delivery to the substrate for aromatization.[42,43] The protonation-deprotonation equilibrium in the aspartic acid residue is allowed by its unusual pKa[42] that is the main responsible for the pH dependence of the catalytic activity in aromatase.

The threonine residue was shown not to be directly involved in proton delivery ad Cpd I could be captured for this mutant. However, a proton gating role for this residue and a stabilization effect for Cpd I were shown to have a crucial role in catalysis. The data presented add new insights into the mechanism of dioxygen activation cytochrome P450.

2.4 Materials and methods

2.4.1 Materials

All chemicals were reagent grade and obtained from commercially available sources. Androstenedione, *meta*-chloroperbenzoic acid (*m*-CPBA), superoxide dismutase (SOD) and nicotinamide adenine dinucleotide phosphate (NADPH) were obtained from Sigma-Aldrich (Milan, Italy). 19-oxo androstenedione was purchased from Biozol (Eching, Germany). Amplex Red hydrogen peroxide/peroxidase assay kit was purchased from Invitrogen (Eugene, USA).

2.4.2 Protein production and purification

The recombinant form of human aromatase (Aro), the mutants (Aro-D309N, Aro-T310A and Aro-R192Q), and cytochrome P450 reductase (CPR) were expressed and purified as previously described.[56,57] The P450venzyme concentration was determined by an Agilent 8453 UV VIS spectrophotometer (Agilent Technologies, Santa Clara, CA, USA) by the reduced carbon monoxide complex in the difference spectrum, using an extinction coefficient at 450 nm of 91,000 M^{-1} cm^{-1}.[58] The CPR concentration was determined by using the extinction coefficient at 456 nm (24,100 M^{-1} cm^{-1}).[59]

2.4.3 Cpd I capture and characterization by stopped-flow kinetics

The compound *m*-CPBA was purified by washing with 100 mM pH 7.5 potassium phosphate buffer for 3~5 times and stirring on ice for 1 hour. The stock solution of *m*-CPBA was prepared in acetonitrile and diluted to the appropriate concentration with potassium phosphate (KPi) buffer. The oxidation of ferric aromatase and the mutants was carried out using a Hi-Tech scientific SF-61 single mixing stopped-flow instrument (TgK Scientific, UK). One of the drive syringes was filled with enzyme (14 µM) in a 100 mM potassium phosphate buffer, 10% glycerol at the chosen pH. The second drive syringe was filled with the *m*-CPBA in the same buffer. All the experiments were carried out at 4 ºC using a circular water bath. The kinetic data were analyzed with Kinetic Studio software, version 5.1.06. (TgK Scientific, UK).

2.4.4 Activity assay enzyme reaction

For the experiment where *m*-CPBA was used to form Cpd I and trigger the reaction, a 1 ml solution of 100 mM potassium phosphate buffer, 10% glycerol containing 7 µM aromatase and 200 µM 19-oxo-androstenedione (19-oxo-ASD) was incubated at 4 °C and titrated with *m*-CPBA (total addition of 200 µM). The reaction was stopped by heating at 90 ºC for 10 min. After centrifugation at 11,000 g for 15 minutes, the supernatant was used for HPLC analysis. In the control experiment, the enzyme was inactivated by heat shock, and then incubated with *m*-CPBA.

For the experiment where Aro activity was studied at different pH values, all the reaction mixtures were set up in 100 mM potassium phosphate buffer (at a chosen pH) containing 0.5 µM aromatase, 0.5 µM CPR, 20 µM 19-oxo-ASD and 0.5 mM NADPH at 30 ºC for 20 min, and the final reaction volume was 0.5 ml. The reaction was stopped by heating at 90 ºC for 10 min. After centrifugation, the supernatant was

further analyzed by HPLC.

2.4.5 NADPH consumption and hydrogen peroxide formation studies

NADPH consumption was measured by an Agilent 8453 UV-vis spectrophotometer at 30 ºC. The reaction mixture contained 0.25 µM Aro, 0.25 µM CPR, 100 µM substrate androstenedione (ASD) or 19-oxo-androstenedione (19-oxo ASD), 150 µM NADPH, in a volume of 400 µl. After adding NADPH, the absorbance of the reaction solution at 340 nm was recorded every 20 s for 10 min. The NADPH consumed was calculated by using an extinction coefficient at 340 nm of 6,220 M^{-1} cm^{-1} for NADPH. The products were quantified by HPLC analysis. The concentration of hydrogen peroxide generated during NADPH consumption was determined by Amplex Red hydrogen peroxide/peroxidase assay kit according to the manufacturer's instructions. The superoxide radical was determined by adding 2 µM SOD under the same conditions.

2.4.6 HPLC analysis

The HPLC analysis was performed on an Agilent 1200 series HPLC system (Agilent Technologies, Santa Clara, CA, USA) equipped with a diode array detector (DAD) and a reverse-phase column (Zorbax Eclipse plus C18, 250 × 4.6 mm, 5 µm, Agilent Technologies, Santa Clara, CA, USA). A sample volume of 85 µl was injected into the HPLC system for each analysis. When 19-oxo ASD was used as the substrate, the mobile phase was water: acetonitrile (50: 50, V/V), the flow rate was 0.5 ml/min, and the wavelength set at 280 nm to detect estrone. When ASD was used as substrate, the reaction solution was analysed by the following program, using water and acetonitrile as mobile phase: 0-3 min, 5% acetonitrile; 3-18 min, linear gradient from 5% to 50% acetonitrile; 18-23 min, linear gradient to 100% acetonitrile; 23-32 min, isocratic at 100% acetonitrile. The flow rate was 0.5 ml/min. In this case, ASD, 19-OH ASD and 19-oxo ASD were detected at 237 nm, and estrone was detected at 280 nm.

2.5 References

[1] Guengerich, F. P. Common and Uncommon Cytochrome P450 Reactions Related to Metabolism and Chemical Toxicity. Chem. Res. Toxicol. 2001, 14 (6), 611–650.

[2] Montellano, P. R. O. d. Cytochrome P450: Structure, Mechanism, and Biochemistry; 3rd ed.; Montellano, P. R. O. d., Ed.; Springer US, 2005. https://doi.org/10.1007/b139087.

[3] Denisov, I. G.; Makris, T. M.; Sligar, S. G.; Schlichting, I. Structure and Chemistry of Cytochrome P450. Chem. Rev. 2005, 105 (6), 2253–2278. https://doi.org/10.1021/cr0307143.

[4] Guengerich, F. P. Human Cytochrome P450 Enzymes. In Cytochrome P450: Structure, Mechanism, and Biochemistry; Montellano, P. R. O. d., Ed.; Springer International Publishing: Cham, 2015; pp 523–785. https://doi.org/10.1007/978-3-319-12108-6_9.

[5] Di Nardo, G.; Gilardi, G. Natural Compounds as Pharmaceuticals: The Key Role of Cytochromes P450 Reactivity. Trends Biochem. Sci. 2020, 45 (6), 511–525. https://doi.org/10.1016/j.tibs.2020.03.004.

[6] Guengerich, F. P. Intersection of the Roles of Cytochrome P450 Enzymes with Xenobiotic and Endogenous Substrates: Relevance to Toxicity and Drug Interactions Chem. Res. Toxicol. 2017, 30 (1), 2–12. https://doi.org/10.1021/acs.chemrestox.6b00226.

[7] Di Nardo, G.; Zhang, C.; Marcelli, A. G.; Gilardi, G. Molecular and Structural Evolution of Cytochrome P450 Aromatase. Int. J. Mol. Sci. 2021, 22 (2), 631. https://doi.org/10.3390/ijms22020631.

[8] Thompson, E. A.; Siiteri, P. K. Utilization of Oxygen and Reduced Nicotinamide Adenine Dinucleotide Phosphate by Human Placental Microsomes during Aromatization of Androstenedione. J. Biol. Chem. 1974, 249 (17), 5364–5372.

[9] Thompson, E. A.; Siiteri, P. K. The Involvement of Human Placental Microsomal Cytochrome P-450 in Aromatization. J. Biol. Chem. 1974, 249 (17), 5373–5378.

[10] Simpson, E. R.; Mahendroo, M. S.; Means, G. D.; Kilgore, M. W.; Hinshelwood, M. M.; Graham-Lorence, S.; Amarneh, B.; Ito, Y.; Fisher, C. R.; Michael, M. D.; Mendelson, C. R.; Bulun, S. E. Aromatase Cytochrome P450, The Enzyme Responsible for Estrogen Biosynthesis. Endocr. Rev. 1994, 15 (3), 342–355. https://doi.org/10.1210/edrv-15-3-342.

[11] Nardo, G. D.; Gilardi, G. Human Aromatase: Perspectives in Biochemistry and Biotechnology. Biotechnol. Appl. Biochem. 2013, 60 (1), 92–101. https://doi.org/10.1002/bab.1088.

[12] Buzdar, A. U.; Robertson, J. F. R.; Eiermann, W.; Nabholtz, J.-M. An Overview of the Pharmacology and Pharmacokinetics of the Newer Generation Aromatase Inhibitors Anastrozole, Letrozole, and Exemestane. Cancer 2002, 95 (9), 2006–2016. https://doi.org/10.1002/cncr.10908.

[13] Smith, I. E.; Dowsett, M. Aromatase Inhibitors in Breast Cancer. N. Engl. J. Med. 2003, 348, 2431-2442. https://doi.org/10.1056/NEJMra023246

[14] Santen, R. J.; Brodie, H.; Simpson, E. R.; Siiteri, P. K.; Brodie, A. History of Aromatase: Saga of an Important Biological Mediator and Therapeutic Target. Endocr. Rev. 2009, 30 (4), 343–375. https://doi.org/10.1210/er.2008-0016.

[15] Chumsri, S.; Howes, T.; Bao, T.; Sabnis, G.; Brodie, A. Aromatase, Aromatase Inhibitors, and Breast Cancer. J. Steroid Biochem. Mol. Biol. 2011, 125 (1), 13–22. https://doi.org/10.1016/j.jsbmb.2011.02.001.

[16] Osawa, Y.; Shibata, K.; Rohrer, D.; Weeks, C.; Duax, W. L. Reassignment of the Absolute Configuration of 19-Substituted 19-Hydroxysteroids and Stereomechanism of Estrogen Biosynthesis. J. Am. Chem. Soc. 1975, 97 (15), 4400–4402. https://doi.org/10.1021/ja00848a046

[17] Arigoni, D.; Battaglia, R.; Akhtar, M.; Smith, T. Stereospecificity of Oxidation at C-19 in Oestrogen Biosynthesis. J. Chem. Soc., Chem. Commun. 1975, No. 6, 185. https://doi.org/10.1039/c39750000185.

[18] Akhtar, M.; Calder, M. R.; Corina, D. L.; Wright, J. N. Mechanistic Studies on C-19 Demethylation in Oestrogen Biosynthesis. Biochem. J. 1982, 201 (3), 569–580. https://doi.org/10.1042/bj2010569

[19] Akhtar, M.; Njar, V. C. O.; Neville Wright, J. Mechanistic Studies on Aromatase and Related C-C Bond Cleaving P-450 Enzymes. J. Steroid Biochem. Mol. Biol. 1993, 44 (4–6), 375–387. https://doi.org/10.1016/0960-0760(93)90241-N.

[20] Poulos, T. L. Heme Enzyme Structure and Function. Chem. Rev. 2014, 114 (7), 3919–3962. https://doi.org/10.1021/cr400415k.

[21] Groves, J. T.; McClusky, G. A. Aliphatic Hydroxylation via Oxygen Rebound. Oxygen Transfer Catalyzed by Iron. J. Am. Chem. Soc. 1976, 98 (3), 859–861. https://doi.org/10.1021/ja00419a049.

[22] Groves, J. T.; McClusky, G. A.; White, R. E.; Coon, M. J. Aliphatic Hydroxylation by Highly Purified Liver Microsomal Cytochrome P-450. Evidence for a Carbon Radical Intermediate. Biochem. Biophys. Res. Commun. 1978, 81 (1), 154–160. https://doi.org/10.1016/0006-291X(78)91643-1.

[23] Rittle, J.; Green, M. T. Cytochrome P450 Compound I: Capture, Characterization, and C-H Bond Activation Kinetics. Science 2010, 330 (6006), 933–937. https://doi.org/10.1126/science.1193478.

[24] Mak, P. J.; Luthra, A.; Sligar, S. G.; Kincaid, J. R. Resonance Raman Spectroscopy

of the Oxygenated Intermediates of Human CYP19A1 Implicates a Compound I Intermediate in the Final Lyase Step. J. Am. Chem. Soc. 2014, 136 (13), 4825–4828. https://doi.org/10.1021/ja500054c.

[25] Khatri, Y.; Luthra, A.; Duggal, R.; Sligar, S. G. Kinetic Solvent Isotope Effect in Steady-State Turnover by CYP19A1 Suggests Involvement of Compound 1 for Both Hydroxylation and Aromatization Steps. FEBS Lett. 2014, 588 (17), 3117–3122. https://doi.org/10.1016/j.febslet.2014.06.050.

[26] Yoshimoto, F. K.; Guengerich, F. P. Mechanism of the Third Oxidative Step in the Conversion of Androgens to Estrogens by Cytochrome P450 19A1 Steroid Aromatase. J. Am. Chem. Soc. 2014, 136 (42), 15016–15025. https://doi.org/10.1021/ja508185d.

[27] Makris, T. M.; Denisov, I.; Schlichting, I.; Sligar, S. G. Activation of Molecular Oxygen by Cytochrome P450. In Cytochrome P450; Ortiz de Montellano, P. R., Ed.; Springer US: Boston, MA, 2005; pp 149–182. https://doi.org/10.1007/0-387-27447-2_5.

[28] Stok, J. E.; Yamada, S.; Farlow, A. J.; Slessor, K. E.; De Voss, J. J. Cytochrome P450cin (CYP176A1) D241N: Investigating the Role of the Conserved Acid in the Active Site of Cytochrome P450s. Biochim. Biophys. Acta Proteins. Proteom. 2013, 1834 (3), 688–696. https://doi.org/10.1016/j.bbapap.2012.12.022.

[29] Ishigooka, M.; Shimizu, T.; Hiroya, K.; Hatano, M. Role of Glu318 at the Putative Distal Site in the Catalytic Function of Cytochrome P450d. Biochemistry 1992, 31 (5), 1528–1531. https://doi.org/10.1021/bi00120a033.

[30] Lee-Robichaud, P.; Akhtar, E. M.; Akhtar, M. An Analysis of the Role of Active Site Protic Residues of Cytochrome P-450s: Mechanistic and Mutational Studies on 17α-Hydroxylase-17,20-Lyase (P-45017α Also CYP17). Biochem. J. 1998, 330 (2), 967–974. https://doi.org/10.1042/bj3300967.

[31] Zhou, D. J.; Korzekwa, K. R.; Poulos, T.; Chen, S. A. A Site-Directed Mutagenesis Study of Human Placental Aromatase. J. Biol. Chem. 1992, 267 (2), 762–768. https://doi.org/10.1016/S0021-9258(18)48349-4.

[32] Lo, J.; Di Nardo, G.; Griswold, J.; Egbuta, C.; Jiang, W.; Gilardi, G.; Ghosh, D. Structural Basis for the Functional Roles of Critical Residues in Human Cytochrome P450 Aromatase. Biochemistry 2013, 52 (34), 5821–5829. https://doi.org/10.1021/bi400669h.

[33] Imai, M.; Shimada, H.; Watanabe, Y.; Matsushima-Hibiya, Y.; Makino, R.; Koga, H.; Horiuchi, T.; Ishimura, Y. Uncoupling of the Cytochrome P-450cam Monooxygenase Reaction by a Single Mutation, Threonine-252 to Alanine or Valine: Possible Role of the Hydroxy Amino Acid in Oxygen Activation. Proc. Natl. Acad. Sci. 1989, 86 (20), 7823–7827. https://doi.org/10.1073/pnas.86.20.7823.

[34] Martinis, S. A.; Atkins, W. M.; Stayton, P. S.; Sligar, S. G. A Conserved Residue of Cytochrome P-450 Is Involved in Heme-Oxygen Stability and Activation. J. Am. Chem. Soc. 1989, 111 (26), 9252–9253. https://doi.org/10.1021/ja00208a031.

[35] Nagano, S.; Poulos, T. L. Crystallographic Study on the Dioxygen Complex of Wild-Type and Mutant Cytochrome P450cam. Implications for the Dioxygen Activation Mechanism. J. Biol. Chem. 2005, 280 (36), 31659–31663. https://doi.org/10.1074/jbc.M505261200.

[36] Coleman, T.; Stok, J. E.; Podgorski, M. N.; Bruning, J. B.; De Voss, J. J.; Bell, S. G. Structural Insights into the Role of the Acid-Alcohol Pair of Residues Required for Dioxygen Activation in Cytochrome P450 Enzymes. J. Biol. Inorg. Chem. 2020, 25 (4), 583–596. https://doi.org/10.1007/s00775-020-01781-4.

[37] Cryle, M. J.; Voss, J. J. D. The Role of the Conserved Threonine in P450BM3 Oxygen Activation: Substrate-Determined Hydroxylation Activity of the Thr268Ala Mutant. ChemBioChem 2008, 9 (2), 261–266. https://doi.org/10.1002/cbic.200700537.

[38] Schlichting, I. The Catalytic Pathway of Cytochrome P450cam at Atomic Resolution. Science 2000, 287 (5458), 1615–1622. https://doi.org/10.1126/science.287.5458.1615.

[39] Raag, R.; Martinis, S. A.; Sligar, S. G.; Poulos, T. L. Crystal Structure of the Cytochrome P-450CAM Active Site Mutant Thr252Ala. Biochemistry 1991, 30 (48) 11420–11429. https://doi.org/10.1021/bi00112a008.

[40] Yeom, H.; Sligar, S. G.; Li, H.; Poulos, T. L.; Fulco, A. J. The Role of Thr268 in Oxygen Activation of Cytochrome P450BM-3. Biochemistry 1995, 34 (45), 14733–14740. https://doi.org/10.1021/bi00045a014.

[41] Ghosh, D.; Griswold, J.; Erman, M.; Pangborn, W. Structural Basis for Androgen Specificity and Oestrogen Synthesis in Human Aromatase. Nature 2009, 457 (7226), 219–223. https://doi.org/10.1038/nature07614.

[42] Di Nardo, G.; Breitner, M.; Bandino, A.; Ghosh, D.; Jennings, G. K.; Hackett, J. C.; Gilardi, G. Evidence for an Elevated Aspartate PKa in the Active Site of Human Aromatase. J. Biol. Chem. 2015, 290 (2), 1186–1196. https://doi.org/10.1074/jbc.M114.595108.

[43] Spinello, A.; Pavlin, M.; Casalino, L.; Magistrato, A. A Dehydrogenase Dual Hydrogen Abstraction Mechanism Promotes Estrogen Biosynthesis: Can We Expand the Functional Annotation of the Aromatase Enzyme? Chemistry 2018, 24 (42), 10840–10849. https://doi.org/10.1002/chem.201802025.

[44] Ghosh, D.; Griswold, J.; Erman, M.; Pangborn, W. X-Ray Structure of Human Aromatase Reveals an Androgen-Specific Active Site. J. Steroid Biochem. Mol. Biol. 2010, 118 (4–5), 197–202. https://doi.org/10.1016/j.jsbmb.2009.09.012.

[45] Munro, A. W.; McLean, K. J.; Grant, J. L.; Makris, T. M. Structure and Function

of the Cytochrome P450 Peroxygenase Enzymes. Biochem. Soc. Trans. 2018, 46 (1), 183–196. https://doi.org/10.1042/BST20170218.

[46] Cupp-Vickery, J. R.; Han, O.; Hutchinson, C. R.; Poulos, T. L. Substrate-Assisted Catalysis in Cytochrome P450eryF. Nat. Struct. Biol. 1996, 3 (7), 632–637. https://doi.org/10.1038/nsb0796-632.

[47] Egawa, T.; Shimada, H.; Ishimura, Y. Evidence for Compound I Formation in the Reaction of Cytochrome P450cam with M-Chloroperbenzoic Acid. Biochem. Biophys. Res. Commun. 1994, 201 (3), 1464–1469. https://doi.org/10.1006/bbrc.1994.1868.

[48] Kellner, D. G.; Hung, S.-C.; Weiss, K. E.; Sligar, S. G. Kinetic Characterization of Compound I Formation in the Thermostable Cytochrome P450 CYP119. J. Biol. Chem. 2002, 277 (12), 9641–9644. https://doi.org/10.1074/jbc.C100745200.

[49] Grant, J. L.; Hsieh, C. H.; Makris, T. M. Decarboxylation of Fatty Acids to Terminal Alkenes by Cytochrome P450 Compound I. J. Am. Chem. Soc. 2015, 137 (15), 4940–4943. https://doi.org/10.1021/jacs.5b01965.

[50] Dornevil, K.; Davis, I.; Fielding, A. J.; Terrell, J. R.; Ma, L.; Liu, A. Cross-Linking of Dicyclotyrosine by the Cytochrome P450 Enzyme CYP121 from Mycobacterium Tuberculosis Proceeds through a Catalytic Shunt Pathway. J. Biol. Chem. 2017, 292 (33), 13645–13657. https://doi.org/10.1074/jbc.M117.794099.

[51] Sheng, X.; Zhang, H.; Im, S.-C.; Horner, J. H.; Waskell, L.; Hollenberg, P. F.; Newcomb, M. Kinetics of Oxidation of Benzphetamine by Compounds I of Cytochrome P450 2B4 and Its Mutants. J. Am. Chem. Soc. 2009, 131 (8), 2971–2976. https://doi.org/10.1021/ja808982g.

[52] Newcomb, M.; Zhang, R.; Chandrasena, R. E. P.; Halgrimson, J. A.; Horner, J. H.; Makris, T. M.; Sligar, S. G. Cytochrome P450 Compound I. J. Am. Chem. Soc. 2006, 128 (14), 4580–4581. https://doi.org/10.1021/ja060048y.

[53] Akhtar, M.; Wright, J. N.; Lee-Robichaud, P. A Review of Mechanistic Studies on Aromatase (CYP19) and 17α-Hydroxylase-17,20-Lyase (CYP17). J. Steroid Biochem. Mol. Biol. 2011, 125 (1–2), 2–12. https://doi.org/10.1016/j.jsbmb.2010.11.003.

[54] Spolitak, T.; Dawson, J. H.; Ballou, D. P. Rapid Kinetics Investigations of Peracid Oxidation of Ferric Cytochrome P450cam: Nature and Possible Function of Compound ES. J. Inorg. Biochem. 2006, 100 (12), 2034–2044. https://doi.org/10.1016/j.jinorgbio.2006.09.026.

[55] Vidakovic, M.; Sligar, S. G.; Li, H.; Poulos, T. L. Understanding the Role of the Essential Asp251 in Cytochrome P450cam Using Site-Directed Mutagenesis, Crystallography, and Kinetic Solvent Isotope Effect. Biochemistry 1998, 37 (26), 9211–9219. https://doi.org/10.1021/bi980189f.

[56] Di Nardo, G.; Breitner, M.; Sadeghi, S. J.; Castrignanò, S.; Mei, G.; Di Venere, A.;

Nicolai, E.; Allegra, P.; Gilardi, G. Dynamics and Flexibility of Human Aromatase Probed by FTIR and Time Resolved Fluorescence Spectroscopy. PLoS One 2013, 8 (12), e82118. https://doi.org/10.1371/journal.pone.0082118.

[57] Zhang, C.; Catucci, G.; Di Nardo, G.; Gilardi, G. Effector Role of Cytochrome P450 Reductase for Androstenedione Binding to Human Aromatase. Int. J. Biol. Macromol. 2020, 164, 510–517. https://doi.org/10.1016/j.ijbiomac.2020.07.163.

[58] Omura, T.; Sato, R. The Carbon Monoxide-binding Pigment of Liver Microsomes. I. Evidence for Its Hemoprotein Nature. J. Biol. Chem. 1964, 239, 2370–2378. https://doi.org/10.1016/S0021-9258(20)82244-3

[59] Porter, T. D.; Wilson, T. E.; Kasper, C. B. Expression of a Functional 78,000 Dalton Mammalian Flavoprotein, NADPH-Cytochrome P-450 Oxidoreductase, in Escherichia Coli. Arch. Biochem. Biophys. 1987, 254 (1), 353–367. https://doi.org/10.1016/0003-9861(87)90111-1.

Chapter 3

Effector Role of Cytochrome P450 Reductase for Androstenedione Binding to Human Aromatase

International Journal of Biological Macromolecules 164 (2020) 510–517

Contents lists available at ScienceDirect

International Journal of Biological Macromolecules

journal homepage: http://www.elsevier.com/locate/ijbiomac

Effector role of cytochrome P450 reductase for androstenedione binding to human aromatase

Chao Zhang, Gianluca Catucci, Giovanna Di Nardo *, Gianfranco Gilardi *

Department of Life Sciences and Systems Biology, University of Torino, Via Accademia Albertina 13, Torino 10123, Italy

ARTICLE INFO

Article history:
Received 28 April 2020
Received in revised form 4 June 2020
Accepted 15 July 2020
Available online 19 July 2020

Keywords:
Aromatase
Cytochrome P450 reductase
Isothermal titration calorimetry

ABSTRACT

Cytochromes P450 constitute a large superfamily of monooxygenases involved in many metabolic pathways. Most of them are not self-sufficient and need a reductase protein to provide the electrons necessary for catalysis. It was shown that the redox partner plays a role in the modulation of the structure and function of some bacterial P450 enzymes.

Here, the effect of NADPH-cytochrome reductase (CPR) on human aromatase (Aro) is studied for what concerns its role in substrate binding. Pre-steady-state kinetic experiments indicate that both the substrate binding rates and the percentage of spin shift detected for aromatase are increased when CPR is present. Moreover, aromatase binds the substrate through a conformational selection mechanism, suggesting a possible effector role of CPR. The thermodynamic parameters for the formation of the CPR-Aro complex were studied by isothermal titration calorimetry. The dissociation constant of the complex formation is 4.5 folds lower for substrate-free compared to the substrate-bound enzyme. The enthalpy change observed when the CPR-Aro complex forms in the absence of the substrate are higher than in its presence, indicating that more interactions are formed/broken in the former case. Taken together, our data confirm that CPR has a role in promoting aromatase conformation optimal for substrate binding.

1. Introduction

Human cytochromes P450 (P450) are membrane-bound proteins present in most tissues of the human body [1]. They play essential roles in the metabolism of steroid hormones, vitamins and fatty acids and they also can oxidize xenobiotics such as carcinogens and drugs. They are not self-sufficient enzymes and most of them share the reduction partner, cytochrome P450 reductase (CPR). Electrons from NADPH are stepwise transferred from CPR to the P450 heme group and protein-protein interaction has been demonstrated to be guided mainly by electrostatic interactions with the positively charged heme-proximal side of the P450 enzyme and the negatively charged residues on FMN-binding domain of CPR [2–4] as well as by hydrophobic interactions [5]. CPR and cytochromes P450 are anchored to the membrane through their hydrophobic N-terminal transmembrane helices. The anchoring of the proteins in the lipid bilayer was shown to play an important role due to the influence of both the lipid environment and the membrane-anchor helices on electron transfer and P450 catalytic efficiency [6,7]. Solid-state NMR studies in membrane-mimicking environments such as lipid nanodiscs have shown that protein-lipid interaction are crucial for the stability, the dynamics and the interaction between human cytochromes P450 and the redox partners CPR [8–12] and cytochrome b_5 [13–15]. Moreover it was shown that CPR and cytochrome b_5 compete for cytochromes P450 binding and that the presence of the substrate affects the interplay between the three proteins promoting the binding of cytochrome b_5 to the P450 enzyme [15].

In addition to electron transfer, different studies have shown that the redox partners can play important roles in regulating the structure and function of some bacterial P450 enzymes [16–20]. As a consequence, the topic of the interaction between cytochromes P450 and its redox partner is attracting more and more attention and an important question is whether CPR plays a role in modulating the structure and function of human P450s.

Here we investigate the role played by CPR in modulating the substrate binding ability of human aromatase. This enzyme is involved in the estrogens synthesis and it catalyzes the conversion of androgens to estrogens via a three-step reaction [21–23]. Due to its important role in breast cancer development and progression [24,25], the structure-function relationship of aromatase has been widely studied [26–32]. This enzyme is highly selective for the androgen substrates with K_M values reported in the low μM–nM range [30,33] and it also shows a high coupling efficiency (87%) [34], when compared to other human more promiscuous cytochromes P450, indicating an optimal interaction with CPR.

* Corresponding authors at: Via Accademia Albertina 13, 10123 Torino, Italy.
E-mail addresses: giovanna.dinardo@unito.it (G. Di Nardo), gianfranco.gilardi@unito.it (G. Gilardi).

https://doi.org/10.1016/j.ijbiomac.2020.07.163
0141-8130/

Many cytochromes P450 have been shown to adopt different conformations ranging from the open form, typical of the ligand free-enzymes, to the closed one that is adopted when a substrate or inhibitor is present [35]. The crystal structure of aromatase is available only in complex with the substrate androstenedione. The protein is in a closed conformation and the substrate is perfectly accommodated in a relatively small active site [26,28,36]. This implies that aromatase needs to undergo structural changes to make the active site accessible to the substrate [27,37,38]. Indeed, FTIR and time-resolved fluorescence spectroscopy studies revealed that in the absence of substrate, the flexibility of aromatase increases with faster dynamics of helix F involved in the substrate access channel [36,39]. Thus, it has been hypothesized that aromatase adopts different conformations according to the presence and absence of the substrate. In general, the study of how the conformational dynamics of cytochromes P450 are associated with ligand binding events is another important topic in the research field. Recently, it has been shown that many human P450 enzymes use a conformational selection mechanism rather than an induced fit one [40,41]. In the induced fit model, the substrate (S) binds to the enzyme (E) and causes a conformational change in the protein to give the optimal ligand-bound conformation, indicated as ES* in Eq. (1) (Scheme 1A):

$$E + S \underset{k_{off}}{\overset{k_{on}}{\rightleftarrows}} ES \underset{k_{-1}}{\overset{k_1}{\rightleftarrows}} ES^* \quad (1)$$

In the conformational selection model, the substrate (S) binds one of the possible conformations of the enzyme that is the one optimal for substrate binding, indicated by E* in Eq. (2) (Scheme 1B):

$$E \underset{k_{-1}}{\overset{k_1}{\rightleftarrows}} E^* + S \underset{k_{off}}{\overset{k_{on}}{\rightleftarrows}} ES^* \quad (2)$$

In the present study, a combination of substrate titrations followed spectrophotometrically, as well as pre-steady state kinetics of substrate binding and isothermal titration calorimetry are used to gain information on the effect of CPR on human aromatase (Aro) ability to bind the substrate and on the thermodynamics of CPR-Aro complex formation. The presence of CPR is found to increase the rates for substrate binding and to increase the number of molecules that are in the optimal conformation to bind the substrate. The results support that Aro binds the substrate through a conformational selection mechanism with the CPR having a higher affinity when the substrate is not present in the active site of the protein.

2. Materials and methods

2.1. Chemicals

All solvents and reagents were of analytical grade and were obtained from Sigma Aldrich.

2.2. Protein expression and purification

The recombinant form of human aromatase used in this work lacks the N-terminal amino acid fragment anchoring the protein to the membrane (residues 1–39) that was replaced by 10 residues (MAKKTSSKGR). Moreover, a four-histidine tag was introduced at the C-terminal [39]. The recombinant protein was expressed and purified as described previously [39]. Briefly, transformed *Escherichia coli* DH5α cells were grown at 37 °C in a Terrific Broth media until the cell density OD_{600} reached 0.6. Protein expression was induced with 1 mM isopropyl-β-D-thiogalactopyranoside and carried out at 28 °C for 48 h. The cells were then harvested and resuspended in 100 mM potassium phosphate (KPi) pH 7.4, 20% glycerol, 1 mM β-mercaptoethanol, 0.1% v/v Tween-20 buffer containing 1 mg/mL lysozyme, 1% v/v Tween-20 and protease inhibitor mixture. After stirring for 45 min, cells were disrupted by sonication and ultra-centrifuged at 40,000 rpm for 25 min at 4 °C. The supernatant was first loaded onto a diethyl

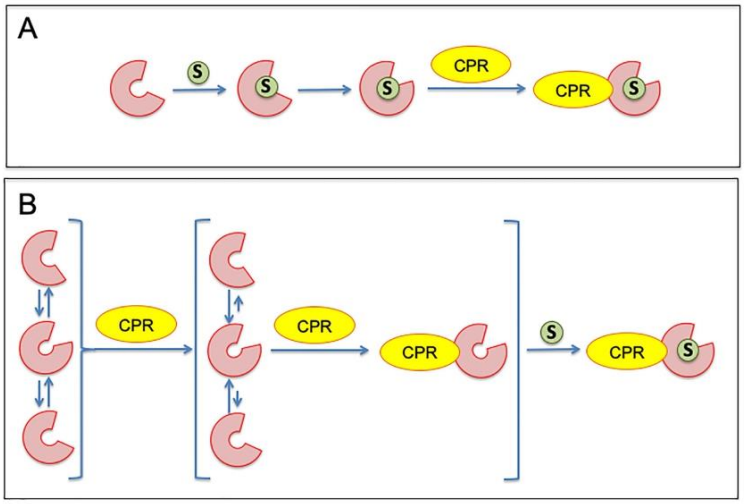

Scheme 1. Models for enzyme-substrate binding in human aromatase and role of cytochrome P450 reductase (CPR). (A) In the induced fit model, the substrate binds the enzyme and induces a conformational rearrangement that optimizes the substrate-enzyme interaction. In a next step, CPR binds the enzyme-substrate complex and has no role in substrate binding. (B) In the conformational selection model, the enzyme shifts between different conformational states. The binding of CPR favors the enzyme conformation that is optimal for substrate binding that occurs in a next step.

aminoethyl (DEAE) ion-exchange chromatography and then further purified by a Nickel-ion affinity chromatography. The target protein was eluted with a linear gradient in which histidine ranging from 10 to 40 mM was added. The eluted fractions were pooled according to the purity ratio (A_{280nm}/A_{418nm}) and concentrated by Amicon centrifugal filters (30 kDa MWCO membrane). Aro concentration was estimated by CO-binding assay, using an extinction coefficient at 450 nm of 91,000 M^{-1} cm^{-1} [42].

Human CPR was expressed as a full-length protein in *Escherichia coli* DH5α. The cells were resuspended in a 100 mM Tris-acetate buffer, pH 7.6, 0.5 M sucrose and 1 mM EDTA buffer and lysed by adding with 0.5 mg/mL lysozyme and 0.1 mM EDTA for 30 min at 4 °C. After centrifugation at 4000 rpm for 20 min, the pellets were resuspended in 100 mM KPi, pH 7.6, 6 mM magnesium acetate, 0.1 mM DTT, 20% glycerol, 0.2 mM PMSF and 0.1 mM DNase I, and disrupted by sonication. The membrane-containing pellets were collected by 40 min centrifugation at 40,000 rpm, suspended in 20 mM KPi, pH 7.6, 20% glycerol, 0.1 mM EDTA, 0.2 mM PMSF, 0.2% sodium cholate and 0.2% Triton X-100, and stirred gently for 2 h. This crude extract was then centrifugated at 40,000 rpm for 1 h, and the supernatant was load onto a pre-equilibrated affinity chromatography of 2′,5′-ADP Sepharose 4B. After different washing steps with the equilibration buffer, where first 250 mM NaCl and then 2 mM adenosine were added, the CPR was eluted with a linear gradient in which $NADP^+$ increased from 0.1 to 1 mM. Fractions containing the full-length CPR, which were monitored by SDS-PAGE analysis, were pooled and concentrated by Amicon centrifugal filters (with 30 kDa MWCO membrane). The CPR concentrations were measured using an extinction coefficient at 456 nm of 24,100 M^{-1} cm^{-1} [43].

2.3. UV–vis spectroscopy and substrate binding titrations

Spectral binding titrations were performed as described previously [30]. In brief, 1 μM of aromatase in 100 mM KPi buffer pH 7.0, 20% glycerol, 1 mM β-mercaptoethanol were incubated with increasing amounts of androstenedione ranging from 0.5 μM to 12 μM. Binding assay was using an Agilent 8453 UV–vis spectrophotometer at 25 °C. UV–visible spectra were recorded after each addition, and the absorbance differences at 394 nm and at 418 nm were plotted against the added substrate concentrations. The data were fitted to the following equation that allowed to calculate the dissociation constants K_D:

$$\Delta A_{394\text{-}418} = \Delta A^{max}{}_{394\text{-}418} \cdot [S]_{free} / (K_D + [S]_{free})$$

where $[S]_{free}$ is $[S]_{total} - [E \cdot S]$ and $[E \cdot S] = \Delta A_{394\text{-}418}\,[E]_{total} / \Delta A^{max}_{394\text{-}418}$.

2.4. Stopped flow absorbance experiments

The pre-steady state kinetics of substrate binding to aromatase was investigated using a Hi-Tech scientific SF-61 single mixing stopped-flow instrument (TgK Scientific, UK). In a typical experiment, one of the drive syringes contained the purified aromatase (2 μM) in a 100 mM potassium phosphate buffer pH 7.0 containing 10% glycerol, 1 mM β-mercaptoethanol. The second drive syringe contained different concentrations of the substrate androstenedione. For the experiments in the presence of CPR, the purified protein (6 μM) was pre-incubated with aromatase in the first drive syringe and then mixed with the substrate androstenedione.

In all the experiments, the temperature was set at 25 °C and controlled by a water bath. For each substrate concentration, 5 to 7 replicates were conducted for each experiment. Each Kinetic trace was derived from observing the changes at 394 nm as a function of time and fitted to a single or double exponential function by Kinetic studio V3 software (TgK Scientific, UK).

2.5. Isothermal titration calorimetry

Isothermal titration calorimetry (ITC) experiments were performed at 25 °C using a MicroCal iTC200 instrument (Malvern Instruments, Malvern, UK). Before the experiment, aromatase and CPR were prepared by extensive buffer-exchange using Amicon centrifugal filters (30 kDa MWCO) and concentrated with the same potassium phosphate buffer (100 mM KPi, 10% glycerol, pH 7.0). For the experiments in the presence of the substrate, aromatase (0.5 μM) was incubated overnight at 4 °C with saturating amounts of the substrate androstenedione (20 μM). The reaction cell was filled with 300 μL of 25 μM aromatase and the injection syringe was filled with 600 μM CPR. CPR was titrated into Aro in potassium phosphate buffer (100 mM KPi, 10% glycerol, pH 7.0) up to a 1:5 (Aro:CPR) molar ratio. The first injection was 0.1 μL with 0.2 s duration and omitted during data analysis. The second injection was 3.5 μL with 7 s duration followed by 9 injections of 4 μL with 8 s duration. Each titration experiment involved a 90 s interval between injections. The reaction cell was continuously stirred at 750 rpm speed. A reference power of 7 was used for each experiment. The data were processed and analyzed by using Origin® 7.0 software. Control experiments were

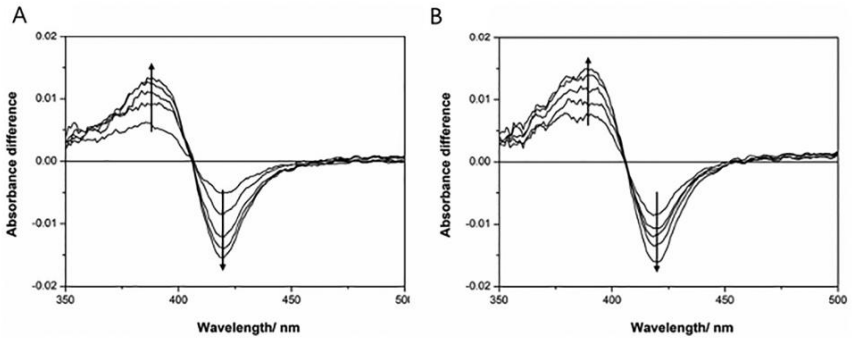

Fig. 1. Substrate binding monitored by stopped-flow analysis. (A) Difference spectra observed after mixing 1 μM Aro with 10 μM androstenedione in the stopped-flow apparatus. (B) Difference spectra observed after mixing 1 μM Aro and 3 μM CPR with 10 μM androstenedione. The traces shown were collected after 0, 0.1, 0.2, 0.3, 0.4 and 0.5 s from mixing.

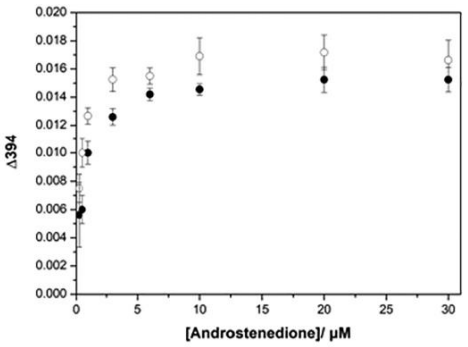

Fig. 2. Plot of the amount of spin shift as a function of the substrate concentration. Black circles represent the amount of spin shift obtained from 1 μM Aro in the absence of CPR; empty circles represent the amount of spin shift obtained from 1 μM Aro pre-mixed with 3 μM CPR (Aro:CPR = 1:3).

carried out by titrating the ligand CPR into the cell containing only the buffer under identical conditions. The heats of dilution were subtracted from the observed titration data.

3. Results and discussion

3.1. Effect of CPR on substrate binding by aromatase

The effect of CPR on the affinity (K_D) of human aromatase toward its substrate was first investigated by UV–vis spectroscopy. In general, the binding of the substrate in the active site of cytochromes P450 is known to alter the spin state of the heme iron, with a spectral transition that for aromatase occurs from 418 to 394 nm [39]. Here the substrate binding curves values were obtained by monitoring the spin shift caused by the addition of increasing concentrations of androstenedione to 1 μM of Aro and data were fitted to one-site saturation binding curves, from which an apparent K_D of 0.98 ± 0.11 μM and 0.72 ± 0.11 μM were found in the absence and in the presence 3-fold excess of CPR, respectively. These results are not significantly different and indicate that CPR does not affect the binding affinity of Aro for the substrate androstenedione.

Pre-steady state kinetics of substrate binding were then investigated by stopped-flow measurements in the absence and presence of CPR. First, different concentrations of the substrate (0.25–30 μM) were used with a fixed concentration of Aro (1 μM) in the absence and presence of 3 μM of CPR. Fig. 1 shows the difference spectra obtained with the typical low-to-high spin transition due to substrate binding. When the percentage of spin shift obtained at different substrate concentrations was measured, the data showed consistent lower values in the absence of CPR (Fig. 2). In particular, at the lowest substrate concentration used (0.25–0.5 μM), the spin shift obtained in the absence of CPR was 40% lower than that obtained in its presence (Fig. 2). These data indicate that CPR increases the population of Aro that binds the substrate, suggesting a possible regulatory role on the conformation on the P450 enzyme, as previously reported for P450cam [20].

The kinetics of substrate binding were followed as the increase of the signal at 394 nm in the first 3 s and the traces obtained were found to better fit to a single exponential function from which the rate constants were derived (Fig. 3). The plot of the rates as a function of substrate concentration shows a linear trend both in the absence and presence of CPR (Fig. 4A). However, the substrate binding rates were increased by up to 30% when saturating amounts of the substrate were tested (Fig. 4A). A linear regression was applied to calculate the apparent second-order rate constants (k_{on} and k_{off}). In the absence of CPR, the obtained k_{on} value was 5.1×10^5 M^{-1} s^{-1} and the k_{off} was 0.17 s^{-1} (Table 1). However, both the apparent k_{on} and k_{off} were increased when an excessive CPR was added. The calculated k_{on} and k_{off} were 7.0×10^5 M^{-1} s^{-1} and was 0.24 s^{-1}, respectively. K_D values calculated from these kinetic constants (k_{off}/k_{on}) are in the same order of magnitude with the K_D values measured by spectroscopic titrations (Table 1).

One of the interesting questions in the cytochrome P450 research field is whether they bind their substrates/inhibitors through conformational selection modes or induced fit.

When an increasing hyperbolic dependence of the binding rates (k_{obs}) as a function of substrate concentration is found, this is diagnostic of an induced fit mechanism [44]. On the other hand, a decreasing dependence in the binding rates (k_{obs}) as a function of substrate concentration is diagnostic of conformational selection [44,45]. However, conformational selection can give rise to increasing trends as well. In this case, a possible way to distinguish between the two modes is to carry out two separate experiments. In a first experiment, the concentration of the enzyme is fixed and the one of the substrate is varied; in a second experiment, the concentration of the substrate is fixed and the one of the enzyme is varied. When the plots of the k_{obs} obtained in the two experiments are constructed, the same trend should be found in the case of an induced fit mechanism

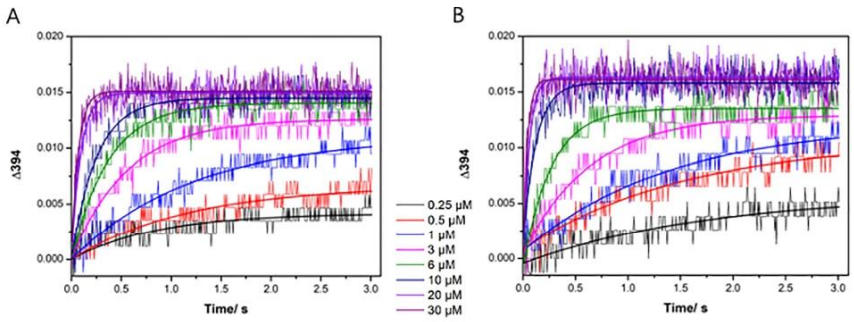

Fig. 3. Kinetics of substrate binding to aromatase. (A) Kinetic traces (ΔA394) obtained after mixing different amounts of the substrate androstenedione (0.25, 0.5, 1, 3, 6, 10, 20, 30 μM) with 1 μM Aro. (B) Kinetic traces (ΔA394) obtained after mixing different amounts of the substrate (0.25, 0.5, 1, 3, 6, 10, 20, 30 μM) with 1 μM Aro and 3 μM CPR (Aro:CPR = 1:3). All curves are fitted to single exponential functions.

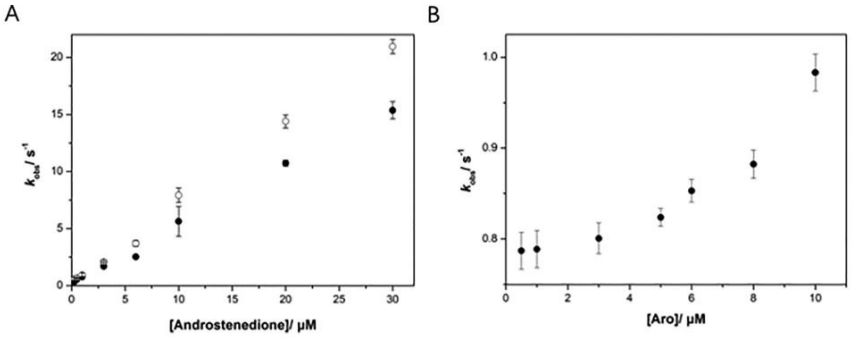

Fig. 4. Analysis of the substrate binding rates. (A) Plot of the binding rates as a function of substrate concentration with a fixed aromatase amount (1 μM) in the absence (solid symbols) and presence (white symbols) of 3 μM CPR (Aro:CPR = 1:3). (B) Plot of the binding rates as a function of aromatase concentration with a fixed substrate amount (2 μM).

Table 1
Binding rates and dissociation constants of aromatase for the substrate androstenedione.

Aro:CPR	K_D[a] (μM)	k_1 (s^{-1})	k_{on} (M^{-1} s^{-1})	k_{off} (s^{-1})	K_D[b] (μM)
1:0	0.98 ± 0.11	15.4 ± 0.8	5.1 ± 0.3 × 10^5	0.17 ± 0.06	0.33 ± 0.13
1:3	0.72 ± 0.11	20.2 ± 0.9	7.0 ± 0.2 × 10^5	0.24 ± 0.05	0.34 ± 0.06

[a] K_D values calculated from spectral equilibrium binding titrations.
[b] K_D values calculated from these kinetic constants (k_{off}/k_{on}).

whereas distinct kinetics are found in the case of the conformation selection mode [44].

In the case of Aro, the plot of the rates as a function of androstenedione concentration (Fig. 4A) shows a linear trend. This suggests a conformational selection mode as an induced fit should have a hyperbolic dependence [44]. To gain further information, a second set of experiments was carried out keeping the substrate concentration fixed at 2 μM while varying the enzyme concentration. The plots obtained (Fig. 4B) show a non-linear dependence. The two plots where either the protein or the ligand are varied should be identical in the case of an induced fit mechanism [44], therefore it can be concluded that a conformational selection mode is taking place in substrate binding by aromatase.

Taken together, the data show that the presence of CPR does not cause any change in the substrate binding affinity of aromatase, but it increases the binding rate for the substrate as well as the fraction of the enzyme that is able to bind the substrate through a conformational selection mechanism. This is consistent with Eq. (2), Scheme 1B.

3.2. Isothermal titration calorimetry (ITC)

The thermodynamic characterization of a binding process is traditionally investigated by isothermal titration calorimetry (ITC). Therefore the binding process of CPR to aromatase in the absence and presence of the substrate androstenedione was followed by ITC. One important issue about this experiment is the reduction state of CPR. Indeed, it is known that the semiquinone state of CPR (CPR_{sq}) has the highest affinity for other human P450s as demonstrated for P450 2C9 [46]. Upon reduction, the fully oxidized CPR (CPR_{ox}) undergoes the conformational changes required for the CPR_{sq} to be able to dock the P450 proximal side. This forms a complex where the FMN of the CPR_{sq} and then heme of the P450 are close enough to allow electron transfer [47,48].

For these reasons, the UV–vis spectra of the CPR and the Aro used in the ITC experiments were collected to confirm the oxidation state of the two proteins (Fig. 5). In particular, the spectrum of CPR in Fig. 5A shows a band at 587 nm with a shoulder at 630 nm, typical of the its semiquinone state (CPR_{sq}). This confirms that CPR is purified in its semiquinone state as previously reported [49,50]. Fig. 5B shows the spectra recorded of Aro in the absence and presence of the substrate androstenedione. The presence of bands at 418 and 394 nm indicate that

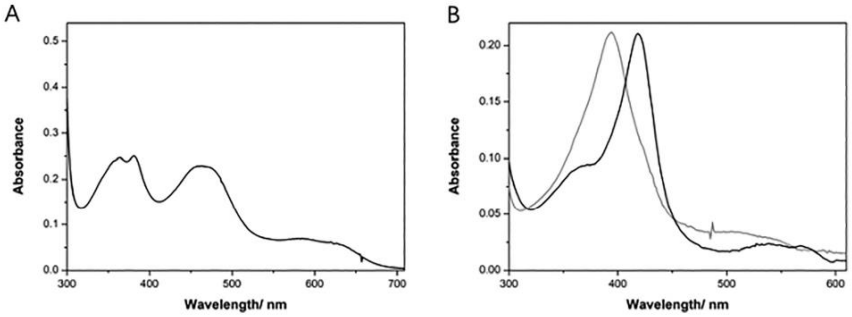

Fig. 5. UV–vis spectra of the protein samples used for ITC measurement. (A) Spectra of 10 μM CPR in potassium phosphate buffer (100 mM KPi, 10% glycerol, pH 7.0). (B) Aromatase spectra in the substrate-free form (black line) and upon incubation with the substrate androstenedione (gray line).

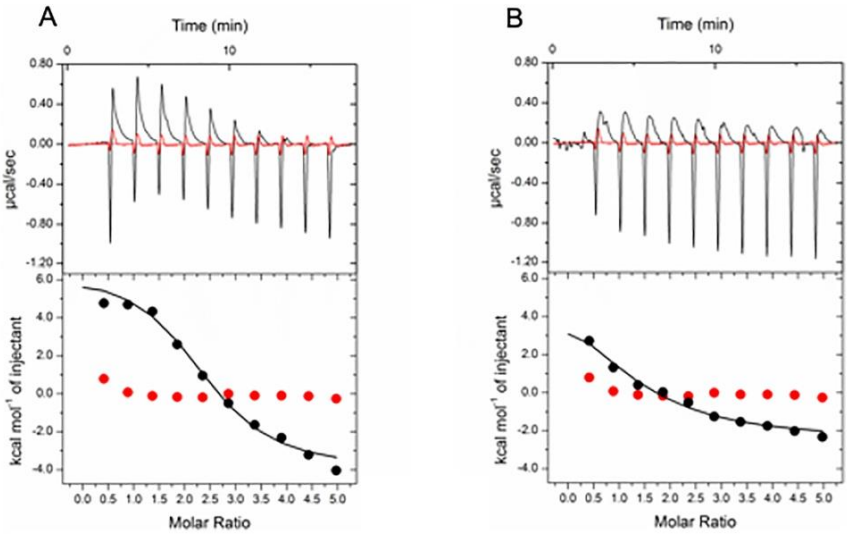

Fig. 6. Isothermal titration calorimetry traces for CPR_{sq}-Aro complex formation. ITC traces were obtained titrating CPR_{sq} in the (A) substrate-free and (B) substrate-bound Aro in 100 mM KPi, 10% glycerol pH 7.0. The top panels show the raw data, the lower panels show the enthalpy changes plotted as a function of the CPR_{sq}: Aro molar ratio. The black curves indicate the best fit to a single site model, the red circles represent the control experiments, where CPR_{sq} was titrated into the ITC only containing buffer.

the protein undergoes the typical low-to-high spin state changes upon substrate binding.

We therefore proceeded to collect the ITC profiles resulting from the titration of CPR_{sq} into the cell containing Aro in experiments carried out both in the presence and absence of androstenedione (Fig. 6). The titration was carried out in a 100 mM KPi pH 7.0 buffer containing 10% glycerol and the final CPR_{sq}:Aro molar ratio achieved was 5:1. In all cases the ITC profiles show the presence of an exothermic followed by an endothermic process. These profiles are not present in control experiments where the CPR_{sq} was titrated in a solution containing only buffer. Moreover, when the heat of the endothermic and the exothermic processes are plotted as a function of the CPR_{sq}: Aro molar ratio, a sigmoidal trend typical of ligand binding is obtained with the endothermic process contributing more to the overall process (data not shown). Thus, the two processes can be assigned to the CPR_{sq}-Aro complex formation. The thermodynamic parameters were obtained by fitting the overall data (Fig. 6) and they are reported in Table 2. In the absence of the substrate, the interaction between Aro and CPR_{sq} yielded a K_D value of 5.4 ± 1.2 μM, while in the presence of the substrate the K_D was 24.2 ± 6.9 μM. These results suggested that CPR_{sq} binds to the substrate-free Aro with a higher affinity compared to the substrate-bound form. Interestingly, the enthalpy changes of the interaction between CPR_{sq} and Aro are also significantly altered by the presence of the substrate. In fact, these are considerably higher than when the substrate is not present, indicating that more interactions are forming and breaking when substrate-free Aro complexes with CPR_{sq}. This finding also suggests that more conformational changes are taking place in CPR_{sq} and aromatase when the substrate is not present.

The overall ΔG resulted negative as well as −TΔS indicating that the binding is entropically driven. This finding suggests a large entropic contribution that can be due to the release or replacement of ordered water molecules from the protein surface and to the proteins' conformational dynamics during complex formation [51]. The positive ΔH values suggest that the binding of CPR_{sq} to aromatase is composed of intramolecular hydrogen bonding and non-covalent interaction following conformational changes of CPR_{sq}. It has to be taken into account that ITC experiments were carried out under a single buffer condition known to maintain protein stability and solubility. Moreover, the proteins are not in their physiological membrane environment that is known to affect and limit their orientation promoting complex formation also through the transmembrane helix [14]. However, the thermodynamic parameters calculated by ITC are in line with those recently calculated by surface plasmon resonance (SPR) for the interaction of CPR_{sq} with many human cytochromes P450, including aromatase [52]. Also in that case, the process resulted entropically driven with a positive value of ΔH [52].

4. Conclusion

In conclusion, this study provides new insights on the interaction of a human cytochrome P450 with the redox partner, indicating an effector role of CPR, as previously observed for bacterial cytochrome P450cam [19,20].

Table 2
Thermodynamic parameters measured from ITC experiments.

Combinations	K_D (μM)	ΔH (kcal mol^{-1})	ΔG (kcal mol^{-1})	−TΔS (kcal mol^{-1})
CPR_{sq}/Aro − substrate	5.4 ± 1.2	9.5 ± 0.4	−7.2 ± 1.6	−16.7 ± 1.6
CPR_{sq}/Aro + substrate	24.2 ± 6.9	6.0 ± 0.2	−6.3 ± 1.4	−12.3 ± 1.4

Here we show not only that human Aro adopts the conformational selection mode to bind the substrate, but also that CPR when bound to substrate-free Aro triggers the conformational changes required for optimal substrate binding (Scheme 1B). These data are consistent with the recent results coming from all-atom molecular dynamics simulations showing that CPR binding alters the motions of human aromatase and reshapes the substrate access channel [53].

The effector role of CPR can be crucial in the physiological environment since the reductase protein is in limited amounts compared to cytochromes P450 [54] and would therefore promote catalysis when already in the semi-reduced form and ready to bind the enzyme. It would be interesting to expand this kind of studies to other human enzymes, such as the more promiscuous cytochromes P450 involved in drug metabolism, to highlight possible preferences of CPR for the different enzymes according to their physiological role in the organism.

Acknowledgements

CZ thanks China Scholarship Council (CSC) for financial support.

Author contributions

CZ, GG, GDN and GG designed the experiments; CZ and GC performed the experiments; CZ, GC, GDN and GG analyzed the data; CZ and GDN wrote the paper. All authors reviewed and approved this article.

Declaration of competing interest

The authors declare that there is no conflict of interest.

References

[1] S.D. Black, Membrane topology of the mammalian P450 cytochromes, FASEB J. 6 (1992) 680–685, https://doi.org/10.1096/fasebj.6.2.1537456.
[2] M. Wang, D.L. Roberts, R. Paschke, T.M. Shea, B.S.S. Masters, J.J. Kim, Three-dimensional structure of NADPH–cytochrome P450 reductase: prototype for FMN- and FAD-containing enzymes, Proc. Natl. Acad. Sci. U. S. A. 94 (1997) 8411–8416, https://doi.org/10.1073/pnas.94.16.8411.
[3] Y. Hong, R. Rashid, S. Chen, Binding features of steroidal and nonsteroidal inhibitors, Steroids 76 (2011) 802–806, https://doi.org/10.1016/j.steroids.2011.02.037.
[4] Y. Hong, H. Li, Y.C. Yuan, S. Chen, Sequence–function correlation of aromatase and its interaction with reductase, J. Steroid Biochem. Mol. Biol. 118 (2010) 203–206, https://doi.org/10.1016/j.jsbmb.2009.11.010.
[5] C. Kenaan, H. Zhang, E.V. Shea, P.F. Hollenberg, Uncovering the role of hydrophobic residues in cytochrome P450−cytochrome P450 reductase interactions, Biochemistry 50 (2011) 3957–3967, https://doi.org/10.1021/bi1020748.
[6] P. Hlavica, Mechanistic basis of electron transfer to cytochromes P450 by natural redox partners and artificial donor constructs, Adv. Exp. Med. Biol. 851 (2015) 247–297, https://doi.org/10.1007/978-3-319-16009-2_10.
[7] U.H.N. Dürr, L. Waskell, A. Ramamoorthy, The cytochromes P450 and b5 and their reductases-promising targets for structural studies by advanced solid-state NMR spectroscopy, Biochim. Biophys. Acta Biomembr. 1768 (2007) 3235–3259, https://doi.org/10.1016/j.bbamem.2007.08.007.
[8] C. Barnaba, K. Gentry, N. Sumangala, A. Ramamoorthy, The catalytic function of cytochrome P450 is entwined with its membrane-bound nature, F1000Res 6 (2017) 662, https://doi.org/10.12688/f1000research.11015.1.
[9] C. Barnaba, A. Ramamoorthy, Picturing the membrane-assisted choreography of cytochrome P450 with lipid nanodiscs, ChemPhysChem 19 (2018) 2603–2613, https://doi.org/10.1002/cphc.201800444.
[10] C. Barnaba, T. Ravula, I.G. Medina-Meza, S.C. Im, G.M. Anantharamaiah, L. Waskell, A. Ramamoorthy, Lipid-exchange in nanodiscs discloses membrane boundaries of cytochrome-P450 reductase, Chem. Commun. 54 (2018) 6336–6339, https://doi.org/10.1039/C8CC02003E.
[11] E. Prade, M. Mahajan, S.C. Im, M. Zhang, K.A. Gentry, G.M. Anantharamaiah, L. Waskell, A. Ramamoorthy, A minimal functional complex of cytochrome P450 and FBD of cytochrome P450 reductase in nanodiscs, Angew. Chem. Int. Ed. 57 (2018) 8458–8462, https://doi.org/10.1002/anie.201802210.
[12] M. Mahajan, T. Ravula, E. Prade, G.M. Anantharamaiah, A. Ramamoorthy, Probing membrane enhanced protein-protein interactions in a minimal redox complex of cytochrome-P450 and P450-reductase, Chem. Commun. 55 (2019) 5777–5780, https://doi.org/10.1039/C9CC01630A.
[13] S. Ahuja, N. Jahr, S.C. Im, S. Vivekanandan, N. Popovych, S.V. Le Clair, R. Huang, R. Soong, J. Xu, K. Yamamoto, R.P. Nanga, A. Bridges, L. Waskell, A. Ramamoorthy, A model of the membrane-bound cytochrome b5-cytochrome P450 complex from NMR and mutagenesis data, J. Biol. Chem. 288 (2013) 22080–22095, https://doi.org/10.1074/jbc.M112.448225.
[14] K. Yamamoto, M.A. Caporini, S.C. Im, L. Waskell, A. Ramamoorthy, Transmembrane interactions of full-length mammalian bitopic cytochrome-P450-cytochrome-b5 complex in lipid bilayers revealed by sensitivity-enhanced dynamic nuclear polarization solid-state NMR spectroscopy, Sci. Rep. 7 (2017) 4116, https://doi.org/10.1038/s41598-017-04219-1.
[15] K.A. Gentry, G.M. Anantharamaiah, A. Ramamoorthy, Probing protein-protein and protein-substrate interactions in the dynamic membrane-associated ternary complex of cytochromes P450, b5, and reductase, Chem. Commun. 55 (2019) 13422–13425, https://doi.org/10.1039/C9CC05904K.
[16] P.J. Bakkes, J.L. Riehm, T. Sagadin, A. Rühlmann, P. Schubert, S. Biemann, M. Girhard, M.C. Hutter, R. Bernhardt, V.B. Urlacher, Engineering of versatile redox partner fusions that support monooxygenase activity of functionally diverse cytochrome P450s, Sci. Rep. 7 (2017) 9570, https://doi.org/10.1038/s41598-017-10075-w.
[17] W. Zhang, Y. Liu, J. Yan, S. Cao, F. Bai, Y. Yang, S. Huang, L. Yao, Y. Anzai, F. Kato, L.M. Podust, D.H. Sherman, S. Li, New reactions and products resulting from alternative interactions between the P450 enzyme and redox partners, J. Am. Chem. Soc. 136 (2014) 3640–3646, https://doi.org/10.1021/ja4130302.
[18] T. Sagadin, J.L. Riehm, M. Milhim, M.C. Hutter, R. Bernhardt, Binding modes of CYP106A2 redox partners determine differences in progesterone hydroxylation product patterns, Commun. Biol. 1 (2018) 99, https://doi.org/10.1038/s42003-018-0104-9.
[19] S. Tripathi, H. Li, T.L. Poulos, Structural basis for effector control and redox partner recognition in cytochrome P450, Science 340 (2013) 1227–1230, https://doi.org/10.1126/science.1235797.
[20] S.A. Hollingsworth, D. Batabyal, B.D. Nguyen, T.L. Poulos, Conformational selectivity in cytochrome P450 redox partner interactions, Proc. Natl. Acad. Sci. 113 (2016) 8723–8728, https://doi.org/10.1073/pnas.1606474113.
[21] E.A. Thompson, P.K. Siiteri, The involvement of human placental microsomal cytochrome P-450 in aromatization, J. Biol. Chem. 249 (1974) 5373–5378.
[22] E.A. Thompson, P.K. Siiteri, Utilization of oxygen and reduced nicotinamide adenine dinucleotide phosphate by human placental microsomes during aromatization of androstenedione, J. Biol. Chem. 249 (1974) 5364–5372.
[23] E.R. Simpson, M.S. Mahendroo, G.D. Means, M.W. Kilgore, M.M. Hinshelwood, S. Graham-Lorence, B. Amarneh, Y. Ito, C.R. Fisher, M.D. Michael, C.R. Mendelson, S.E. Bulun, Aromatase cytochrome P450, the enzyme responsible for estrogen biosynthesis, Endocr. Rev. 15 (1994) 342–355, https://doi.org/10.1210/edrv-15-3-342.
[24] A. Brodie, G. Sabnis, D. Jelovac, Aromatase and breast cancer, J. Steroid Biochem. Mol. Biol. 102 (2006) 97–102, https://doi.org/10.1016/j.jsbmb.2006.09.002.
[25] R.J. Santen, H. Brodie, E.R. Simpson, P.K. Siiteri, A. Brodie, History of aromatase: saga of an important biological mediator and therapeutic target, Endocr. Rev. 30 (2009) 343–375, https://doi.org/10.1210/er.2008-0016.
[26] D. Ghosh, J. Griswold, M. Erman, W. Pangborn, Structural basis for androgen specificity and oestrogen synthesis in human aromatase, Nature 457 (2009) 219–223, https://doi.org/10.1038/nature07614.
[27] D. Ghosh, J. Lo, D. Morton, D. Valette, J. Xi, J. Griswold, S. Hubbell, C. Egbuta, W. Jiang, J. An, H.M.L. Davies, Novel aromatase inhibitors by structure-guided design, J. Med. Chem. 55 (2012) 8464–8476, https://doi.org/10.1021/jm300930n.
[28] J. Lo, G. Di Nardo, J. Griswold, C. Egbuta, W. Jiang, G. Gilardi, D. Ghosh, Structural basis for the functional roles of critical residues in human cytochrome P450 aromatase, Biochemistry 52 (2013) 5821–5829, https://doi.org/10.1021/bi400669h.
[29] G. Di Nardo, G. Gilardi, Human aromatase: perspectives in biochemistry and biotechnology, Biotechnol. Appl. Biochem. 60 (2013) 92–101, https://doi.org/10.1002/bab.1088.
[30] G. Di Nardo, M. Breitner, A. Bandino, D. Ghosh, G.K. Jennings, J.C. Hackett, G. Gilardi, Evidence for an elevated aspartate pKa in the active site of human aromatase, J. Biol. Chem. 290 (2015) 1186–1196, https://doi.org/10.1074/jbc.M114.595108.
[31] R. Baravalle, G. Di Nardo, A. Bandino, I. Barone, S. Catalano, S. Andò, G. Gilardi, Impact of R264C and R264H polymorphisms in human aromatase function, J. Steroid Biochem. Mol. Biol. 167 (2017) 23–32, https://doi.org/10.1016/j.jsbmb.2016.09.022.
[32] D. Ghosh, C. Egbuta, J. Lo, Testosterone complex and non-steroidal ligands of human aromatase, J. Steroid Biochem. Mol. Biol. 181 (2018) 11–19, https://doi.org/10.1016/j.jsbmb.2018.02.009.
[33] C.D. Sohl, F.P. Guengerich, Kinetic analysis of the three-step steroid aromatase reaction of human cytochrome P450 19A1, J. Biol. Chem. 285 (2010) 17734–17743, https://doi.org/10.1074/jbc.M110.123711.
[34] R. Baravalle, A. Ciaramella, F. Baj, G. Di Nardo, G. Gilardi, Identification of endocrine disrupting chemicals acting on human aromatase, Biochim. Biophys. Acta BBA Proteins Proteomics. 1866 (2018) 88–96, https://doi.org/10.1016/j.bbapap.2017.05.013.
[35] X. Yu, V. Cojocaru, R.C. Wade, Conformational diversity and ligand tunnels of mammalian cytochrome P450s, Biotechnol. Appl. Biochem. 60 (2013) 134–145, https://doi.org/10.1002/bab.1074.
[36] W. Jiang, D. Ghosh, Motion and flexibility in human cytochrome P450 aromatase, PLoS One 7 (2012), e32565. https://doi.org/10.1371/journal.pone.0032565.
[37] A. Magistrato, J. Sgrignani, R. Krause, A. Cavalli, Single or multiple access channels to the CYP450s active site? An answer from free energy simulations of the human aromatase enzyme, J. Phys. Chem. Lett. 8 (2017) 2036–2042, https://doi.org/10.1021/acs.jpclett.7b00697.
[38] G. Di Nardo, G. Cimicata, R. Baravalle, V. Dell'Angelo, A. Ciaramella, G. Catucci, P. Ugliengo, G. Gilardi, Working at the membrane interface: ligand-induced changes in dynamic conformation and oligomeric structure in human aromatase, Biotechnol. Appl. Biochem. 65 (2018) 46–53, https://doi.org/10.1002/bab.1613.
[39] G. Di Nardo, M. Breitner, S.J. Sadeghi, S. Castrignanò, G. Mei, A. Di Venere, E. Nicolai, P. Allegra, G. Gilardi, Dynamics and flexibility of human aromatase probed by FTIR

and time resolved fluorescence spectroscopy, PLoS One 8 (2013), e82118. https://doi.org/10.1371/journal.pone.0082118.

[40] F.P. Guengerich, C.J. Wilkey, T.T.N. Phan, Human cytochrome P450 enzymes bind drugs and other substrates mainly through conformational-selection modes, J. Biol. Chem. 294 (2019) 10928–10941, https://doi.org/10.1074/jbc.RA119.009305.

[41] F.P. Guengerich, C.J. Wilkey, S.M. Glass, M.J. Reddish, Conformational selection dominates binding of steroids to human cytochrome P450 17A1, J. Biol. Chem. 294 (2019) 10028–10041, https://doi.org/10.1074/jbc.RA119.008860.

[42] T. Omura, R. Sato, The carbon monoxide-binding pigment of liver microsomes: I. Evidence for its hemoprotein nature, J. Biol. Chem. 239 (1964) 2370–2378.

[43] T.D. Porter, T.E. Wilson, C.B. Kasper, Expression of a functional 78,000 dalton mammalian flavoprotein, NADPH-cytochrome P-450 oxidoreductase, in Escherichia coli, Arch. Biochem. Biophys. 252 (1987) 353–367, https://doi.org/10.1016/0003-9861(87)90111-1.

[44] S. Gianni, J. Dogan, P. Jemth, Distinguishing induced fit from conformational selection, Biophys. Chem. 189 (2014) 33–39, https://doi.org/10.1016/j.bpc.2014.03.003.

[45] A.D. Vogt, E. Di Cera, Conformational selection or induced fit? A critical appraisal of the kinetic mechanism, Biochemistry 51 (2012) 5894–5902, https://doi.org/10.1021/bi3006913.

[46] C. Barnaba, E. Taylor, J.A. Brozik, Dissociation constants of cytochrome P450 2C9/cytochrome P450 reductase complexes in a lipid bilayer membrane depend on NADPH: a single-protein tracking study, J. Am. Chem. Soc. 139 (2017) 17923–17934, https://doi.org/10.1021/jacs.7b08750.

[47] C. Barnaba, M.J. Martinez, E. Taylor, A.O. Barden, J.A. Brozik, Single-protein tracking reveals that NADPH mediates the insertion of cytochrome P450 reductase into a biomimetic of the endoplasmic reticulum, J. Am. Chem. Soc. 139 (2017) 5420–5430, https://doi.org/10.1021/jacs.7b00663.

[48] W.C. Huang, J. Ellis, P.C.E. Moody, E.L. Raven, G.C.K. Roberts, Redox-linked domain movements in the catalytic cycle of cytochrome P450 reductase, Structure 21 (2013) 1581–1589, https://doi.org/10.1016/j.str.2013.06.022.

[49] M.J.I. Paine, N.S. Scrutton, A.W. Munro, A. Gutierrez, G.C.K. Roberts, C. Roland Wolf, Electron transfer partners of cytochrome P450, in: P.R. Ortiz de Montellano (Ed.), Cytochrome P450: Structure, Function, and Biochemistry, Kluwer Academic/Plenum Publishers, New York 2005, pp. 115–148.

[50] B. Louerat-Oriou, A. Perret, D. Pompon, Differential redox and electron-transfer properties of purified yeast, plant and human NADPH-cytochrome P-450 reductases highly modulate cytochrome P-450 activities, Eur. J. Biochem. 258 (1998) 1040–1049, https://doi.org/10.1046/j.1432-1327.1998.2581040.x.

[51] T. Abraham, R.N.A.H. Lewis, R.S. Hodges, R.N. McElhaney, Isothermal titration calorimetry studies of the binding of a rationally designed analogue of the antimicrobial peptide gramicidin s to phospholipid bilayer membranes, Biochemistry 44 (2005) 2103–2112, https://doi.org/10.1021/bi048077d.

[52] E.O. Yablokov, T.A. Sushko, P.V. Ershov, A.V. Florinskaya, O.V. Gnedenko, T.V. Shkel, I.P. Grabovec, N.V. Strushkevich, L.A. Kaluzhskiy, S.A. Usanov, A.A. Gilep, A.S. Ivanov, A large-scale comparative analysis of affinity, thermodynamics and functional characteristics of interactions of twelve cytochrome P450 isoforms and their redox partners, Biochimie 162 (2019) 156–166, https://doi.org/10.1016/j.biochi.2019.04.020.

[53] I. Ritacco, A. Saltalamacchia, A. Spinello, E. Ippoliti, A. Magistrato, All-atom simulations disclose how cytochrome reductase reshapes the substrate access/egress routes of its partner CYP450s, J. Phys. Chem. Lett. 11 (2020) 1189–1193, https://doi.org/10.1021/acs.jpclett.9b03798.

[54] G.F. Cawley, C.J. Batie, W.L. Backes, Substrate-dependent competition of different P 450 isoenzymes for limiting NADPH-cytochrome P 450 reductase, Biochemistry 34 (1995) 1244–1247, https://doi.org/10.1021/bi00004a018.

Chapter 4

Molecular and Structural Evolution of Cytochrome P450 Aromatase

International Journal of
Molecular Sciences

MDPI

Article

Molecular and Structural Evolution of Cytochrome P450 Aromatase

Giovanna Di Nardo *, Chao Zhang, Anna Giulia Marcelli and Gianfranco Gilardi *

Department of Life Sciences and Systems Biology, University of Torino, via Accademia Albertina 13, 1023 Torino, Italy; chao.zhang@unito.it (C.Z.); anna.marcelli@edu.unito.it (A.G.M.)
* Correspondence: giovanna.dinardo@unito.it (G.D.N.); gianfranco.gilardi@unito.it (G.G.)

Abstract: Aromatase is the cytochrome P450 enzyme converting androgens into estrogen in the last phase of steroidogenesis. As estrogens are crucial in reproductive biology, aromatase is found in vertebrates and the invertebrates of the genus *Branchiostoma*, where it carries out the aromatization reaction of the A-ring of androgens that produces estrogens. Here, we investigate the molecular evolution of this unique and highly substrate-selective enzyme by means of structural, sequence alignment, and homology modeling, shedding light on its key role in species conservation. The alignments led to the identification of a core structure that, together with key and unique amino acids located in the active site and the substrate recognition sites, has been well conserved during evolution. Structural analysis shows what their roles are and the reason why they have been preserved. Moreover, the residues involved in the interaction with the redox partner and some phosphorylation sites appeared late during evolution. These data reveal how highly substrate-selective cytochrome P450 has evolved, indicating that the driving forces for evolution have been the optimization of the interaction with the redox partner and the introduction of phosphorylation sites that give the possibility of modulating its activity in a rapid way.

Keywords: cytochrome P450; aromatase; estrogens; molecular evolution; structural alignment; substrate recognition sites; conservation

Citation: Di Nardo, G.; Zhang, C.; Marcelli, A.G.; Gilardi, G. Molecular and Structural Evolution of Cytochrome P450 Aromatase. *Int. J. Mol. Sci.* **2021**, *22*, 631. https://doi.org/10.3390/ijms22020631

Received: 21 December 2020
Accepted: 7 January 2021
Published: 10 January 2021

1. Introduction

Aromatase is the enzyme that converts androgens into estrogens through a three-step reaction that allows the aromatization of the A-ring of the steroid molecule [1,2]. The enzyme belongs to the cytochrome P450 (P450s) superfamily that comprises thousands of enzymes involved in the metabolism of endogenous and exogenous substrates [3–5]. The origin of such a large number of enzymes is still controversial, even though the presence of a common ancient precursor, CYP51 (lanosterol 14alpha-demethylase), for both prokaryotes and eukaryotes has been hypothesized [6].

The P450 superfamily is composed of two groups of enzymes. Depending on their substrate recognition abilities, one group comprises P450s that catalyze specific reactions on specific endogenous substrates; a second group includes enzymes that have evolved towards broad substrate selectivity, usually employed for xenobiotic metabolism, as in the case of mammalian liver proteins. While for the second group, it can be hypothesized that evolution has widened their substrate selectivity, for the first one, it is not clear how molecular evolution has worked.

Aromatase belongs to the first group as it carries out the conversion of androgens into estrogens across different classes of living organisms. From an evolutionary point of view, its gene and activity have been found in invertebrates of the genus *Branchiostoma*, belonging to cephalochordates [7]. Indeed, aromatase, together with other P450 enzymes involved in steroidogenesis, have been found in the gonads of the invertebrate *Branchiostoma belcheri*, which is considered to be evolutionarily closer to vertebrates than other invertebrates [8,9].

The enzyme is present in all vertebrates as the product of expression of a single gene, with some exceptions represented by pigs and teleosts, where duplication events have produced three and two isoforms, respectively [10–13]. Furthermore, the protein is expressed in different tissues in vertebrates, where it plays an essential role in reproductive biology as estrogens are responsible for ovarian differentiation, development of the reproductive system, sex differentiation, and reproduction [14]. Moreover, a critical role of estrogens has also been demonstrated in brain, bone, skin, fat, and cardiovascular tissues [15–20]. In humans, tissue-specific regulation of aromatase gene expression is allowed by the presence of eleven promoters and alternative first exons [21]. However, a wide tissue distribution of the aromatase protein and a complex regulatory region in its gene is already present in fishes [22].

Vertebrates have been used as models to understand the roles of aromatase and estrogens in the different tissues where it is expressed. For example, in birds and mammals, it has been demonstrated that in the brain, there is a rapid modulation of aromatase activity through phosphorylation and that estrogens can be considered neurotransmitters [23]. Moreover, estrogens are involved in different processes, such as neurogenesis, neuroprotection, and cognition [22,24].

In reptiles and amphibians, temperature regulates aromatase expression and is responsible for temperature-dependent sex determination [25–27]. In some hermaphrodite fishes, sex changes occur in response to environmental cues related to social interactions, and aromatase is involved in the remodeling of the gonads during this process [28,29]. Due to the phenotypic effects as a consequence of androgen/estrogen unbalance, amphibians and fishes are widely used as model organisms to understand the possible effect of many compounds that also target human aromatase [30,31], known as endocrine-disrupting chemicals (EDCs) [32,33].

Among fishes, teleosts represent the only case where two isoforms are present (CYP19A1 and CYP19B1), and they are preferentially expressed in the gonads and brain, respectively. Interestingly, these isoforms have also been reported to have different catalytic activity in comparison to the human enzyme [34,35], indicating that functional differences can be present. Thus, it is interesting to understand the phylogenetic origins of these differences.

In this work, comparative sequence and structural analysis are used to investigate if and how the substrate-selective nature of aromatase has evolved, both in structural and functional terms. Its highly substrate-selective nature, calibrated for catalysis on androgens, makes it an optimal candidate for evolutionary studies, with the aim of (1) understanding if and how molecular evolution has structurally optimized this enzyme in order to make it more efficient and (2) determining what the conserved structural scaffold is and which are the amino acids that are essential for its function. Moreover, by identifying the functional amino acids that have not changed during evolution and excluding the ones shared with the other P450s, it is possible to obtain the fingerprint sequences of this enzyme. Structural analysis also allows us to identify a possible role for these residues and the rational basis for conservation. The most different aromatase sequences were also subjected to homology modeling to visualize where evolution has structurally modified the enzyme.

2. Results

2.1. Multiple Sequence Alignment

2.1.1. Structural Conservation

In order to identify the most conserved structural elements in aromatase, 365 sequences, ranging from invertebrates to mammals, were used for multiple sequence alignment. Out of the 365 sequences aligned, 66 were from mammals, 8 from birds, 12 from reptiles, 18 from amphibians, 259 from fishes, and 2 from the invertebrates of the genus *Branchiostoma*.

For all the analyses performed in this work, the residue numbers refer to the sequence of human aromatase (CYP19A1, Uniprot ID P11511).

When the positions of the most conserved regions were analysed in the crystal structure of the human enzyme, they resulted as part of helix A (65–78), the β-sheet formed by strands β1 (83–88) and β2 (93–97), helix E (187–205), part of helix F (221–224), the central part of helix I (residues 302–318 in human aromatase), helix K (354–366), the K-β3 loop and the β3 strand (368–376), the β6 strand (393–396), and helix L and part of the L-K" loop (427–448) (Figure 1). Helices C, D, F, and H carry conserved amino acids oriented toward the core of the protein and nonconserved amino acids exposed to the solvent. Thus, the conserved structural core in cytochrome P450 is formed by a four-helix bundle formed by helices D, E, I, and L that is conserved among aromatase sequences; an exception is made for the residues of helix D, exposed to the solvent (Figure 1) [36]. Helix G is not conserved, whereas the F-G loop and the first part of helix F, known to be important for opening the access channel in cytochrome P450, are conserved.

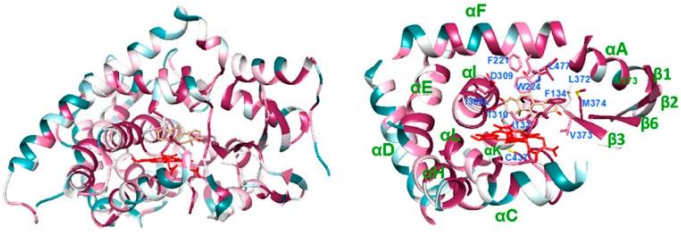

(**a**) (**b**)

Figure 1. Crystal structure of human aromatase (PDB ID 4KQ8), colored according to the conservation. The violet areas correspond to the more conserved regions, whereas the dark green ones correspond to the most variable. Heme is shown in red and the substrate androstenedione in light brown. (**a**) Overall structure of human aromatase. (**b**) The core structure of aromatase, carrying the most conserved regions. The residues important for substrate binding are also shown.

The key cysteine residue coordinating heme iron is obviously conserved in all the sequences, and it is within a consensus sequence formed by FGFGPRX_1CX_2GK/R, where X_1 is variable (G, A, S, T, or N) whereas X_2 is A, V, L, or I. This consensus sequence is also well-conserved in cytochrome P450 (FXXGX(H/R)XCXG), together with the meander region, a loop preceding the cysteine residue [36], which is also well-conserved in most aromatase sequences.

The three Arg residues involved in salt bridges with heme propionyl groups (R115, R145, and R435 in human aromatase) are also present in all the sequences, together with Trp141, and are involved in an H-bond with the heme propionyl group.

A highly conserved motif in cytochrome P450 is the EX_1X_2R motif located in helix K and involved in salt bridge interactions that are important for its tertiary structure and the correct incorporation of the heme cofactor [36]. This motif is conserved in all sequences; X_1 is a serine residue, whereas X_2 is L or M in most aromatase sequences.

2.1.2. Functional Conservation

The level of conservation of amino acids that are relevant for substrate binding and catalysis was then verified in the multiple alignments. A highly conserved alcohol–acid pair is present on helix I in cytochrome P450, and it is part of the proton relay network that allows the formation of the reactive intermediate (Compound I) in the catalytic cycle. In aromatase, the alcohol–acid pair is formed by an aspartic acid residue (D309 in human aromatase) and a threonine residue (T310) that are conserved (exception is made for two fish sequences), and they are preceded by a proline residue (P308) in all the sequences analyzed. When compared to other P450s, this proline residue is unique to aromatase, and it is responsible for the shift of the I-helix axis observed in the crystal structure of the human enzyme [37]. Such a shift is important as it allows the 3-keto moiety of the

substrate androstenedione to be accommodated near the fifth turn of the I-helix that is formed by M303 and A307. These two residues are conserved, with some exceptions. The methionine is substituted by an isoleucine in five fish sequences, one amphibian sequence, and one mammal sequence; there is an alanine residue that is a glycine residue in 4.5% of fish sequences and in two invertebrates. Moreover, the shift of the I-helix allows the formation of a hydrogen bond between D309 and the 3-keto oxygen of the substrate. Such an aspartic acid residue has never been changed into a glutamic acid during evolution due to its important role in substrate binding and catalysis [38]. All these residues (303–310) are located on helix I, and they are part of one of six substrate recognition sites (SRSs), namely, SRS-4. The residues involved in androstenedione binding are highly conserved, with some exceptions represented by few fish sequences (Table 1).

Table 1. Conservation of the residues involved in substrate binding and catalysis in human aromatase. The scores are normalized so that the average score for all residues is zero and the standard deviation is one. The lowest score represents the most conserved position in a protein. For reference, the lowest score associated with a fully conserved residue was −1.103, whereas the highest score obtained for a nonconserved residue in human aromatase was +2.844.

Residue	Location	Conservation Score	Notes
C437	K″-L helix loop	−1.095	
I305	I-helix	−0.936	L/V only in invertebrate *Branchiostoma*
A306	I-helix	−1.002	T in the mammal *Capra hircus*
D309	I-helix	−1.058	Q in CYP19B1 of the fish *Halichoeres tenuispinis*
T310	I-helix	−1.011	I in the fish *Maylandia zebra*
F221	F-helix	−0.805	
W224	F-helix	−0.896	
I133	B-C loop	−1.038	M in pig aromatase isoform 3
F134	B-C loop	−1.073	
V370	K-helix—β3 loop	−1.001	
L372	K-helix—β3 loop	−0.202	Phe in fishes
V373	K-helix—β3 loop	−0.583	S/ T in most fishes and in CYP19A1 of zebrafish and goldfish
M374	β3	−1.031	
L477	β8–β9 loop	−1.011	
S478	β8–β9 loop	−0.828	A in many sequences, starting from mammals to amphibians. S in fishes.
R192	Helix E	−0.974	C or H in some mammals, birds and fishes, including the two isoforms of zebrafish
E483	β9–β10 loop	−0.761	Conserved in the two isoforms of zebrafish and goldfish

Two other residues are important for aromatase function; they are predicted to be part of the proton relay network that allows the formation of the reactive Compound I in the typical P450 catalytic cycle: R192 and E483. These residues form a salt bridge in the same position as the one found in the crystal structure of the bacterial cytochrome P450cam [39]. The residues R192 and E483 are highly conserved, starting from the sequences of aromatase from invertebrates. The crystal structure of the bacterial camphor-hydroxylating P450cam from *Pseudomonas putida* shows that this salt bridge is broken when the P450cam interacts with the redox partner that stabilizes the open conformation of the enzyme, exerting an effector role [39–41]. For human aromatase, the redox partner cytochrome P450 reductase (CPR) has been shown to promote substrate binding, acting as an effector [42], and the

presence of the R192-E483 salt bridge in the same structural position as P450cam suggests that a similar effect can be exerted by its redox partner CPR.

2.1.3. Conservation of the Substrate Recognition Sites (SRSs)

Six regions have been identified to be important for substrate recognition and binding in P450s: these are the so-called substrate recognition sites (SRSs). They are considered to be the most variable regions among cytochrome P450 as their variation during evolution is associated with new substrate selectivity. According to this idea, it is expected that the SRSs of aromatase, a nonpromiscuous enzyme that is highly selective for androgen substrates, have been highly conserved during evolution. Thus, the level of conservation of the six SRSs was checked and is shown in Table S1. As it can be seen, SRS-4 is the most highly conserved one (69.7% of the amino acids are conserved) as it carries amino acids crucial for catalysis, whereas SRS-3 has been highly variable during aromatase evolution (15.4% of conserved amino acids). In the other SRSs, about 40% of the amino acids are conserved.

As mentioned before, some residues in SRSs are shared in all P450s as they are essential for their catalysis. For example, in SRS-4, the acid–alcohol pair is not unique for aromatase as it is part of the proton relay network that allows the formation of reactive intermediates. Thus, in order to identify the residues that are conserved and unique for aromatase in the SRSs, multiple structural alignments of the 57 human P450s were performed using the server PROMALS3D. For structural alignment, the server uses the crystal structures available; their PDB IDs are used as input. When the structures are not available, the input sequences are aligned after secondary structure prediction, and 3D structure constraints are assigned based on homolog structures [43]. The multiple alignments obtained were then evaluated by the ConSurf server to assign a conservation score for each amino acid position.

Table S2 shows the residues belonging to the six SRSs in aromatase and the corresponding conservation score obtained from the alignment of the 363 sequences analyzed. Moreover, it shows the conservation score for the same positions obtained from the alignment with all the other human P450s. This comparison was performed to identify the residues conserved in the SRSs of all the human enzymes (shown in green in Table S2) and the ones specific for aromatase (shown in red in Table S2).

In SRS-1, helix C carries a Trp residue (W141 in aromatase) that is an aromatic amino acid in all P450s, important for heme binding. In many of them, it is followed by a positively charged residue (present in all CYP2, CYP3, and CYP26 members). R145 is conserved in most P450s as it is involved in heme binding, and the last two residues are small hydrophobics in many of them. K150/A151 are conserved and specific for aromatase. The helix B region is highly variable in human P450s. In aromatase, M127 is conserved as it delineates the active site cavity, whereas N135 is part of an H-bond network also involving R435, important for heme binding. The role of N135 is important as it bridges G131 and N137, keeping the B-C loop in a conformation that allows the highly conserved I133 and F134 to be part of the active site and to contact the substrate (Figure 2a).

SRS-2 is highly variable in P450s, and it carries conserved residues in aromatase. They are located on helix F and on the F-G loop. They are important flexible elements in P450s, including aromatase [44], as they are involved in the conformational changes that allow ligand access to the active site [45]. Out of them, Tyr220 forms an important H-bond with N295 that is part of SRS-4 and, with I125, defines the substrate access channel (Figure 2b).

In SRS-3, the cluster of three basic residues is not specific for aromatase as it is present in all CYP4F members, CYP46A1, and, within the same helix (helix G), CYP51. Interestingly, a glutamic acid is present before the cluster in all CYP4F members. EK is also present in some CYP26/27 members. Interesting, all these P450 families are involved in steroid, leukotriene, and retinoic and fatty acid processing [46–50].

SRS-4 and SRS-5 are the most conserved in human P450s. However, there are residues specific for aromatase, including I305 and M374, that are involved in substrate binding. In SRS5, the consensus sequence XEXXR is well conserved.

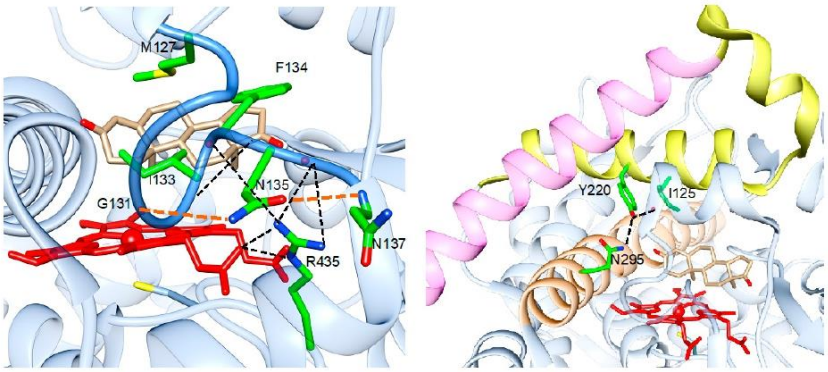

(**a**) (**b**)

Figure 2. Role of the highly conserved residues in human aromatase (PDB ID 4KQ8). (**a**) Involvement of the highly conserved N135 in bridging G131 and N137 via H-bonds (shown in orange), which is important to maintain the B-C loop (blue) conformation and provide M127 and F134 to the active site of the protein. The H-bond network is shown in black. (**b**) Involvement of the highly conserved Y220 in H-bonds that connect N295 and I125. N295 is part of SRS-4, shown in orange, Y220 is part of SRS-2, shown in yellow, and SRS-3 is shown in magenta.

SRS-6 carries two His residues that are conserved in aromatase sequences that are part of a β-hairpin, whereas the other residues are not conserved.

2.1.4. Consensus Sequence for Post-Translational Modifications

Post-translational modifications on human aromatase have been reported to alter its activity [51–54].

The region between amino acids 262 and 268 is a consensus sequence for different kinases such as PKA (R-X_{1-2}-S/T-X) and PKG ((R/K)$_{2-3}$-X-S/T-X). In human aromatase, the sequence is KRRRIST, where a cluster of four basic residues gives a positively charged patch on the surface that can attract opposite charges. However, only K and the first R are highly conserved, whereas the S and T residues are not conserved in fishes and the two invertebrate sequences (Figure 3). This means that the consensus sequence for PKA is present starting from amphibians. On the other hand, the consensus for PKG that includes two or three basic residues is present in only 15% of mammal aromatase sequences.

The other residue reported to be phosphorylated is S118, which is very well conserved, together with an arginine residue presenting two amino acids before (R116). The only exceptions are represented by six aromatase sequences from fishes and the two from invertebrates where serine is substituted by N or D (Figure 3). Thus, this consensus sequence for PKA is present starting from vertebrates.

The other important residue known to be phosphorylated is Y361. This residue is present in most mammal sequences (83%) and appears in amphibians, where it is present in 75% of the sequences. In mammals, where it is not present, it is substituted by N, as in most fishes, where a tyrosine residue is found only in 2.8% of the sequences analyzed (Figure 3).

2.1.5. Interaction with the Redox Partner

The interaction of P450s with their redox partner is crucial for their function and catalytic efficiency. The docking site of cytochrome P450 reductase (CPR) and the P450 enzyme is the proximal side, and it is mainly triggered by electrostatic interactions between the positively charged surface of P450s and the negatively charged surface of CPR [55–57].

For aromatase, many basic residues have been identified and suggested to be involved in the interaction with CPR by site-directed mutagenesis experiments [58] and computational studies [59–61]. The conservation of these residues was checked in the multiple alignments, and the results are shown in Table 2. The conservation score is included for each position, together with the result of the visual analysis that allows us to identify the sequences where the amino acids are not conserved.

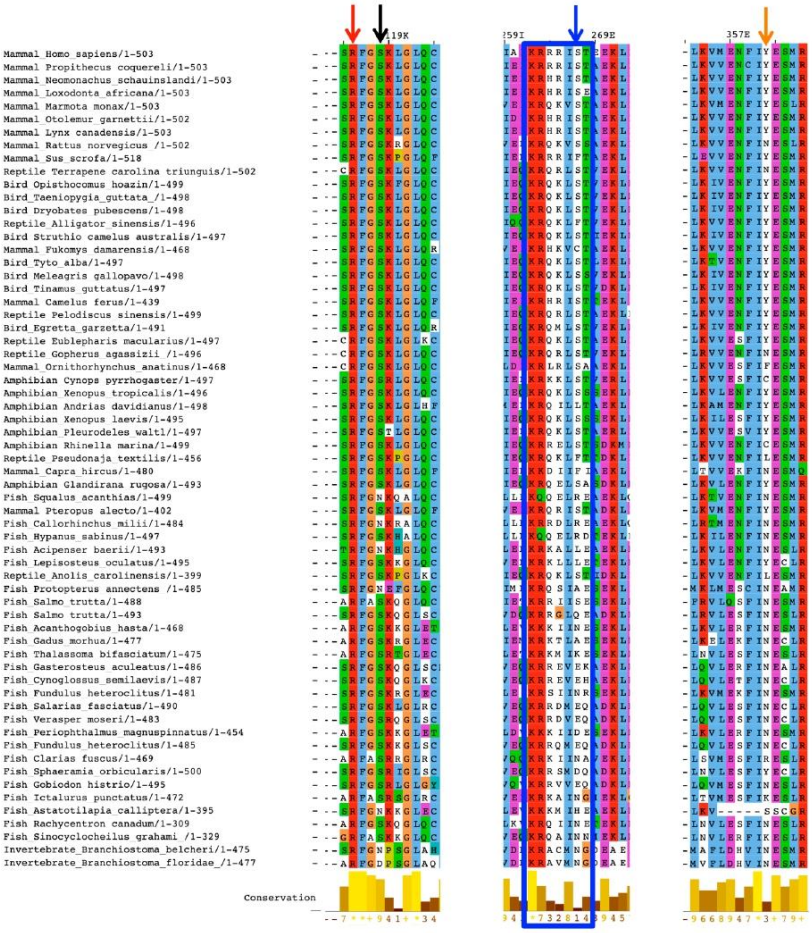

Figure 3. Multiple sequence alignments showing only representative aromatase sequences from the different classes of vertebrates and the two invertebrates. The three regions shown are the ones carrying the phosphorylation sites: S118 is indicated by the black arrow, and R116, which forms the consensus for PKA, is indicated by the red arrow. S267 is indicated by the blue arrow, and the cluster KRRIST, present on human aromatase, is shown in the blue box. Y361 is indicated by the orange arrow.

Table 2. Conservation of the residues involved in the interaction with the redox partner in human aromatase. The scores are normalized, so that the average score for all residues is zero and the standard deviation is one. The lowest score represents the most conserved position in a protein. For reference, the lowest score associated with a fully conserved residue was −1.103, whereas the highest score obtained for a nonconserved residue in human aromatase was +2.844.

Residue	Conservation Score	Notes
K99	0.287	R in most fishes and *Branchiostoma floridae*, not conserved in 1 amphibian, 1 reptile, in 15% of fishes and *Branchiostoma belcheri* (S)
K108	−0.024	Always substituted by R
R145	−0.972	Well conserved
K352	1.293	Conserved only in mammals
K389	0.767	Not conserved in invertebrates (P) and 70% of fishes (including only isoform CYP19A1 in zebrafish)
K390	−0.231	K or R
K420	0.472	Not conserved in two mammals, 20% of fishes (including CYP19B1 of zebrafish) and E in invertebrates
R425	−0.881	Well conserved with some exceptions in fishes and the invertebrates (T)
K440	−0.897	R in invertebrates
S153	−0.533	T in invertebrates and most fishes
Q351	0.799	Conserved in 90% of mammals
Y424	0.308	Conserved in mammals
Y441	−0.553	Conserved in mammals and amphibians, H in 97% of fishes and T in invertebrates

Out of the nine basic residues that form the positively charged proximal site (Figure S1), six are conserved as their mutation, when present, is conservative. The other three residues appear during evolution at different times, as K352 is conserved in mammals and K389 and K420 are well-conserved starting from amphibians. Concerning the four residues predicted to form hydrogen bonds with CPR, two of them are conserved, and, interestingly, Q351 and Y424 are conserved only in mammals.

These data indicate that a patch of basic amino acids had already appeared in invertebrates, and it has been highly conserved during evolution. However, other residues were introduced later; these comprise the amino acids that reinforce the positively charged proximal site as well as two residues that protrude from the proximal site of the enzyme (Figure S1) to form H-bonds with the redox partner. These data suggest that the interaction with the redox partner has been one of the driving forces for evolution in aromatase.

2.2. Homology Modeling of Evolutionarily Old Aromatase

Based on the sequence alignment, homology modeling was applied to two aromatase sequences as it was found that they carry significant insertions, in addition to mutations, in key positions.

The invertebrate aromatase sequence from *Branchiostoma floridae* was selected as it shows an amino acid insertion, 40% of identity, and 60% of homology with the human one. Thus, a homology model was built to study where the main differences between the two aromatase enzymes are located.

A six-amino-acid insertion is present in the invertebrate sequence compared to all the other sequences analyzed (between M276 and D277 in human aromatase), and the model shows that such an insertion elongates the loop connecting helices H′ and the H loop (Figure 4). Moreover, the analysis of the location of the substitutions shows that they are all on the protein surface and on structural elements such as helix G, which are the least

conserved ones in aromatase. There are no mutations in the core structure of the protein and the active site, indicating that the main structural scaffold of aromatase was already present in this old protein. Moreover, many mutations are located in the SRSs, indicating that these areas have evolved in vertebrates.

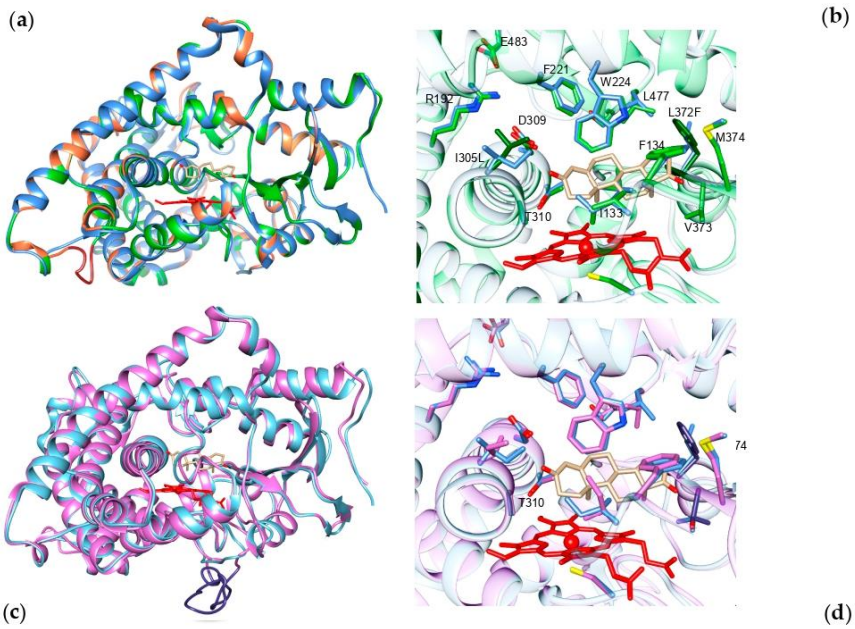

Figure 4. Homology models of evolutionarily old aromatase. (**a**) Homology model for aromatase from the invertebrate *Branchiostoma floridae* (green) superimposed onto the crystal structure of human aromatase (blue). The nonconserved regions are shown in orange, and the grey shadow shows the location of the insertion. (**b**) Zoomed-in view of the active site showing the conserved (green) and nonconserved residues (dark green) involved in substrate binding and catalysis. (**c**) Homology model for aromatase from the pufferfish *Takifugu rubripes* (magenta) superimposed to the crystal structure of human aromatase (blue). The grey shadow shows the location of the long insertion (violet). (**d**) Zoomed-in view of the active site showing the conserved (magenta) and nonconserved residues (dark purple) involved in substrate binding and catalysis. Heme is shown in red and the substrate androstenedione in light brown.

The multiple sequence alignment also shows the presence of some important mutations together with a long insertion in aromatase from some fish species, including the one from pufferfish *Takifugu rubripes*. In this case, the fish sequence shares 52% of identity and 70% of homology with the human one. A homology model was built in order to predict the possible effect of the substitutions found in the active site. Figure 4 shows the model carrying a long insertion between N421 and V422, which corresponds to the loop connecting helix K" and helix L.

Since this long insertion is modeled as a long loop, secondary structure prediction tools were used to verify a possible elongation of the K" helix. However, both PsiPred and I-Tasser servers did not predict any secondary structure formation for the amino acids present in that loop. Such a result justifies the absence of such a long and not-necessary loop in the other aromatase sequences.

Concerning the active site, while the substitution of L372 with a phenylalanine does not seem to affect the polarity and dimensions of the catalytic pocket, the substitution of V373 with the polar threonine residue, which in some species is a serine, can be predicted to affect the polarity of the active site (Figure 4). As the substrate carries at least two keto- (as in androstenedione) groups or one keto- group and one hydroxyl group (as in testosterone), the presence of a serine/threonine residue can be predicted to possibly affect the orientation and positioning of the substrate in the active site of the enzyme. Indeed, the Thr/Ser residue could form a hydrogen bond with the substrate. Thus, this substitution seems to be important to properly orient the substrate in the active site for efficient catalysis.

3. Discussion

Aromatase is a unique enzyme carrying out a three-step reaction on the androgen substrate, with the third step leading to the aromatization of the A-ring of the steroid molecule. This intriguing reaction has been the subject of many studies aimed at understanding the mechanism of the third aromatization step [62,63]. Moreover, the crystal structure of the human enzyme has indicated the amino acids within the protein matrix involved in substrate binding and catalysis, and their role has been confirmed by site-directed mutagenesis [64,65].

In this work, sequence and structural alignments were performed with aromatase sequences available on databases. Unfortunately, the number of sequences for the different classes of vertebrates is very different as most of the sequences are available from fishes and mammals and, therefore, a bias is introduced in the conservation score. However, we performed a qualitative analysis in order to see the effect of mutations in key positions using the conservation score as an indicator for the level of conservation.

The multiple alignment shows that the enzyme structural scaffold and the key functional residues have been highly conserved during evolution, with only few exceptions in the aromatase sequences from fishes and invertebrates. Thus, the structural core elements of the protein carrying the residues involved in substrate binding are evolutionarily old and this is reasonable as they guarantee the specific function that aromatase has in species conservation. On the other hand, while some SRSs have also been well-conserved during evolution, SRS-3 has shown the lowest level of conservation (15% of the residues are highly conserved). SRS-3 is located on helix G, a flexible element, which, together with helix F and the F-G loop, is known to be involved in the opening and closure of the access channel for the substrate. Interestingly, helix F and the F-G loop are much more conserved as they belong to SRS-2, which shows 40% of the residues to be highly conserved. Out of the conserved residues, we could identify the ones unique to aromatase, thanks to a structural alignment with the other human P450 enzymes. The data show that some conserved and unique amino acids, such as N135 and Y220, are involved in H-bond networks and have a structural role that supports the positioning of the residues involved in substrate binding in the active site.

A lower level of conservation is found in some of the amino acids that form the positively charged proximal side and in some other residues that are involved in the interaction with the redox partner through the formation of H-bonds. This finding is very interesting as CPR is shared between many P450 enzymes within the same organism. Moreover, we have recently demonstrated that human CPR has an effector role as it facilitates substrate binding by stabilizing the aromatase open conformation, which is optimal for substrate access to the active site [42]. Thus, the data suggest that one of the driving forces for evolution has been the optimization of the interface between aromatase and CPR in order to make aromatase more competitive for the same shared redox partner. Such an optimization involves the introduction of positively charged residues as well as amino acids that form H-bonds and facilitate CPR binding, which, in turn, promotes catalysis.

The other interesting finding is the poor conservation of some residues known to be involved in post-translational modifications. Phosphorylation is a rapid way to modulate enzyme activity compared to regulation at the gene level. Aromatase activity is affected

by phosphorylation, and some of the residues that can undergo this post-translational modification have been identified [51–54]. Phosphorylation of S118 has been reported to decrease aromatase activity in human cell lines [54]. The residue S118 is highly conserved in aromatase sequences from vertebrates, together with R115, which forms the consensus sequence for PKA. This consensus is missing in invertebrates and in few fish sequences (3%).

Another consensus sequence for PKA, as well as for PKG, involves S267 and/or Thr268. These residues are not present in fishes, whereas the consensus sequence for PKA is present in amphibians. On the other hand, the consensus for PKG, which includes two or three basic residues, has appeared late during evolution as it is present in only 15% of the mammal aromatase sequences. Interestingly, this consensus sequence includes R264 in human aromatase that is mutated into a Cys or His in some polymorphisms that are also reported to alter aromatase activity when used in combination with polymorphic variants of CPR [66]. Moreover, they have been associated with an increased risk for estrogen-dependent pathologies such as breast cancer and polycystic ovary syndrome [67–70].

The other residue known to be phosphorylated is Y361, which appears in amphibians but is not fully conserved even within mammals. Aromatase phosphorylation in this position has been associated with tumor progression in breast cancer cell lines [52]. Indeed, short exposure to estradiol was found to increase aromatase activity through phosphorylation of a tyrosine residue (Y361) by c-Src kinase in estrogen-dependent MCF-7 breast cancer epithelial cells. The authors hypothesized the presence of a positive nongenomic autocrine loop between estradiol and aromatase in MCF-7 breast cancer cells [52]. Moreover, it was also demonstrated that estradiol impairs the ability of the tyrosine phosphatase PTP1B to dephosphorylate aromatase, resulting in increased aromatase activity and estrogen production [71]. The multiple sequence alignment shows that the tyrosine residue in position 361, located on helix K, which is one of the most conserved structural elements in aromatase, appears in few fish species, but it is poorly conserved even among mammals, where it is substituted by an asparagine residue, as in most fishes.

Taken together, the results of the conservation of the phosphorylation sites show that evolution has introduced and is still introducing amino acids in key surface positions that can be phosphorylated and consensus sequences in order to modulate aromatase activity. Thus, the need for quickly and locally altering the estrogen concentration in cells seems to be the other driving force for the evolution of this enzyme. This finding is supported by the fact that a rapid regulation of aromatase activity is known to occur in neurons [72,73] and teleost fishes express aromatase only in glial cells, indicating that the ability to synthesize estrogens in neurons has been acquired during evolution [74,75]. In the brain, the acquisition of phosphorylable sites may be explained by the need to modulate estrogen production in higher vertebrate neurons, where rapid changes in estrogen levels, as a consequence of aromatase phosphorylation, have been associated with important physiological and behavioral responses [73].

It is interesting to note that if, on the one hand, the introduction of phosphorylation sites can be evolutionarily beneficial, as in the case of brain aromatase, on the other hand, phosphorylation of residues that increases aromatase activity can strengthen the negative effects of estrogens, as in the case of breast cancer.

In conclusion, this study on aromatase shows that molecular evolution has worked to maintain a high selectivity for a substrate-specific human cytochrome P450 such as aromatase. However, based on the mutations introduced in key sites, it has been observed that evolution has introduced residues that optimize the interaction with the redox partner and phosphorylation sites that give the possibility of rapidly modulating its activity through phosphorylation. It will be interesting to extend the study to other P450s that are highly substrate-selective to understand how molecular evolution has worked for this group of P450s.

4. Materials and Methods

4.1. Multiple Sequence and Structural Alignments

A total of 365 aromatase sequences from vertebrates and the one available from the cephalochordate *Branchiostoma* were retrieved from the Uniprot database [76] using the ConfSurf server [77] in two different searches. The first one included up to 500 sequences closest to the human aromatase sequence, with at least 40% of identity from the reference database "Clean Uniprot". The second search was performed by searching for up to 500 sequences that sample the list of homologs to the query that was the sequence of human aromatase. In this case, the minimal percentage of identity was 40%. The sequence was extrapolated from the crystal structure (PDB ID 3S79) so that the server could automatically calculate evolutionary conservation scores and map them on the aromatase structure [78]. These parameters were chosen on the basis that they allowed the retrieval of only aromatase sequences that were manually verified.

Out of the 365 sequences aligned, 66 were from mammals, 8 from birds, 12 from reptiles, 18 from amphibians, 259 from fishes, and 2 from the invertebrates of the genus *Branchiostoma*.

The sequences were aligned through the HMMER algorithm [79] and visualized and analyzed with Jalview software [80]. Position-specific conservation scores were computed using the empirical Bayesian algorithm [81]. The scores were normalized so that the average score for all residues was zero and the standard deviation was one. In aromatase, the lowest score associated with a fully conserved residue was −1.103 (N135), whereas the highest score obtained for a nonconserved residue was +2.844 (E181). The amino acid conservation output, together with the structural conservation from ConSurf server, was checked by visual inspection. Visual inspection is always needed to check correct alignment.

The substrate recognition sites (SRSs) in human aromatase were identified from a structural alignment with the crystal structure of CYP2C8 (PDB ID 2NNJ) [82] performed using the software UCSF Chimera [83]. Indeed, the SRSs were annotated [84] based on the CYP2C family [85].

Structural alignments between aromatase and all the other human P450s were performed using PROMALD3D, a multiple-structure-based alignment refined in combination with sequence constraints [43]. The alignment took into account the crystal structures available and the prediction of secondary structure elements for the unknown structures. Once structurally aligned, the conservation score was assigned using the ConSurf server.

The structural analysis of the conserved amino acids was performed using UCSF Chimera software that was also used for figure preparation [83].

4.2. Homology Modeling

Homology models were built using the software Modeller 9.25 [86], I-tasser [87], and the crystal structure of human aromatase (PDB ID 3S79, 3EQM) as a template. The best model was selected according to the Z-DOPE score, with energy minimized using Amberff14SB forcefield [88] and subjected to validation using Molprobity [89], ProSA [90], and QMEAN [91].

The homology model of aromatase from *Branchiostoma floridae* was obtained from Modeller with a Z-DOPE score of −1.0. The validation from the ProSA server showed a Z-score of −9.44 that is within the values of known 3D structures of similar length. The QMEN4 value was −2.89, and the Ramachandran plot showed that 94% were in the favored regions.

The homology model of pufferfish was first obtained from Modeller (Z-DOPE score −1.23). The long insertion was modeled as a long loop, as expected. Thus, a secondary structure prediction was carried out using the PSIPred server [92] and I-Tasser [87]. The validation from the ProSA server showed a Z-score of −7.86, which is within the values of known 3D structures of similar length, whereas the QMEAN4 value was −3.05. The Ramachandran plot showed that 94.57% of the residues were in the favored regions.

Supplementary Materials: Supplementary materials can be found at https://www.mdpi.com/1422-0067/22/2/631/s1.

Author Contributions: Conceptualization, G.D.N. and G.G.; methodology, G.D.N. and G.G.; software, G.D.N., C.Z., and A.G.M.; validation, G.D.N., C.Z., and A.G.M.; formal analysis, G.D.N., C.Z., and A.G.M.; investigation, G.D.N., C.Z., and A.G.M.; resources, G.D.N. and G.G.; data curation, G.D. and C.Z.; writing—original draft preparation, G.D.N.; writing—review and editing, G.D.N., C.Z., and G.G.; visualization, G.D.N., C.Z., and A.G.M.; supervision, G.D.N. and G.G.; project administration, G.D.N. and G.G.; funding acquisition, G.D.N. and G.G. All authors have read and agreed to the published version of the manuscript.

Funding: This research received no external funding.

Institutional Review Board Statement: Not applicable.

Informed Consent Statement: Not applicable.

Data Availability Statement: The data presented in this study are available on request from the corresponding author.

Conflicts of Interest: The authors declare no conflict of interest.

References

1. Thompson, E.A.; Siiteri, P.K. Utilization of oxygen and reduced nicotinamide adenine dinucleotide phosphate by human placental microsomes during aromatization of androstenedione. *J. Biol. Chem.* **1974**, *249*, 5364–5372. [CrossRef]
2. Simpson, E.R.; Mahendroo, M.S.; Means, G.D.; Kilgore, M.W.; Hinshelwood, M.M.; Graham-Lorence, S.; Amarneh, B.; Ito, Y.; Fisher, C.R.; Michael, M.D.; et al. Aromatase cytochrome P450, the enzyme responsible for estrogen biosynthesis. *Endocr. Rev.* **1994**, *15*, 342–355. [CrossRef] [PubMed]
3. Coon, M.J. Cytochrome P450: Nature's most versatile biological catalyst. *Annu. Rev. Pharmacol. Toxicol.* **2005**, *45*, 1–25. [CrossRef] [PubMed]
4. Guengerich, F.P. Cytochrome p450 enzymes in the generation of commercial products. *Nat. Rev. Drug. Discov.* **2002**, *1*, 359–366. [CrossRef] [PubMed]
5. Di Nardo, G.; Gilardi, G. Natural compounds as pharmaceuticals: The key role of cytochromes p450 reactivity. *Trends Biochem. Sci.* **2020**, *45*, 511–525. [CrossRef]
6. Nelson, D.R.; Goldstone, J.V.; Stegeman, J.J. The Cytochrome P450 Genesis Locus: The Origin and Evolution of Animal Cytochrome P450s. *Philos. Trans. R. Soc. Lond B Biol. Sci.* **2013**, *368*, 20120474. [CrossRef]
7. Callard, G.V.; Tarrant, A.M.; Novillo, A.; Yacci, P.; Ciaccia, L.; Vajda, S.; Chuang, G.-Y.; Kozakov, D.; Greytak, S.R.; Sawyer, S.; et al. Evolutionary origins of the estrogen signaling system: Insights from amphioxus. *J. Steroid Biochem. Mol. Biol.* **2011**, *127*, 176–188. [CrossRef]
8. Callard, G.V.; Pudney, J.A.; Kendall, S.L.; Reinboth, R. In vitro conversion of androgen to estrogen in amphioxus gonadal tissues. *Gen. Comp. Endocrinol.* **1984**, *56*, 53–58. [CrossRef]
9. Mizuta, T.; Kubokawa, K. Presence of sex steroids and cytochrome P450 genes in amphioxus. *Endocrinology* **2007**, *148*, 3554–3565. [CrossRef]
10. Kishida, M.; Callard, G.V. Distinct cytochrome P450 aromatase isoforms in zebrafish (Danio rerio) brain and ovary are differentially programmed and estrogen regulated during early development. *Endocrinology* **2001**, *142*, 740–750. [CrossRef]
11. Tchoudakova, A.; Kishida, M.; Wood, E.; Callard, G.V. Promoter characteristics of two cyp19 genes differentially expressed in the brain and ovary of teleost fish. *J. Steroid Biochem. Mol. Biol.* **2001**, *78*, 427–439. [CrossRef]
12. Conley, A.J.; Corbin, C.J.; Hughes, A.L. Adaptive evolution of mammalian aromatases: Lessons from Suiformes. *J. Exp. Zool. Part A: Ecol. Genet. Physiol.* **2009**, *311*, 346–357. [CrossRef] [PubMed]
13. Corbin, C.J.; Hughes, A.L.; Heffelfinger, J.R.; Berger, T.; Waltzek, T.B.; Roser, J.F.; Santos, T.C.; Miglino, M.A.; Oliveira, M.F.; Braga, F.C.; et al. Evolution of suiform aromatases: Ancestral duplication with conservation of tissue-specific expression in the collared peccary (Pecari tayassu). *J. Mol. Evol.* **2007**, *65*, 403–412. [CrossRef] [PubMed]
14. Hamilton, K.J.; Hewitt, S.C.; Arao, Y.; Korach, K.S. Estrogen hormone biology. *Curr. Top. Dev. Biol.* **2017**, *125*, 109–146. [CrossRef]
15. McEwen, B.S.; Milner, T.A. Understanding the broad influence of sex hormones and sex differences in the brain. *J. Neurosci. Res.* **2017**, *95*, 24–39. [CrossRef]
16. Galea, L.A.M.; Frick, K.M.; Hampson, E.; Sohrabji, F.; Choleris, E. Why estrogens matter for behavior and brain health. *Neurosci. Biobehav. Rev.* **2017**, *76*, 363–379. [CrossRef]
17. Almeida, M.; Laurent, M.R.; Dubois, V.; Claessens, F.; O'Brien, C.A.; Bouillon, R.; Vanderschueren, D.; Manolagas, S.C. Estrogens and androgens in skeletal physiology and pathophysiology. *Physiol. Rev.* **2017**, *97*, 135–187. [CrossRef]
18. Brincat, M.P.; Baron, Y.M.; Galea, R. Estrogens and the skin. *Climacteric* **2005**, *8*, 110–123. [CrossRef]
19. Knowlton, A.A.; Lee, A.R. Estrogen and the cardiovascular system. *Pharmacol. Ther.* **2012**, *135*, 54–70. [CrossRef]

20. Bernasochi, G.B.; Rupasinghe, T.T.W.; Bell, J.R.; Roessner, U.; Boon, W.C.; Delbridge, L.M.D. A novel mass spectrometric methodology facilitates quantification of testosterone and progesterone, but not estrogens in cardiac and adipose tissues. *J. Mol. Cell. Cardiol.* **2020**, *140*, 11–12. [CrossRef]
21. Wang, H.; Li, R.; Hu, Y. The alternative noncoding exons 1 of aromatase (Cyp19) gene modulate gene expression in a posttranscriptional manner. *Endocrinology* **2009**, *150*, 3301–3307. [CrossRef] [PubMed]
22. Piferrer, F.; Blázquez, M. Aromatase distribution and regulation in fish. *Fish Physiol. Biochem.* **2005**, *31*, 215–226. [CrossRef] [PubMed]
23. Cornil, C.A.; Ball, G.F.; Balthazart, J. The dual action of estrogen hypothesis. *Trends Neurosci.* **2015**, *38*, 408–416. [CrossRef] [PubMed]
24. Coumailleau, P.; Pellegrini, E.; Adrio, F.; Diotel, N.; Cano-Nicolau, J.; Nasri, A.; Vaillant, C.; Kah, O. Aromatase, estrogen receptors and brain development in fish and amphibians. *Biochim. Biophys. Acta* **2015**, *1849*, 152–162. [CrossRef] [PubMed]
25. Pieau, C.; Dorizzi, M. Oestrogens and temperature-dependent sex determination in reptiles: All is in the gonads. *J. Endocrinol.* **2004**, *181*, 367–377. [CrossRef]
26. Matsumoto, Y.; Buemio, A.; Chu, R.; Vafaee, M.; Crews, D. Epigenetic control of gonadal aromatase (cyp19a1) in temperature-dependent sex determination of red-eared slider turtles. *PLoS ONE* **2013**, *8*, e63599. [CrossRef]
27. Flament, S. Sex Reversal in Amphibians. *Sex Dev.* **2016**, *10*, 267–278. [CrossRef]
28. Nakamura, M.; Kobayashi, T.; Chang, X.-T.; Nagahama, Y. Gonadal Sex Differentiation in Teleost Fish. *J. Exp. Zool.* **1998**, *281*, 362–372. [CrossRef]
29. Sunobe, T.; Nakamura, M.; Kobayashi, Y.; Kobayashi, T.; Nagahama, Y. Aromatase immunoreactivity and the role of enzymes in steroid pathways for inducing sex change in the hermaphrodite gobiid fish Trimma Okinawae. *Comp. Biochem. Physiol.* **2005**, *141*, 54–59. [CrossRef]
30. Baravalle, R.; Ciaramella, A.; Baj, F.; Di Nardo, G.; Gilardi, G. Identification of endocrine disrupting chemicals acting on human aromatase. *Biochim. Biophys. Acta Proteins Proteom.* **2018**, *1866*, 88–96. [CrossRef]
31. Zhang, C.; Schilirò, T.; Gea, M.; Bianchi, S.; Spinello, A.; Magistrato, A.; Gilardi, G.; Di Nardo, G. Molecular basis for endocrine disruption by pesticides targeting aromatase and estrogen receptor. *Int. J. Environ. Res. Public Health* **2020**, *17*, 5664. [CrossRef] [PubMed]
32. Kloas, W. Amphibians as a model for the study of endocrine disruptors. *Int. Rev. Cytol.* **2002**, *216*, 1–57. [CrossRef] [PubMed]
33. Scholz, S.; Renner, P.; Belanger, S.E.; Busquet, F.; Davi, R.; Demeneix, B.A.; Denny, J.S.; Léonard, M.; McMaster, M.E.; Villeneuve, D.L.; et al. Alternatives to in vivo tests to detect endocrine disrupting chemicals (edcs) in fish and amphibians—Screening for estrogen, androgen and thyroid hormone disruption. *Crit. Rev. Toxicol.* **2013**, *43*, 45–72. [CrossRef] [PubMed]
34. Zhao, J.; Mak, P.; Tchoudakova, A.; Callard, G.; Chen, S. Different catalytic properties and inhibitor responses of the goldfish brain and ovary aromatase isozymes. *Gen. Comp. Endocrinol.* **2001**, *123*, 180–191. [CrossRef] [PubMed]
35. Tong, S.K.; Chiang, E.F.; Hsiao, P.H.; Chung, B. Phylogeny, expression and enzyme activity of zebrafish cyp19 (P450 aromatase) genes. *J. Steroid Biochem. Mol. Biol.* **2001**, *79*, 299–303. [CrossRef]
36. Hasemann, C.A.; Kurumbail, R.G.; Boddupalli, S.S.; Peterson, J.A.; Deisenhofer, J. Structure and function of cytochromes P450: A comparative analysis of three crystal structures. *Structure* **1995**, *3*, 41–62. [CrossRef]
37. Ghosh, D.; Griswold, J.; Erman, M.; Pangborn, W. Structural basis for androgen specificity and oestrogen synthesis in human aromatase. *Nature* **2009**, *457*, 219–223. [CrossRef]
38. Di Nardo, G.; Breitner, M.; Bandino, A.; Ghosh, D.; Jennings, G.K.; Hackett, J.C.; Gilardi, G. Evidence for an elevated aspartate pK_a in the active site of human aromatase. *J. Biol. Chem.* **2015**, *290*, 1186–1196. [CrossRef]
39. Tripathi, S.; Li, H.; Poulos, T.L. Structural basis for effect or control and redox partner recognition in cytochrome P450. *Science* **2013**, *340*, 1227–1230. [CrossRef]
40. Liou, S.-H.; Mahomed, M.; Lee, Y.-T.; Goodin, D.B. Effector roles of putidaredoxin on cytochrome P450cam conformational states. *J. Am. Chem. Soc.* **2016**, *138*, 10163–10172. [CrossRef]
41. Hollingsworth, S.A.; Batabyal, D.; Nguyen, B.D.; Poulos, T.L. Conformational selectivity in cytochrome P450 redox partner interactions. *Proc. Natl. Acad. Sci. USA* **2016**, *113*, 8723–8728. [CrossRef] [PubMed]
42. Zhang, C.; Catucci, G.; Di Nardo, G.; Gilardi, G. Effector role of cytochrome P450 reductase for androstenedione binding to human aromatase. *Int. J. Biol. Macromol.* **2020**, *164*, 510–517. [CrossRef] [PubMed]
43. Pei, J.; Kim, B.H.; Grishin, N.V. PROMALS3D: A tool for multiple protein sequence and structure alignments. *Nucleic Acids Res.* **2008**, *36*, 2295–2300. [CrossRef] [PubMed]
44. Di Nardo, G.; Breitner, M.; Sadeghi, S.J.; Castrignanò, S.; Mei, G.; Di Venere, A.; Nicolai, E.; Allegra, P.; Gilardi, G. Dynamics and flexibility of human aromatase probed by FTIR and time resolved fluorescence spectroscopy. *PLoS ONE* **2013**, *8*, e82118. [CrossRef] [PubMed]
45. Poulos, T.L. Cytochrome P450 flexibility. *Proc. Natl. Acad. Sci. USA* **2003**, *100*, 13121–13122. [CrossRef]
46. Kalsotra, A.; Strobel, H.W. Cytochrome P450 4F subfamily: At the crossroads of eicosanoid and drug metabolism. *Pharm. Ther.* **2006**, *112*, 589–611. [CrossRef]
47. Mast, N.; Norcross, R.; Andersson, U.; Shou, M.; Nakayama, K.; Bjorkhem, I.; Pikuleva, I.A. Broad substrate specificity of human cytochrome P450 46A1 which initiates cholesterol degradation in the brain. *Biochemistry* **2003**, *42*, 14284–14292. [CrossRef]

48. Lepesheva, G.I.; Waterman, M.R. Sterol 14α-demethylase cytochrome P450 (CYP51), a P450 in all biological kingdoms. *Biochim. Biophys. Acta* **2007**, *1770*, 467–477. [CrossRef]
49. Ray, W.J.; Bain, G.; Yao, M.; Gottlieb, D.I. CYP26, a novel mammalian cytochrome P450, is induced by retinoic acid and defines a new family. *J. Biol. Chem.* **1997**, *272*, 18702–18708. [CrossRef]
50. Cali, J.J.; Russell, D.W. Characterization of human sterol 27-hydroxylase. A mitochondrial cytochrome P-450 that catalyzes multiple oxidation reaction in bile acid biosynthesis. *J. Biol. Chem.* **1991**, *266*, 7774–7778. [CrossRef]
51. Baravalle, R.; Di Nardo, G.; Bandino, A.; Barone, I.; Catalano, S.; Andò, S.; Gilardi, G. Impact of R264C and R264H polymorphisms in human aromatase function. *J. Steroid. Biochem. Mol. Biol.* **2017**, *167*, 23–32. [CrossRef] [PubMed]
52. Catalano, S.; Barone, I.; Giordano, C.; Rizza, P.; Qi, H.; Gu, G.; Malivindi, R.; Bonofiglio, D.; Andò, S. Rapid estradiol/ERα signaling enhances aromatase enzymatic activity in breast cancer cells. *Mol. Endocrinol.* **2009**, *23*, 1634–1645. [CrossRef] [PubMed]
53. Hayashi, T.; Harada, N. Post-translational dual regulation of cytochrome P450 aromatase at the catalytic and protein levels by phosphorylation/dephosphorylation. *FEBS J.* **2014**, *281*, 4830–4840. [CrossRef] [PubMed]
54. Miller, T.W.; Shin, I.; Kagawa, N.; Evans, D.B.; Waterman, M.R.; Arteaga, C.L. Aromatase is phosphorylated in situ at serine-118. *J. Steroid. Biochem. Mol. Biol.* **2008**, *112*, 95–101. [CrossRef] [PubMed]
55. Shimizu, T.; Tateishi, T.; Hatano, M.; Fujii-Kuriyama, Y. Probing the role of lysines and arginines in the catalytic function of cytochrome P450d by site-directed mutagenesis. Interaction with NADPH-cytochrome P450 reductase. *J. Biol. Chem.* **1991**, *266*, 3372–3375. [CrossRef]
56. Shen, S.J.; Strobel, H.W. Role of lysine and arginine residues of cytochrome P450 in the interaction between cytochrome P4502B1 and NADPH-cytochrome P450 reductase. *Arch. Biochem. Biophys.* **1993**, *304*, 257–265. [CrossRef] [PubMed]
57. Šrejber, M.; Navrátilová, V.; Paloncýová, M.; Bazgier, V.; Berka, K.; Anzenbacher, P.; Otyepka, M. Membrane-attached mammalian cytochromes P450: An overview of the membrane's effects on structure, drug binding, and interactions with redox partners. *J. Inorg. Biochem.* **2018**, *183*, 117–136. [CrossRef]
58. Hong, Y.; Li, H.; Ye, J.; Miki, Y.; Yuan, Y.-C.; Sasano, H.; Evans, D.B.; Chen, S. Epitope characterization of an aromatase monoclonal antibody suitable for the assessment of intratumoral aromatase activity. *PLoS ONE* **2009**, *4*, e8050. [CrossRef]
59. Hong, Y.; Rashid, R.; Chen, S. Binding features of steroidal and nonsteroidal inhibitors. *Steroids* **2011**, *76*, 802–806. [CrossRef]
60. Ritacco, I.; Spinello, A.; Ippoliti, E.; Magistrato, A. Post-translational regulation of CYP450s metabolism as revealed by all-atoms simulations of the aromatase enzyme. *J. Chem. Inf. Model.* **2019**, *59*, 2930–2940. [CrossRef]
61. Ritacco, I.; Saltalamacchia, A.; Spinello, A.; Ippoliti, E.; Magistrato, A. All-atom simulations disclose how cytochrome reductase reshapes the substrate access/egress routes of its partner CYP450s. *J. Phys. Chem. Lett.* **2020**, *11*, 1189–1193. [CrossRef]
62. Yoshimoto, F.K.; Guengerich, F.P. Mechanism of the third oxidative step in the conversion of androgens to estrogens by cytochrome P450 19A1 steroid aromatase. *J. Am. Chem. Soc.* **2014**, *136*, 15016–15025. [CrossRef] [PubMed]
63. Khatri, Y.; Luthra, A.; Duggal, R.; Sligar, S.G. Kinetic solvent isotope effect in steady-state turnover by CYP19A1 suggests involvement of Compound 1 for both hydroxylation and aromatization steps. *FEBS Lett.* **2014**, *588*, 3117–3122. [CrossRef] [PubMed]
64. Lo, J.; Di Nardo, G.; Griswold, J.; Egbuta, C.; Jiang, W.; Gilardi, G.; Ghosh, D. Structural basis for the functional roles of critical residues in human cytochrome P450 aromatase. *Biochemistry* **2013**, *52*, 5821–5829. [CrossRef] [PubMed]
65. Di Nardo, G.; Gilardi, G. Human aromatase: Perspectives in biochemistry and biotechnology: Human Aromatase. *Biotechnol. Appl. Biochem.* **2013**, *60*, 92–101. [CrossRef]
66. Parween, S.; Rojas Velazquez, M.N.; Udhane, S.S.; Kagawa, N.; Pandey, A.V. Variability in loss of multiple enzyme activities due to the human genetic variation P284T located in the flexible hinge region of NADPH cytochrome P450 oxidoreductase. *Front. Pharmacol.* **2019**, *10*, 1187. [CrossRef]
67. Hemimi, N.; Shaafie, I.; Alshawa, H. The study of the impact of genetic polymorphism of aromatase (CYP19) enzyme and the susceptibility to polycystic ovary syndrome (575.5). *FASEB J.* **2014**, *28*, 575-5. [CrossRef]
68. Jin, J.L.; Sun, J.; Ge, H.J.; Cao, Y.X.; Wu, X.K.; Liang, F.J.; Sun, H.X.; Ke, L.; Yi, L.; Wu, Z.W.; et al. Association between CYP19 gene SNP rs2414096 polymorphism and polycystic ovary syndrome in Chinese women. *BMC. Med. Genet.* **2009**, *10*, 139. [CrossRef]
69. Mehdizadeh, A.; Kalantar, S.M.; Sheikhha, M.H.; Aali, B.S.; Ghanei, A. Association of SNP rs.2414096 CYP19 gene with polycystic ovarian syndrome in Iranian women. *Int. J. Reprod. Biomed.* **2017**, *15*, 491–496. [CrossRef] [PubMed]
70. Lee, K.M.; Abel, J.; Ko, Y.; Harth, V.; Park, W.Y.; Seo, J.S.; Yoo, K.Y.; Choi, J.Y.; Shin, A.; Ahn, S.H.; et al. Genetic polymorphisms of cytochrome P450 19 and 1B1, alcohol use, and breast cancer risk in Korean women. *Br. J. Cancer* **2003**, *88*, 675–678. [CrossRef]
71. Barone, I.; Giordano, C.; Malivindi, R.; Lanzino, M.; Rizza, P.; Casaburi, I.; Bonofiglio, D.; Catalano, S.; Andò, S. Estrogens and PTP1B function in a novel pathway to regulate aromatase enzymatic activity in breast cancer cells. *Endocrinology* **2012**, *153*, 5157–5166. [CrossRef] [PubMed]
72. Cornil, C.A.; Ball, G.F.; Balthazart, J. Functional significance of the rapid regulation of brain estrogen action: Where do the estrogens come from? *Brain Res.* **2006**, *1126*, 2–26. [CrossRef] [PubMed]
73. Balthazart, J.; Choleris, E.; Remage-Healey, L. Steroids and the brain: 50 years of research, conceptual shifts and the ascent of non-classical and membrane-initiated actions. *Horm. Behav.* **2018**, *99*, 1–8. [CrossRef] [PubMed]
74. Forlano, P.M.; Deitcher, D.L.; Myers, D.A.; Bass, A.H. Anatomical distribution and cellular basis for high levels of aromatase activity in the brain of teleost fish: Aromatase enzyme and mRNA expression identify glia as source. *J. Neurosci.* **2001**, *21*, 8943–8955. [CrossRef] [PubMed]

75. Diotel, N.; Le Page, Y.; Mouriec, K.; Tong, S.-K.; Pellegrini, E.; Vaillant, C.; Anglade, I.; Brion, F.; Pakdel, F.; Chung, B.-C.; et al. Aromatase in the brain of teleost fish: Expression, regulation and putative functions. *Front. Neuroendocrinol.* **2010**, *31*, 172–192. [CrossRef]
76. The UniProt Consortium. UniProt: A worldwide hub of protein knowledge. *Nucleic Acids Res.* **2019**, *47*, D506–D515. [CrossRef]
77. Ashkenazy, H.; Abadi, S.; Martz, E.; Chay, O.; Mayrose, I.; Pupko, T.; Ben-Tal, N. ConSurf 2016: An improved methodology to estimate and visualize evolutionary conservation in macromolecules. *Nucleic Acids Res.* **2016**, *44*, W344–W350. [CrossRef]
78. Landau, M.; Mayrose, I.; Rosenberg, Y.; Glaser, F.; Martz, E.; Pupko, T.; Ben-Tal, N. ConSurf 2005: The projection of evolutionary conservation scores of residues on protein structures. *Nucleic Acids Res.* **2005**, *33*, W299–W302. [CrossRef]
79. Finn, R.D.; Clements, J.; Eddy, S.R. HMMER web server: Interactive sequence similarity searching. *Nucleic Acids Res.* **2011**, *39*, W29–W37. [CrossRef]
80. Clamp, M.; Cuff, J.; Searle, S.M.; Barton, G.J. The Jalview Java alignment editor. *Bioinformatics* **2004**, *20*, 426–427. [CrossRef]
81. Mayrose, I.; Graur, D.; Ben-Tal, N.; Pupko, T. Comparison of site-specific rate-inference methods for protein sequences: Empirical bayesian methods are superior. *Mol. Biol. Evol.* **2004**, *21*, 1781–1791. [CrossRef] [PubMed]
82. Schoch, G.A.; Yano, J.K.; Sansen, S.; Dansette, P.M.; Stout, C.D.; Johnson, E.F. Determinants of cytochrome p450 2c8 substrate binding: Structures of complexes with montelukast, troglitazone, felodipine, and 9-cis-retinoic acid. *J. Biol. Chem.* **2008**, *283*, 17227–17237. [CrossRef] [PubMed]
83. Pettersen, E.F.; Goddard, T.D.; Huang, C.C.; Couch, G.S.; Greenblatt, D.M.; Meng, E.C.; Ferrin, T.E. UCSF Chimera-A visualization system for exploratory research and analysis. *J. Comput. Chem.* **2004**, *25*, 1605–1612. [CrossRef] [PubMed]
84. Midlik, A.; Navrátilová, V.; Moturu, T.R.; Koča, J.; Svobodová, R.; Berka, K. Uncovering of cytochrome P450 anatomy by SecStrAnnotator. *bioRxiv* **2020**. [CrossRef]
85. Gotoh, O. Substrate recognition sites in cytochrome P450 family 2 (CYP2) proteins inferred from comparative analyses of amino acid and coding nucleotide sequences. *J. Biol. Chem.* **1992**, *267*, 83–90. [CrossRef]
86. Webb, B.; Sali, A. Comparative protein structure modeling using MODELLER. *Curr. Protoc. Bioinform.* **2016**, *54*, 5.6.1–5.6.37. [CrossRef]
87. Yang, J.; Yan, R.; Roy, A.; Xu, D.; Poisson, J.; Zhang, Y. The I-Tasser Suite: Protein structure and function prediction. *Nat. Methods* **2015**, *12*, 7–8. [CrossRef]
88. Maier, J.A.; Martinez, C.; Kasavajhala, K.; Wickstrom, L.; Hauser, K.E.; Simmerling, C. ff14SB: Improving the accuracy of protein side chain and backbone parameters from ff99SB. *J. Chem. Theor. Comput.* **2015**, *11*, 3696–3713. [CrossRef]
89. Chen, V.B.; Arendall, W.B.; Headd, J.J.; Keedy, D.A.; Immormino, R.M.; Kapral, G.J.; Murray, L.W.; Richardson, J.S.; Richardson, D.C. MolProbity: All-atom structure validation for macromolecular crystallography. *Acta Crystallogr. D Biol. Crystallogr.* **2010**, *66*, 12–21. [CrossRef]
90. Wiederstein, M.; Sippl, M.J. ProSA-web: Interactive web service for the recognition of errors in three-dimensional structures of proteins. *Nucleic Acids Res.* **2007**, *35*, W407–W410. [CrossRef]
91. Benkert, P.; Biasini, M.; Schwede, T. Toward the estimation of the absolute quality of individual protein structure models. *Bioinformatics* **2011**, *27*, 343–350. [CrossRef] [PubMed]
92. Jones, D.T. Protein secondary structure prediction based on position-specific scoring matrices. *J. Mol. Biol.* **1999**, *292*, 195–202. [CrossRef] [PubMed]

Chapter 5

Polymorphism on human aromatase affects protein dynamics and substrate binding: spectroscopic evidence

Di Nardo et al. Biology Direct (2021) 16:8
https://doi.org/10.1186/s13062-021-00292-9

Biology Direct

RESEARCH Open Access

Polymorphism on human aromatase affects protein dynamics and substrate binding: spectroscopic evidence

Giovanna Di Nardo[1†], Almerinda Di Venere[2†], Chao Zhang[1], Eleonora Nicolai[2], Silvia Castrignanò[1], Luisa Di Paola[3], Gianfranco Gilardi[1*] and Giampiero Mei[2*]

Abstract

Human aromatase is a member of the cytochrome P450 superfamily, involved in steroid hormones biosynthesis. In particular, it converts androgen into estrogens being therefore responsible for the correct sex steroids balance. Due to its capacity in producing estrogens it has also been considered as a promising target for breast cancer therapy. Two single-nucleotide polymorphisms (R264C and R264H) have been shown to alter aromatase activity and they have been associated to an increased or decreased risk for estrogen-dependent pathologies. Here, the effect of these mutations on the protein dynamics is investigated by UV/FTIR and time resolved fluorescence spectroscopy. H/D exchange rates were measured by FTIR for the three proteins in the ligand-free, substrate- and inhibitor-bound forms and the data indicate that the wild-type enzyme undergoes a conformational change leading to a more compact tertiary structure upon substrate or inhibitor binding. Indeed, the H/D exchange rates are decreased when a ligand is present. In the variants, the exchange rates in the ligand-free and –bound forms are similar, indicating that a structural change is lacking, despite the single amino acid substitution is located in the peripheral shell of the protein molecule. Moreover, the fluorescence lifetimes data show that the quenching effect on tryptophan-224 observed upon ligand binding in the wild-type, is absent in both variants. Since this residue is located in the catalytic pocket, these findings suggest that substrate entrance and/or retention in the active site is partially compromised in both mutants. A contact network analysis demonstrates that the protein structure is organized in two main clusters, whose connectivity is altered by ligand binding, especially in correspondence of helix-G, where the amino acid substitutions occur. Our findings demonstrate that SNPs resulting in mutations on aromatase surface modify the protein flexibility that is required for substrate binding and catalysis. The cluster analysis provides a rationale for such effect, suggesting helix G as a possible target for aromatase inhibition.

Keywords: Aromatase polymorphism, Ligand binding, Fluorescence, Molecular modeling

* Correspondence: gianfranco.gilardi@unito.it; mei@med.uniroma2.it
†Giovanna Di Nardo and Almerinda Di Venere contributed equally to this work.
[1]Dipartimento di Scienze della Vita e Biologia dei Sistemi, Università di Torino, Via Accademia Albertina 13, 10123 Turin, Italy
[2]Dipartimento di Medicina Sperimentale, Università di Roma Tor Vergata, Via Montpellier 1, 00133 Rome, Italy
Full list of author information is available at the end of the article

Background

Structural flexibility is a crucial property of proteins, since it allows the molecular rearrangements required for most of their biological functions. Such rearrangements include large conformational changes (i.e. those characterizing cargo and contractile proteins), long distance displacements (for instance, those occurring in some integral membrane receptors), or even smaller, local conformational changes (as those required for the action of most enzymes). Flexibility allows substrates binding, products release and it is needed to confer allosteric properties to enzymes that control and regulate metabolic pathways and cells growth. Cytochromes P450 are a very good example of such enzymes as they are heme-containing monooxygenases involved in key metabolic pathways and xenobiotic detoxification. Moreover, they are known to undergo conformational changes to allow substrate access, catalysis and product release [1]. In particular, structural data demonstrate that some elements such as the F- and G- helices and the loop connecting them (F-G loop) are highly flexible and can open and close channels connecting the surface of the protein to the active site [2, 3].

Human cytochromes P450 are highly polymorphic and some single nucleotide polymorphisms (SNPs) are known to affect the enzyme activity by decreasing the catalytic efficiency. Although the effect of many SNPs can be rationalized by the location of the mutations in the protein structure, for others it is very difficult to predict. This is the case of two SNPs present in human aromatase, a cytochrome P450 with a key role in steroidogenesis as it catalyzes the conversion of androgens into estrogens [4]. The correct activity of this protein is crucial, because alterations in the equilibrium between androgens and estrogens, hypo- or hyperproduction of estrogens are associated to a series of disorders that range from neurological diseases to breast cancer [5]. We have previously characterized the common R264C (rs700519) and the rarer R264H (rs2304462) polymorphic variants showing that the activity of these variants is modified by an alteration of the kinetic parameters [6, 7] and by a different phosphorylation propensity, as R264 is part of a consensus sequence for phosphorylation [6]. However, this residue lies on the protein surface, being part of the G-helix and it is therefore difficult to understand how its mutation can impact the catalytic parameters only based on the location.

We previously demonstrated that aromatase requires dynamic flexibility to bind and process its substrates [8]. In this paper we have used a combination of experimental techniques (namely infrared and fluorescence spectroscopy) to evaluate the impact that a single point mutation (R264C or R264H) on the external surface of human aromatase has on its tridimensional structure and on its biological function. In parallel to such experimental approach, a contact network analysis of the protein structure has been also performed. In the last decade the application of this computational methodology to proteins has allowed to look at these complex molecules from a new perspective, since such kind of algorithms use a few descriptors to characterize the spatial inter-connections among amino acids. In this way, clusters of residues are localized within the protein tridimensional structure and long-range interactions, cooperative effects and segmental mobility can be predicted. The applications of this methodology span from protein-protein interaction [9, 10] to allosteric regulation of enzymes [11, 12], allowing, in very recent researches, to speculate on possible binding sites for drugs against degenerative diseases [13] or viruses [14]. We demonstrate that the combination of this approach with experimental data might suggest a molecular explanation to the loss of biological activity observed in R264C and R264H variants.

Results

H/D exchange followed by FTIR

Fourier transform infrared spectroscopy (FTIR) was applied to determine the kinetics of H/D exchange in Recombinant human aromatase (Aro) and its polymorphic variants, to detect possible differences in the kinetics of deuteration arising from protein conformational changes induced by ligand binding. Figure 1 shows the FTIR spectra recorded at the beginning and at the end of a typical H/D exchange kinetic experiment, in the case of substrate-free Aro.

The band between 1670 cm^{-1} and 1620 cm^{-1} has been assigned to the amide I, whereas the band between 1470 cm^{-1} and 1420 cm^{-1} has been attributed to the amide II. The H/D exchange was thus followed as the increase of the absorbance of the amide II band at 1460 cm^{-1} (Fig. 1, inset), in a time range of 160 min.

The time dependence of the fraction of protons exchanged shows a dramatic increase in the first ten minutes, while a much slower kinetics takes place in the next 2–3 h (Fig. 2). The data are, in fact, best fitted to a double exponential curve (cfr. Methods), which yields two distinct rate values (Table 1). The Aro wt sample is characterized by the faster initial transition ($k_1 \approx 0.4$ m^{-1}), a process that is considerably slowed down by ligand binding (Fig. 1, panel A), the k_1 value being reduced to one half both in the presence of the substrate and the inhibitor molecules (Table 1). No significant differences are instead observed in the long-term component (k_2), indicating that the slower part of the kinetic is independent of the binding process. In the H/D exchange kinetics, unlike Aro wt, the presence of the substrate

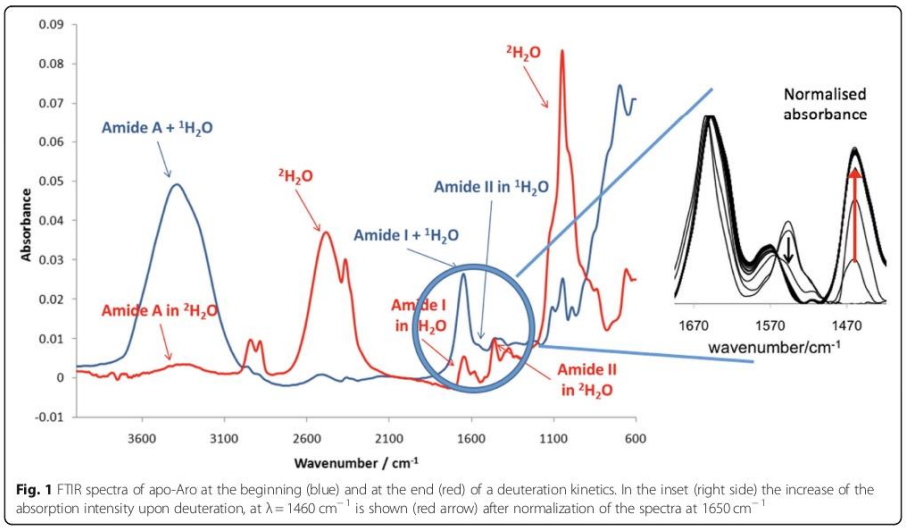

Fig. 1 FTIR spectra of apo-Aro at the beginning (blue) and at the end (red) of a deuteration kinetics. In the inset (right side) the increase of the absorption intensity upon deuteration, at $\lambda = 1460\ cm^{-1}$ is shown (red arrow) after normalization of the spectra at $1650\ cm^{-1}$

androstenedione and the inhibitor anastrozole on polymorphic variants is less relevant (Fig. 2b, c). In particular, the raw data are characterized by a slower increase in the initial part of the process ($t \approx 0–20$ min, Fig. 2), whose fit yields a lower rate constant ($k_1 \approx 0.2\ min^{-1}$, Table 1), with respect to that of the wt protein. Again, the introduction of androstenedione or anastrozole in both mutants does not affect the second step of the kinetics (Fig. 2b, c) and, in fact, no significant changes are observed in the second rate constant value ($k_2 \approx 0.016\ min^{-1}$, Table 1).

The presence of a complex kinetics (Table 1) indicates a heterogeneity in the protons populations. Indeed, a biphasic behaviour of the H/D exchange process in proteins is generally explained in terms of two groups of peptide hydrogens, one more accessible to the solvent molecules (and thus subject to a higher exchanging rate) and a second one located in more buried protein segments, less accessible to water [15–18]. Since the H/D exchange process at the protein surface would be too fast to be detected, the two rate constants must be assigned to partially exposed (k_1) or buried (k_2) residues protons. In such a context, a relevant meaning may be attributed to the pre-exponential factors m_i of the respective fits, as they represent the initial fractions (i.e. at time = 0) of each protons population. As shown in Table 1, the m_1 value of the wt protein is the highest (≈ 0.60) in the absence of any ligand, and the lowest (≈ 0.20) when one of the ligands is present, thus indicating that a large change, $\Delta m_1 \approx -65\%$, occurs in the population of the partially exposed protons upon binding.

On the contrary, the decrease observed in the case of the two mutants results to be smaller ($\Delta m_1 \approx -40\%$ for R264H and $\Delta m_1 \approx -23\%$ in the case of R264C), suggesting less pronounced structural effects induced by ligand binding.

Intrinsic fluorescence dynamics

Ligand-induced changes in the intrinsic fluorescence of aromatase have been characterized through the phase-shift and demodulation technique and the results of data analysis are shown in Fig. 3. As previously observed [8], the protein emission decay is quite heterogeneous, being characterized by four distinct lifetime components, ranging from tenths of nanoseconds to 6–9 ns. Such a complexity is due to the presence of five tryptophan residues, located in different environments of the protein scaffolding. The main feature of the wt sample in the presence of either substrate or inhibitor is a large decrease of the fractional contribution at ≈ 5 ns (Fig. 3a). Such a considerable quenching effect has been attributed by previous fluorescence measurements to the interaction between the substrate and a specific tryptophan residue, namely W224, which is buried in the core of the protein matrix [8].

As shown in Fig. 3b and c, no changes were instead detected in the fractional contribution at 5 ns of both R264H and R264C upon ligands addition, indicating that

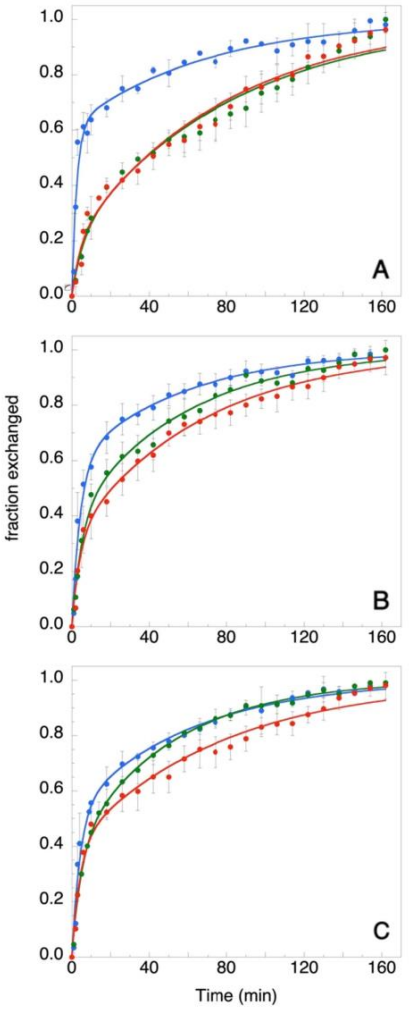

Fig. 2 Kinetics of H/D exchange followed by FTIR for wt-Aro (panel **a**, blue symbols) and the two polymorphic variants (namely R264H, panel **b**, and R264C, panel **c**, blue symbols). The kinetics in the presence of the substrate androstenedione (green symbols) and the inhibitor anastrozole (red symbols) are also reported. The solid lines correspond to the best double exponential fitting curves, whose parameters are reported in Table 1

Table 1 Results of the double exponential fits performed on the data reported in Fig. 2

sample	m_1(*) (min)	$k_1(m^{-1})$ (min^{-1})	$k_2(m^{-1})$ (min^{-1})
Aro wt	0.61 ± 0.03	0.40 ± 0.04	0.014 ± 0.002
Aro wt + sub	0.20 ± 0.05	0.18 ± 0.05	0.012 ± 0.001
Aro wt + inib	0.19 ± 0.03	0.23 ± 0.06	0.012 ± 0.001
R264H	0.59 ± 0.03	0.22 ± 0.05	0.017 ± 0.001
R264H + sub	0.39 ± 0.03	0.19 ± 0.03	0.017 ± 0.002
R264H + inib	0.32 ± 0.02	0.23 ± 0.04	0.015 ± 0.001
R264C	0.52 ± 0.03	0.23 ± 0.05	0.017 ± 0.002
R264C + sub	0.38 ± 0.03	0.20 ± 0.02	0.020 ± 0.001
R264C + inib	0.40 ± 0.03	0.25 ± 0.04	0.013 ± 0.002

(*) $m_2 = 1 - m_1$

in the mutants the binding of either substrate or inhibitor molecules does not produce significant effect in the environment of W224, suggesting a different local conformation with respect to that of the wt cavity.

This hypothesis has been further tested by studying the protein rotational dynamics. The presence of the long lifetime component, in fact, allows to perform anisotropy measurements using the aromatase intrinsic fluorescence. The corresponding phase shift and demodulation data are reported in Fig. 4, for Aro wt and R264C or R264H mutants. The results demonstrate that both mutated forms display slower rotational dynamics, with respect to the wt protein, the data being shifted toward a lower frequency range.

In fact, the phase and demodulation curves of each aromatase type crosses each other at ≈ 150, 63, and 93 MHz, respectively in the case wt, R264H and R264C, indicating that R264H is the form characterized by the slowest dynamics. Non-linear fitting of the phase shift and demodulation points reported in Fig. 4 yielded the results illustrated in Fig. 5. Each data set required two rotational correlation times, ϕ_1, and ϕ_2. The first one, ϕ_1, ranges from 21 ns (wt) to 33 ns (R264H) and it is compatible with the rotational motion of whole protein, as shown in the cartoon sketched in the left side of Fig. 5. Indeed, the predicted turning on a principal axis of a spherical hydrated molecule with the same size of aromatase (≈ 58,000) would be $\phi_{sph} \approx 24$ ns [19]. Longer $\phi_1$values, such those characterizing R264C and R264H, suggest a more swelled tridimensional form, since an expanded tertiary structure would produce a slower motion.

In the case of the wt sample, the entrance of the substrate (or inhibitor) in the protein binding cavity produced a considerable decrease in the $\phi_1$value (≈ − 23%, Fig. 5), thus implying a faster rotational dynamics. This trend was also observed in the mutated forms but with two important differences: i) the extent of the relative

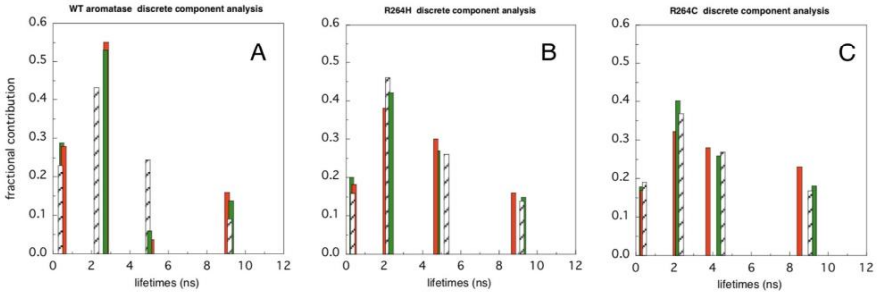

Fig. 3 Lifetime components of wt-Aro fluorescence decay (panel **a**), R264H (panel **b**) and R264C (panel **c**) in the absence (dashed bars) and in the presence of substrate (green) or inhibitor (red)

change in ϕ_1 is less pronounced (≈ – 11% and – 15%, respectively); ii) in both samples, the ϕ_1 value remains above 23 ns, independently of the ligand (substrate or inhibitor) used (Fig. 5).

The second rotational lifetime,ϕ_2,is much shorter being on the order of ≈ 400–500 ps, in the case of wt and R264C aromatase and ≈ 800 ps, as regards R264H (Fig. 5). Such values reflect a faster dynamics (with respect to ϕ_1), that can be ascribed to the average local motions of tryptophan(s) environment. The presence of the ligands in the binding pocket slows down such movements in the case of the wt and the R264C samples, the substrate molecule being the most efficient, since $\phi_2$isalmost doubled in the holo-form (Fig. 5). On the contrary, the addition of the substrate or the inhibitor does not produce significant changes in the local dynamics of R264H, as shown by the similarity of ϕ_2 the values.

ANS binding

8-Anilino-1-naphthalenesulfonic acid (ANS) is a hydrophobic probe, which increases its fluorescence intensity upon binding to surface cavities and pockets of proteins [20]. For such reason, it is particularly suitable to study the conformational changes that modify the

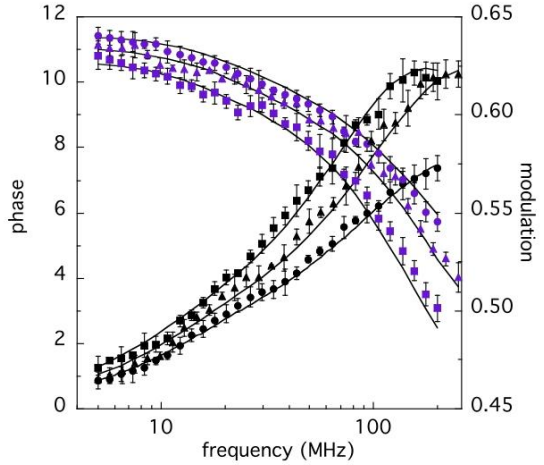

Fig. 4 Phase shift (black symbols) and demodulation data (purple symbols) of wt-Aro (circles), R264H (squares) and R264C (triangles). The solid lines correspond to the best fit obtained using two rotational correlation times

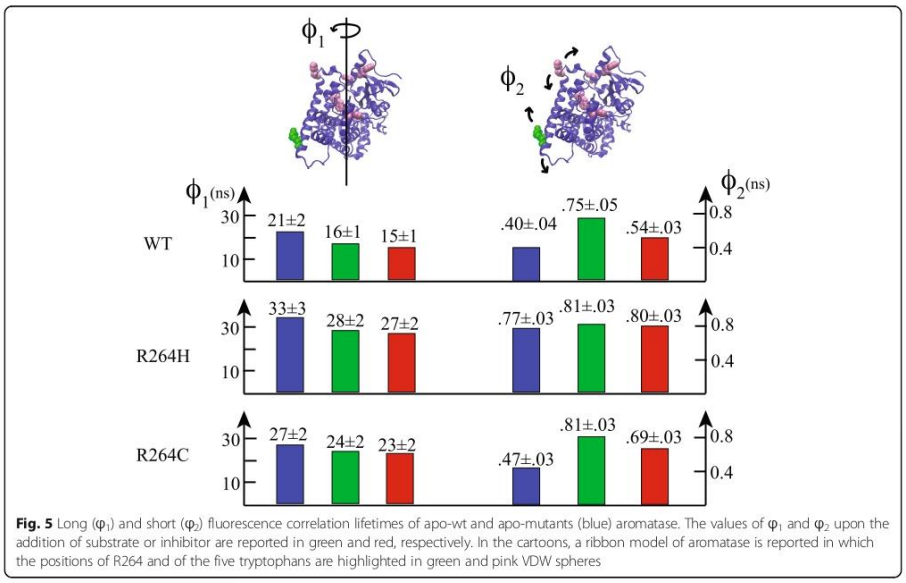

Fig. 5 Long (φ_1) and short (φ_2) fluorescence correlation lifetimes of apo-wt and apo-mutants (blue) aromatase. The values of φ_1 and φ_2 upon the addition of substrate or inhibitor are reported in green and red, respectively. In the cartoons, a ribbon model of aromatase is reported in which the positions of R264 and of the five tryptophans are highlighted in green and pink VDW spheres

compactness of a protein tridimensional structure, such as those produced by temperature [21], pH [22], pressure [23] and substrate binding [24]. In order to characterize to what extent the presence of substrate (or inhibitor) in the active site of aromatase alter the roughness and accessibility of the protein surface, we added increasing amounts of ANS to the ligand-containing samples and compared the respective titration curves and fit in Fig. 6. As shown also by the respective dissociation constants (reported in Table 2), the wt protein displays a lower affinity for ANS, its K_d value being 3 times larger than that obtained in the case of R264H and 2 times with respect to R264C (Table 2). Interestingly, in all samples the ANS binding process does not depend on the ligand used, giving the same results for the substrate and the inhibitor (Fig. 6 and Table 2).

Contact network analysis

A topological characterization of the aromatase structure has been attempted using the available crystallographic model of substrate-containing aromatase (PDB code 4kq8), and an in silico version of the ligand-free protein, obtained through a molecular dynamics simulation [25]. A contact network approach consists of a coarse-graining algorithm that reduces the amino acids of a protein into "nodes" of a tridimensional grid, identifying the position of each residue with that of its α-carbon. Each couple of amino acids distance is than evaluated and an (N x N) matrix built, consisting in "1" and "0" elements, corresponding to interacting or non-interacting elements of the network (according to a discriminating distance, fixed a priori). Eventually, "modules" are identified within the protein structure, thanks to a clustering procedure that groups nodes on the basis of the number of their mutual interactions. In the case of aromatase, such analysis allowed the identification of two distinct regions of the protein, as shown in Fig. 7 left panel, where each module of the crystal structure has been highlighted with a different color, red and green, respectively.

The clustering application does not result into an evident domain partition (such as regions with a preponderant kind of secondary structure or areas characterized by specific biological activity), nor the two clusters part in two distinct sections of the sequence. The spatial distribution of each one of the two clusters is uniform and the border may be approximated by a plane perpendicular to the heme group. As shown in Fig. 7 rigth panel, such an abstract plane is placed just below the channel used by the substrate to reach the catalytic site [26] indicating that the boundary between the two clusters is a critical region for the protein biological function. This feature can be more quantitatively described evaluating the so-called "participation

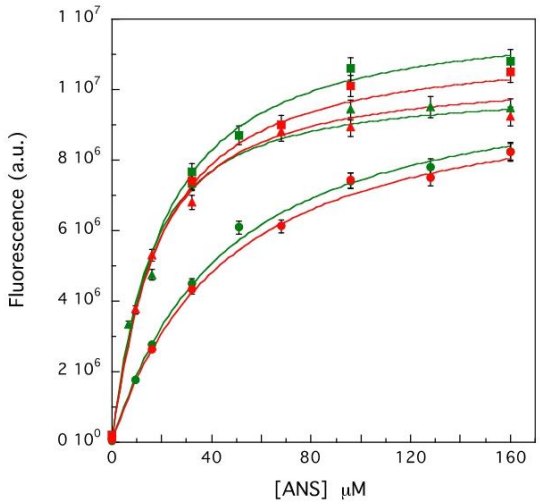

Fig. 6 ANS-binding curves of wt-Aro (circles) and mutants R264H (squares) or R264C (triangles) in the presence of saturating concentration of substrate (green) or inhibitor (red). The concentration of all the proteins is 6.4 μM. The solid lines correspond to the best fit obtained for each sample by a chi-squared minimization procedure (see materials and methods)

coefficient", P, a parameter that reflects the tendency of each node contained in one cluster to establish connections with nodes belonging to the other group [11]. Such connectivity index ranges from 0 to 1 (Fig. 8a) and the average protein value, <P>, calculated on the whole sequence, results to be $<P> \approx 0.076$ (Fig. 8b). Much higher *P* values characterize, instead, the residues lying at the clusters border, including those that form the central section of helix G (dashed rectangle, Fig. 8b). The participation coefficient has been also evaluated in the case of the substrate-bound aromatase model, P_{sb}, and the difference obtained between the holo- and apo-form, $\Delta P = P_{sb} - P$, is represented in Fig. 8c.

While the majority of the protein residues is not affected by the ligand binding process, the topological analysis suggest that a significant increase in the participation coefficient occurs in the case of those residues that form the binding channel (Fig. 8c). The central section of helix G displays, instead, an opposite effect characterized by the largest decrease in the P value, suggesting that the presence of the ligand reduces the connectivity role that that region has in the open, ligand-free protein form.

Table 2 ANS-aromatase dissociation constants yielded by the fits reported in Fig. 6

Sample	K_d (mM)
Aro wt + sub.	40 ± 2
Aro wt + inh.	41 ± 3
R264H + sub.	11 ± 1
R264H + inh.	13 ± 1
R264C + sub	17 ± 2
R264C + inh.	16 ± 2

Discussion

Polymorphism of human proteins is a well-known phenomenon [27] that has recently raised a large interest in the scientific community, due to the possibility that cancer predictive studies (based on enzyme variants analyses) have in precision medicine [28]. The systematic study of proteins' variants databases through new algorithms [29, 30] has considerably improved the accuracy of cancer survival predictions [28, 31–33], giving insights on drugs-induced damages [34] and allowing the identification of new, promising biomarkers [35]. In this general framework, the structural and functional characterization of aromatase polymorphisms is particularly important, as this enzyme is considered as a potential target for breast cancer therapy [36].

The crystallographic structures of placental [37] and recombinant [38] aromatase have demonstrated that the protein has a compact, globular fold and that R264 is localized on the protein surface, far away from the

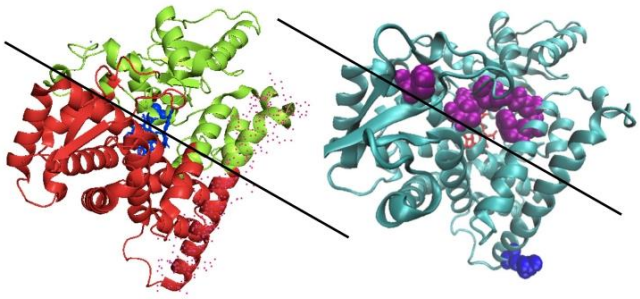

Fig. 7 in the left side of the figure the two clusters (red and green) identified on the basis of the contact network analysis applied to the 4kq8 pdb file are reported (the heme group is also shown in blue). The G-helix has been highlighted by a red dot cloud. On the right side, the same structure is reported together with residue R264 (blue, VDW) and those aminoacids (purple, VDW) which form the access channel for the substrate androstenedione (according to Sgrignani and Magistrato, 2012) and the heme group (in red). The black line in both pictures marks the frontier of the two clusters

substrate binding site. Despite such a peripherical location, the conversion of ARG to HIS or CYS is known to influence the protein functional properties, reducing its ability to bind the substrate and decreasing its catalytic efficiency [6]. Circular dichroism spectroscopy showed that the two polymorphic variants retain the overall wt secondary structure, but are characterized by a lower thermal stability suggesting that the mutation might change the motility of the helix G to which R264 belongs [6]. Structural studies and molecular dynamics simulations of bacterial P450 have revealed that such alpha helix is involved, through the adjacent helix F, in the opening of the channel which provides the access of substrate to the active site [26, 39, 40].

The contact network analysis reported in the present study has identified two main clusters (Fig. 7), which are "communicating" through residues mainly dislocated along the channel that allows the entrance of the substrate in the active site. Such topological analysis thus suggests that large conformational changes characterize the substrate binding process of aromatase, involving long-range interactions between the two modules. Helices F and G are no exception: their central sections contain a relevant number of crucial nodes connecting the two clusters (Fig. 8a and b) and undergo the largest (negative) change in their participation coefficient, P, as the protein binds the substrate molecule (Fig. 8c). The kinetics of H/D exchange in Aro wt (Fig. 2a and Table 1) indicates that these conformational changes produce

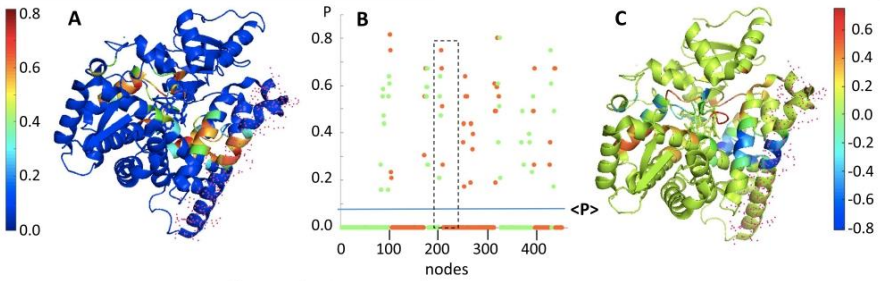

Fig. 8 in panel **a** the participation coefficient, P, of each amino acid of wt-Aro is shown, according to the colors code whose numerical value is reported in the left scale. In panel **b** the distribution of the *P* values is presented as a function of the sequence position (X-axis) and of the belonging to one of the two clusters (red or green) identified in Fig. 7. <P> is the protein average participation coefficient. The area of the dashed rectangle corresponds to the G-helix residues. In panel **c** the difference $\Delta P = P_{sb} - P$ between the P values of the holo and apo forms is reported. The green color has been attributed to those residues whose P value does not change ($\Delta P = 0$) upon ligand binding

a large decrease in the fractionof the more exposed protons in the presence of both androstenedione and anastrozole. Trivial explanations (such as a screening effect exerted by the ligands) seem to be excluded by fluorescence anisotropy measurements, that demonstrate how in the ligand-bound form the protein assumes a more compact tertiary structure through a conformational change that confers the molecule a faster rotational dynamics (Fig. 5). The results obtained for the two polymorphic variants demonstrate that these samples undergo much smaller changes in the H/D kinetics (Table 1) and in the long rotational correlation time (Fig. 5). More importantly, in the presence of both ligands, they retain a higher ANS binding capability, with respect to that of Aro wt (Figure and Table 2), confirming that they lack that compactness which characterize ligand-bound Aro wt. As a consequence, the correct entrance of the substrate (or inhibitor) molecule to the protein active site is compromised, as demonstrated by dynamic fluorescence measurements. Indeed, in a previous study [8], we have demonstrated that the lifetime component at 4.5–5.0 ns can be attributed to W224, since it is not present in mutants such as W224F [8]. Since this tryptophan resides in the proximity of aromatase binding site and it is dramatically quenched by the entrance of androstenedione or anastrozole (Fig. 3a), it can be used to monitor ligand-induced structural changes in the specific region of the active site. The absence of any significant difference of this specific fluorescence lifetime component in the two polymorphic variants (Fig. 3b,c) demonstrates that the local perturbation introduced at the extremity of helix G upon the substitution of R264 impairs the correct placement of the ligand in the active site, thus providing a structural rationale for the decreased activity of the mutants [6].

The normal mode analysis of aromatase [25] has demonstrated that the protein displays a very rigid core (corresponding approximately to the heme group), which is surrounded by concentric shells of progressively more flexible regions. The helices F and G and their interconnecting loop are one of such external mobile structural areas [38]. Indeed, long-range effects connected to the flexibility of helix G has been already reported in the case of bacterial cytochromes P450 [41]. In particular, it was demonstrated that the breaking of the salt bridge which involves ASP 251 has crucial consequences on ligands recognition and binding.

According to the contact network analysis reported in this study, the protein could be figured as a sort of sandwich, the central slice corresponding to the substrate channel (Figs. 7 and 8). In this picture, the packing of the sandwich would be controlled by the clamping effected exerted by helices F and G, whose hinge mechanism resides in their highly inter-connected central elements (Fig. 8). The substitution of R264 with residues characterized by a different geometry (HIS and CYS), length and charge (CYS) must severely affect the salt bridge interaction with ASP 251, altering the "pivot" mechanism by which the flexible F-G group controls the interconnection between the two clusters.

Conclusion

In conclusion, the data reported in this study demonstrate by two independent spectroscopic techniques that human aromatase assumes a more compact tridimensional conformation upon ligand binding. On the contrary, mutants R264C and R264H (that impair the correct binding of both substrate and inhibitor molecules) undergo a less efficient packing process, suggesting a minor flexibility of their mobile segments. A rationale to such behavior could be envisaged thanks to a contact network analysis of the protein structure, which has revealed the connecting role of helices F and G between the two clusters that form the substrate channel to the active site. Thus, based on in vitro measurements, such an explanation shed new light on molecular impact that the two polymorphisms have in living beings.

Methods

Materials

Recombinant human aromatase was expressed in *E. coli* and purified as previously described [7, 8]. Both wild-type and mutants were purified with the same type of buffer, i.e. 100 mM phosphate buffer pH 7.4 containing 20% glycerol, 1 mM β-mercaptoethanol, 0.1% Tween-20.

All chemicals used for protein purification were purchased from Sigma–Aldrich (St. Louis, MO USA) and were analytical grade.

Proteins (wt and mutants) concentration for all fluorescence experiments was about 6.5 μM, while if present, androstenedione and anastrozole concentrations were 20 μM and 10 μM, respectively.

H/D exchange kinetics experiments by ATR-FTIR

Kinetics of H/D exchange was followed by FTIR as reported by Di Nardo et al. [8]. Experiments were performed at room temperature using an infrared spectrophotometer Bruker Model Tensor 27 (Bruker Instruments, USA) coupled with an attenuated total reflectance (ATR) sampling tool (Harrick Scientific Products, USA). The working parameters were set as follows: scan velocity 10 kHz; resolution 4 cm^{-1}; spectra acquisition frequency limits 4000 and 800 cm^{-1}. Protein sample was analysed by depositing a thin protein film (30 μL, 50 μM) directly on ATR germanium crystal. In particular, Aro was analysed in ligand free form and in ligand bound form, obtained by incubating the enzyme

with androstenedione as substrate or anastrozole as inhibitor. The correct binding of both substrate and inhibitor to the active site of Aro was examined by UV/vis spectroscopy by monitoring a shift of the maximum absorbance from 418 nm to 394 nm for Androstenedione and from 418 nm to 422 nm for anastrozole. During acquisition, the spectrophotometer sample chamber was continuously purged with D_2O enriched nitrogen. Spectra were collected at intervals of 1 min, for the first 10 min, and every 8 min for the following 160 min. For each time point 60 scans were collected and averaged. Spectra were collected at least in quadruplicate and averaged for each time point, corrected by the contribution of control sample, represented by protein storage buffer, and normalized. The H/D exchange kinetics was studied by following the absorbance increase at about 1460 cm^{-1}, corresponding to the shift of the Amide II band upon deuteration. The relative absorbance values were plotted as function of time, fitted to a double exponential function and the deuteration rates were calculated and compared by ANOVA statistical analysis using SigmaPlot software.

Fluorescence measurements

Fluorescence spectra were collected using a K2-ISS (ISS, Inc.,Champaign, IL, USA) photon-counting fluorimeter thermo-stated at 20 °C using an external bath circulator. ANS binding was studied measuring the fluorescence emission spectra from 450 to 550 nm of the probe using an excitation wavelength of 350 nm. All spectra were corrected by blank subtraction.

8-Anilino-1-naphthalenesulfonic acid (ANS) binding curves were analyzed assuming a simple binding equilibrium, namely, ANS + P ↔ ANS-P, and fitting the total fluorescence, F, at increasing concentration of ANS, [ANS], according to:

$$F = F_\infty\left(([ANS] + P_0 + K_d) - \sqrt{([ANS] + P_0 + K_d)^2 - 4[ANS]P_0}\right)/(2\,P_0)$$

where P_0 is the total aromatase concentration and K_d the dissociation constant of the process.

Lifetimes and dynamic fluorescence anisotropies were performed using the phase shift and demodulation technique on a KOALA-ISS fluorimeter. The excitation source was a 300-nm laser diode, and the emission was collected through a WG320-nm cutoff filter to avoid scattering. Anisotropy decays were collected through Glan-Thompson polarizers taking into account the G-factor correction. All measurements were repeated in triplicate to obtain a good statistic, using a set of at least 30 frequencies. The data have been analyzed with the software provided by ISS.

Contact network analysis

Protein contact networks (PCNs) rely on a minimalist perspective on protein structures, seen as networks of active contacts between residues (network nodes are the protein residues, and the active contacts between pair of residues are the network links). The definition of active contacts is crucial in defining the properties emerging from the network analysis. In this work, we define "active contact" any contact corresponding to a distance between residues comprised between 4 and 8 Å. This choice includes only significant noncovalent bonds, sensible to the environmental cues. The distance between residues is computed starting from the coordinates of the residues' α-carbons.

The mathematical description of PCNs is provided by the adjacency matrix, defined as:

$$A_{ij} = \begin{cases} 1 & if\, 4\mathring{A} < d_{ij} < 8\mathring{A} \\ 0 & otherwise \end{cases}$$

Once the network has been built up, it is possible to derive several network descriptor. The most important and simple is the node degree k_i, defined as:

$$k_i = \sum\nolimits_j A_{ij}$$

Based on the node degree, we applied a spectral clustering algorithm to partition PCN into clusters. We applied the method to the network Laplacian, defined as follows:

$$\boldsymbol{L} = \boldsymbol{D} - \boldsymbol{A}$$

A being the adjacency matrix and D the degree matrix, i.e. a diagonal matrix whose diagonal is the degree vector. The eigenvalue decomposition is applied to the laplacian L: the eigenvector corresponding to the second minor of eigenvalue v2 is of interest for the clustering partition. Considering the partition in two clusters, for instance, nodes are divided into the two clusters according to the sign of the corresponding components of the vector v2.

The partition is binary and hierarchical; the number of cluster (power of 2) is an input value.

In this work, we partitioned the structures into two clusters, so we applied just once the spectral clustering algorithm to the PCNs.

Once the network clustering has been applied, it is possible to derive a clustering descriptor, the participation coefficient Pi, for the i-th residue (node) defined as:

$$P_i = 1 - \left(\frac{k_{si}}{k_i}\right)^2$$

k_{si} is the i node degree including only links with nodes belonging to the same cluster s and k_i the node i degree.

Thus, P addresses the role of nodes in signal transmission between different clusters (domains in PCNs).

Abbreviations
SNPs: Single nucleotide polymorphisms; Aro: Recombinant human aromatase; FTIR: Fourier transform infrared spectroscopy; ATR: Attenuated total reflectance; ANS: 8-Anilino-1-naphthalenesulfonic acid; PCNs: Protein contact networks

Acknowledgements
Not applicable.

Authors' contributions
G.D.N. and A.D.V.: designed the experiments, interpreted the data and contributed to manuscript writing; C.Z.: contributed to engineering the mutants, purified and characterized the wild type and the mutants; E.N.: designed, performed and interpreted fluorescence experiments; C.S.: designed, performed and interpreted the FT/IR experiments; L.D.P.: designed, performed and interpreted Contact network analysis and contributed to manuscript writing; G. G and G.M.: designed the research project, designed the experiments, interpreted the data and contributed to manuscript writing. The authors read and approved the final manuscript.

Authors' information
Not applicable.

Funding
Not applicable.

Availability of data and materials
Not applicable.

Declarations

Ethics approval and consent to participate
Not applicable.

Consent for publication
Not applicable.

Competing interests
The authors declare that they have no competing interests.

Author details
[1]Dipartimento di Scienze della Vita e Biologia dei Sistemi, Università di Torino, Via Accademia Albertina 13, 10123 Turin, Italy. [2]Dipartimento di Medicina Sperimentale, Università di Roma Tor Vergata, Via Montpellier 1, 00133 Rome, Italy. [3]Dipartimento di Ingegneria, Unità di Fondamenti Chimico-Fisici dell'Ingegneria Chimica, Università Campus Bio-Medico di Roma, via Álvaro del Portillo 21, 00128 Rome, Italy.

Received: 3 April 2021 Accepted: 8 April 2021
Published online: 26 April 2021

References

1. Cojocaru V, Peter JW, Wade RC. The ins and outs of cytochrome P450s. Biochim Biophys Acta. 2007;1770:90–401.
2. Poulos TL. Cytochrome P450 flexibility. PNAS. 2003;100(23):13121–2. https://doi.org/10.1073/pnas.2336095100.
3. Pochapsky TC, Kazanis S, Dang M. Conformational plasticity and structure/function relationships in cytochromes P450. Antioxid Redox Signal. 2010;13(8):1273–96. https://doi.org/10.1089/ars.2010.3109.
4. Di Nardo G, Gilardi G. Human aromatase: perspectives in biochemistry and biotechnology. Biotechnol Appl Biochem. 2013;60(1):92–101. https://doi.org/10.1002/bab.1088.
5. Patel S. Disruption of aromatase homeostasis as the cause of a multiplicity of ailments: a comprehensive review. J Steroid Biochem Mol Biol. 2017;168:19–25. https://doi.org/10.1016/j.jsbmb.2017.01.009.
6. Baravalle R, Di Nardo G, Bandino A, Barone I, Catalano S, Andò S, et al. Impact of R264C and R264H polymorphisms in human aromatase function. J Steroid Biochem Mol Biol. 2017;167:23–32. https://doi.org/10.1016/j.jsbmb.2016.09.022.
7. Parween S, Di Nardo G, Baj F, Zhang C, Gilardi G, Pandey AV. Differential effects of variations in human P450 oxidoreductase on the aromatase activity of CYP19A1 polymorphisms R264C and R264H. J Steroid Biochem Mol Biol. 2020;196:105507. https://doi.org/10.1016/j.jsbmb.2019.105507.
8. Di Nardo G, Breitner M, Sadeghi SJ, Castrignanò S, Mei G, Di Venere A, et al. Dynamics and flexibility of human aromatase probed by FTIR and time resolved fluorescence spectroscopy. PLoS One. 2013;8(12):e82118. https://doi.org/10.1371/journal.pone.0082118.
9. Di Paola L, Mei G, Di Venere A, Giuliani A. Exploring the stability of dimers through protein structure topology. Curr Protein Pept Sci. 2016;17(1):30–6. https://doi.org/10.2174/1389203716666150923104054.
10. Minicozzi V, Di Venere A, Nicolai E, Giuliani A, Caccuri AM, Di Paola L, et al. Non-symmetrical structural behavior of a symmetric protein: the case of homo-trimeric TRAF2 (tumor necrosis factor-receptor associated factor 2). J Biomol Struct Dyn. 2020;13:1–11.
11. Di Paola L, Giuliani A. Protein contact network topology: a natural language for allostery. Curr Opin Struct Biol. 2015;31:43–8. https://doi.org/10.1016/j.sbi.2015.03.001.
12. Di Paola L, Mei G, Di Venere A, Giuliani A. Disclosing allostery through protein contact networks. Methods Mol Biol. 2021;2253:7–20. https://doi.org/10.1007/978-1-0716-1154-8_2.
13. Platania CB, Di Paola L, Leggio GM, Romano GL, Drago F, Salomone S, et al. Molecular features of interaction between VEGFA and anti-angiogenic drugs used in retinal diseases: a computational approach. Front Pharmacol. 2015;6:248.
14. Di Paola L, Hadi-Alijanvand H, Song X, Hu G, Giuliani A. The discovery of a putative allosteric site in SARS-CoV-2 spike protein by an integrated structural/dynamic approach. J Proteosome Res. 2020;19(11):4576–86. https://doi.org/10.1021/acs.jproteome.0c00273.
15. Yu S, Fan F, Flores FC, Mei F, Cheng X. Dissecting the mechanism of Epac activation via hydrogen-deuterium exchange FT-IR and structural modelling. Biochemistry. 2006;45(51):15318–26. https://doi.org/10.1021/bi061701x.
16. Kim KS, Fuchs JA, Woodward CK. Hydrogen exchange identifies native-state motional domains important in protein folding. Biochemistry. 1993;32(37):9600–8. https://doi.org/10.1021/bi00088a012.
17. de Jongh HH, Goormaghtigh E, Ruysschaert JM. Tertiary stability of native and methionine-80 modified cytochrome c detected by proton-deuterium exchange using on-line Fourier transform infrared spectroscopy. Biochemistry. 1995;34(1):172–9. https://doi.org/10.1021/bi00001a021.
18. Li J, Cheng X, Lee JC. Structure and dynamics of the modular halves of Escherichia coli cyclic AMP receptor protein. Biochemistry. 2002;41(50):14771–8. https://doi.org/10.1021/bi026383q.
19. Cantor CH, Schimmel PR. Biophysical chemistry Vol. II. San Francisco: W.H. Freeman and Company; 1980.
20. Lakowicz JR. Principles of fluorescence spectroscopy. New York: Kluwer Academic/Plenum Publishers; 1999. https://doi.org/10.1007/978-1-4757-3061-6.
21. Kim KH, Yun S, Lee EK. Thermodynamic analysis of ANS binding to partially unfolded α-lactalbumin: correlation of endothermic to exothermic changeover with formation of authentic molten globules. J Mol Recognit. 2016;29(9):446–51. https://doi.org/10.1002/jmr.2543.
22. Varriale A, Marabotti A, Mei G, Staiano M, D'Auria S. Correlation spectroscopy and molecular dynamics simulations to study the structural features of proteins. PLoS One. 2013;8(6):e64840. https://doi.org/10.1371/journal.pone.0064840.
23. Ceccarelli A, Di Venere A, Nicolai E, De Luca A, Minicozzi V, Rosato N, et al. TNFR-associated factor-2 (TRAF2): not only a trimer. Biochemistry. 2015;54(40):6153–61. https://doi.org/10.1021/acs.biochem.5b00674.
24. Benítez-Rangel E, Rodríguez-Hernández A, Velasco-García R. The substrate of the glucose-6-phosphate dehydrogenase of Pseudomonas aeruginosa provides structural stability. Biochim Biophys Acta, Proteins Proteomics. 1868;2020:140331.
25. Di Nardo G, Cimicata G, Baravalle R, Dell'Angelo V, Ciaramella A, Catucci G, et al. Working at the membrane interface: ligand-induced changes in dynamic conformation and oligomeric structure in human aromatase. Biotechnol Appl Biochem. 2018;65(1):46–53. https://doi.org/10.1002/bab.1613.
26. Sgrignani J, Magistrato A. Influence of the membrane lipophilic environment on the structure and on the substrate access/egress routes of

the human aromatase enzyme. A computational study. J. Chem. Inf. Model. 2012;52:1595–606.
27. Lewis W. Polymorphism of Human Enzyme Proteins. Nature. 1971;230(5291): 215–8. https://doi.org/10.1038/230215a0.
28. Amelio I, Bertolo R, Bove P, Candi E, Chiocchi M, Cipriani C, et al. Cancer predictive studies. Biol Direct. 2020;15(1):18. https://doi.org/10.1186/s13062-020-00274-3.
29. Mihaylov I, Kańdula M, Krachunov M, Vassilev D. A novel framework for horizontal and vertical data integration in cancer studies with application to survival time prediction models. Biol Direct. 2019;14(1):22. https://doi.org/10.1186/s13062-019-0249-6.
30. Werner J, Géron A, Kerssemakers J, Matallana-Surget S. mPies: a novel metaproteomics tool for the creation of relevant protein databases and automatized protein annotation. Biol Direct. 2019;14(1):21. https://doi.org/10.1186/s13062-019-0253-x.
31. Han Y, Ye X, Wang C, Liu Y, Zhang S, Feng W, et al. Integration of molecular features with clinical information for predicting outcomes for neuroblastoma patients. Biol Direct. 2019;14(1):16. https://doi.org/10.1186/s13062-019-0244-y.
32. Han Y, Ye X, Cheng J, Zhang S, Feng W, Han Z, et al. Integrative analysis based on survival associated co-expression gene modules for predicting neuroblastoma patients' survival time. Biol Direct. 2019;14(1):4. https://doi.org/10.1186/s13062-018-0229-2.
33. Kim SY, Jeong HH, Kim J, Moon JH, Sohn KA. Robust pathway-based multi-omics data integration using directed random walks for survival prediction in multiple cancer studies. Biol Direct. 2019;14(1):8. https://doi.org/10.1186/s13062-019-0239-8.
34. Chierici M, Francescatto M, Bussola N, Jurman G, Furlanello C. Predictability of drug-induced liver injury by machine learning. Biol Direct. 2020;15(1):3. https://doi.org/10.1186/s13062-020-0259-4.
35. Liu L, Wang G, Wang L, Yu C, Li M, Song S, et al. Computational identification and characterization of glioma candidate biomarkers through multi-omics integrative profiling. Biol Direct. 2020;15(1):10. https://doi.org/10.1186/s13062-020-00264-5.
36. Adhikari N, Amin SA, Saha A, Jha T. Combating breast cancer with non-steroidal aromatase inhibitors (NSAIs): understanding the chemico-biological interactions through comparative SAR/QSAR study. Eur J Med Chem. 2017; 137:365–438. https://doi.org/10.1016/j.ejmech.2017.05.041.
37. Ghosh D, Griswold J, Erman M, Pangborn W. Structural basis for androgen specificity and oestrogen synthesis in human aromatase. Nature. 2009; 457(7226):219–23. https://doi.org/10.1038/nature07614.
38. Lo J, Di Nardo G, Griswold J, Egbuta C, Jiang W, Gilardi G, et al. Structural basis for the functional roles of critical residues in human cytochrome P450 aromatase. Biochemistry. 2013;52(34):5821–9. https://doi.org/10.1021/bi400669h.
39. Jiang W, Ghosh D. Motion and flexibility in human cytochrome p450 aromatase. PLoS One. 2013;7:e32565.
40. Park J, Czapla L, Amaro RE. Molecular simulations of aromatase reveal new insights into the mechanism of ligand binding. J Chem Inf Model. 2013; 53(8):2047–56. https://doi.org/10.1021/ci400225w.
41. Di Nardo G, Dell'Angelo V, Catucci G, Sadeghi SJ, Gilardi G. Subtle structural changes in the Asp251Gly/Gln307His P450 BM3 mutant responsible for new activity toward diclofenac, tolbutamide and ibuprofen. Arch Biochem Biophys. 2016;602:106–15. https://doi.org/10.1016/j.abb.2015.12.005.

Publisher's Note

Chapter 6

Molecular basis for endocrine disruption by pesticides targeting aromatase and estrogen receptor

International Journal of
Environmental Research and Public Health

MDPI

Article

Molecular Basis for Endocrine Disruption by Pesticides Targeting Aromatase and Estrogen Receptor

Chao Zhang [1], Tiziana Schilirò [2], Marta Gea [2], Silvia Bianchi [1], Angelo Spinello [3], Alessandra Magistrato [3], Gianfranco Gilardi [1] and Giovanna Di Nardo [1,*]

1 Department of Life Sciences and Systems Biology, University of Torino, 10123 Torino, Italy; chao.zhang@unito.it (C.Z.); silvia.bianchi.04@hotmail.it (S.B.); gianfranco.gilardi@unito.it (G.G.)
2 Department of Public Health and Pediatrics, University of Torino, 10126 Torino, Italy; tiziana.schiliro@unito.it (T.S.); marta.gea@unito.it (M.G.)
3 National Research Council-Institute of Materials (CNR-IOM) at International School for Advanced Studies (SISSA), 34165 Trieste, Italy; angelo.spinello@sissa.it (A.S.); alessandra.magistrato@sissa.it (A.M.)
* Correspondence: giovanna.dinardo@unito.it; Tel.: +390-116-704-689

Received: 10 July 2020; Accepted: 3 August 2020; Published: 5 August 2020

Abstract: The intensive use of pesticides has led to their increasing presence in water, soil, and agricultural products. Mounting evidence indicates that some pesticides may be endocrine disrupting chemicals (EDCs), being therefore harmful for the human health and the environment. In this study, three pesticides, glyphosate, thiacloprid, and imidacloprid, were tested for their ability to interfere with estrogen biosynthesis and/or signaling, to evaluate their potential action as EDCs. Among the tested compounds, only glyphosate inhibited aromatase activity (up to 30%) via a non-competitive inhibition or a mixed inhibition mechanism depending on the concentration applied. Then, the ability of the three pesticides to induce an estrogenic activity was tested in MELN cells. When compared to 17β-estradiol, thiacloprid and imidacloprid induced an estrogenic activity at the highest concentrations tested with a relative potency of 5.4×10^{-10} and 3.7×10^{-9}, respectively. Molecular dynamics and docking simulations predicted the potential binding sites and the binding mode of the three pesticides on the structure of the two key targets, providing a rational for their mechanism as EDCs. The results demonstrate that the three pesticides are potential EDCs as glyphosate acts as an aromatase inhibitor, whereas imidacloprid and thiacloprid can interfere with estrogen induced signaling.

Keywords: aromatase; estrogen receptor; endocrine disrupting chemical; pesticides; neonicotinoids; estrogenic activity; gene reporter assay; MELN allosteric inhibition; molecular dynamics

1. Introduction

Under the modern lifestyle, humans are exposed to various chemicals such as pesticide residuals in fruits and vegetables, antibiotics in meat and milk, preservatives in cosmetics and personal care products [1,2]. These chemicals are usually in low doses and may not have a short term significant impact on the human body, but they can cause long term damages to health [3]. The effects of low-dose compounds on human health are mainly related to the endocrine system [4–6]. These compounds can in fact mimic or influence the action of endogenous hormones through various mechanisms, being therefore referred to as endocrine disrupting chemicals (EDCs) [7,8].

The modern industrial and agricultural system relies heavily on pesticides. The compelling need of high food crop increasingly demands the use of chemicals. This results in the extensive applications of millions of tons of pesticides every year [9,10]. Among the many pesticides available on the market, glyphosate is one of the most widely used herbicides in the world. In plants, it affects the synthesis

of essential aromatic amino acids by inhibiting the activity of 5-enolpyruvylshikimate-3-phosphate synthase (EPSPS) in the shikimate pathway [11]. As a result, glyphosate is considered harmless to mammals since they do not contain the EPSPS enzyme [12]. Conversely, neonicotinoids are currently the most widely used agricultural insecticides [13]. These selective insecticides specifically bind to the α -subunit of nicotinic acetylcholine receptors (nAChR), which is common in all insects [14,15]. Due to their difficulty to penetrate the blood-brain barrier, they should exert low toxicity in vertebrates. However, different direct, indirect, and suspect toxic effects of these compounds on vertebrate wildlife and human health have been reported [16–18]. Neonicotinoids were introduced in the market in the 1990s, therefore their sales volume has enormously proliferated in recent decades, exceeding 25% of the market in 2010 [19]. Imidacloprid has become the world's best-selling insecticide next to glyphosate [20]. Although the European Union banned the outdoor application of imidacloprid, clothianidin, and thiamethoxam in 2018 due to a high risk for bees that are responsible for pollinating most crops worldwide [21], neonicotinoids remain the most extensively applied insecticides in the world [22].

The intensive use of glyphosate-based herbicides and neonicotinoid insecticides has caused the contamination of soil, water, air, and agricultural products [23–28]. The half-life of glyphosate in the field is usually 47 days and it is primarily degraded into aminomethylphosphonic acid (AMPA) and glyoxylic acid by soil microorganisms [29]. Neonicotinoids can exist for a long time in soil and water, and their half-life being as long as three years [22]. Given these observations and the increased use of pesticides, concerns are raising about their potential impact on human health and the environment. In particular, mounting evidence discloses that exposure to pesticides can affect the endocrine system. Toxicological and epidemiological studies indicate possible genotoxic and cytotoxic effects as well as birth defects and neurotoxicity in different cell lines and animal models [18,30].

Aiming at establishing the interference of pollutants with human health, we monitored the effect of glyphosate and two neonicotinoids on two critical targets of the endocrine system: Aromatase, the enzyme responsible for estrogen biosynthesis, and estrogen receptor (ER) alpha, the main protein promoting estrogen signaling.

Aromatase catalyzes the transformation of androgens to estrogens [31]. In vitro experiments showed that glyphosate causes changes of aromatase mRNA levels and activity in placental JEG3 cells and human HEK293 cells, thus interfering with steroid conversion to estradiol [32,33]. In addition, the expression of androgen and ERα was inhibited in glyphosate treated HepG2 cells [34,35] where also the transcription and activity of aromatase were altered [35]. Insecticides such as thiacloprid, thiamethoxam, and imidacloprid affect aromatase expression and activity in a co-culture model of fetoplacental steroidogenesis, increasing estrone and estradiol production, while estriol production is decreased [36]. Thiacloprid, imidacloprid, and thiamethoxam have also been demonstrated to increase aromatase expression and activity in H295R and Hs578t cells [37,38].

Here, a recombinant form of human aromatase is used to test the possible effect of the three pesticides on estrogen biosynthesis, gaining new information at molecular level [39–41]. Moreover, all-atom molecular dynamics simulations provided structural insights on the ability of these molecules to target the aromatase enzyme.

At a cellular level, the estrogen-regulated signaling is mainly due to estrogen receptors (ERs). The main ERs are the ERα and ERβ nuclear receptors and the G-protein-coupled estrogen receptor 1, which is a membrane receptor [42]. Estrogen receptor α (ERα) is a nuclear hormone receptor and a ligand-regulated transcription factor, which mediates the activity of estrogens in vital processes (i.e., reproduction, cardiovascular maintenance, bone density/remodeling). ERα is composed of five functional domains, among which the ligand-binding domain, activated upon estrogen binding, stimulates cell growth and proliferation. After the menopause, increased estrogen levels due to a deregulated activity of aromatase bind as an agonist to ERα, exerting a pro-oncogenic effect by either decreasing apoptosis or promoting cell proliferation [43]. Therefore, estrogen selective modulators

have been developed and one of them, tamoxifen, is extensively used in adjuvant therapy of breast cancer for its ability to act as an ERα antagonist.

Previous studies have investigated the ability of glyphosate to induce an estrogenic activity mediated by ERs. The results of the study of Thongprakaisang et al., 2013 [44] demonstrated that glyphosate induces an ER-mediated estrogenic activity, mediated by ER activation, similar to 17β-estradiol (E2) on T47D-KBluc cells. However, recently another study, using the same cells, showed that this pesticide induces an estrogenic activity, mediated by ER activation, lower than E2 and that this activation is probably induced by a ligand-independent mechanism [45]. Moreover, additional studies on different transfected cells showed that glyphosate did not induce any ER-mediated estrogenic activity and did not produce any anti-estrogenic effect when tested in combination with E2 [35,46]. Therefore, whether glyphosate can trigger an ER-mediated estrogenic activity remains controversial. To our knowledge, only three studies have been performed on the estrogenic activity of imidacloprid and thiacloprid. In particular, in the study of Mesnage et al., 2018 [47] the proliferative effect of both pesticides was investigated on estrogen-sensitive cells, while Kojima et al., 2004 [46] and Westlund and Yargeau, 2017 [48] assessed the ER-mediated estrogenic activity of imidacloprid and thiacloprid on mammalian or yeast cells, respectively. The results of the three studies demonstrated that the two pesticides induce no proliferative effect and no estrogenic activity was mediated by ERs, while an anti-estrogenic activity was detected testing imidacloprid in combination with E2 on yeast cells.

In this work, in order to increase the knowledge on the estrogenic activity of glyphosate, imidacloprid, and thiacloprid, the gene reporter assay on estrogen-sensitive human breast cancer MCF-7 cells transfected with the ERE-βGlob-Luc-SVNeo plasmid (MELN cells) is applied to test the three pesticides for their possible ER-mediated estrogenic activity.

Possible additive and/or antagonist effects are also investigated. Moreover, docking simulations provide atomic level insights on the potential binding mode of these molecules to the primary ligand (estrogen) binding site as well as to a peripheral allosteric site which may be responsible for the experimental observed additive effect of the pollutant with the endogenous ligand.

2. Materials and Methods

2.1. Materials

All reagents are analytically pure by purchase from Sigma-Aldrich (St. Louis, MO, USA). Stock solutions of chemical compounds were prepared in absolute ethanol or dimethyl sulfoxide (DMSO). Before each experiment, the test sample was diluted into a fresh buffer solution, and the final organic solvent concentration was less than 0.1%. The recombinant human aromatase (Aro) and the human recombinant cytochrome P450 reductase (hCPR) were expressed and purified as previously described [39,49].

2.2. ELISA Assay

An estrone direct competitive ELISA kit (BioVendor, Brno, Czech Republic) was used to evaluate the effect of pesticides on aromatase activity. Different reaction mixtures were set up by mixing 5 nM Aro, 5 nM hCPR, 0.5 mM NADPH, 50 nM androstenedione, and three concentrations of pesticides (500, 1000, and 1500 nM) in a 100 mM potassium buffer (KPi) containing 20% glycerol, 1 mM β-mercaptoethanol at pH 7.0. Reactions were carried out for 10 min at 30 °C, heat-inactivated for 10 min at 90 °C, and centrifuged for 10 min at 11,000 rpm. After centrifugation, the supernatant was diluted 1:8 in the Calibrator A provided by the ELISA kit and the product estrone quantified performing ELISA according to the manufacturer's instructions. Reactions in the presence of anastrozole or without hCPR were used as negative controls. The concentration of estrone was extrapolated from a calibration curve with known concentrations of estrone.

For the experiment where the catalytic parameters were derived, four substrate concentrations were applied in the reaction mixture (ranging from 25 to 250 nM) in the absence and presence of 1000 and 5000 nM of glyphosate.

2.3. Computational Studies

In order to explain the molecular terms for the action of glyphosate on the aromatase enzyme we docked it into the two possible allosteric sites previously identified [50]. Docking has been performed with the GLIDE software, release 2020-1 (Schrödinger, LLC, New York, NY, USA) using the single-precision protocol [51]. The two neonicotinoids, thiacloprid and imidacloprid, were instead docked into the ERαs active site, using as a starting structure the crystal structure of 17-β-estradiol (EST)-bound ERα dimer (PDB id: 1qku) [52]. In this structure, we have searched for putative allosteric pockets using the SiteMap algorithm [53].

In order to account for its flexibility of the receptor and since is flexibility resulted to be of paramount importance for the identification of novel allosteric inhibitors [54], we performed classical Molecular Dynamics (MD) simulations on the complex with the aromatase enzyme. We employed as a starting structure of our simulation the equilibrated enzyme model which was embedded in a mimic of a membrane bilayer by using the CHARMMGUI webserver [55]. This consisted of POPC (1-palmitoyl-2-oleoyl-sn-glycero-3-phosphocholine) and 6 wt% of cholesterol (CHL) in order to mimic the endoplasmic reticulum membrane. Physiological protonation states were calculated with the webserver H++ [56]. Asp309 was considered in its neutral form consistently with other literature studies [57]. The glyphosate molecule was considered in the most likely protonation state at physiological pH. According to literature data, the first protonation of the molecule occurs on its phosphate group [58].

The Parm99SB AMBER force field (FF) [59,60] and lipid14 FF [61] were used for the protein and the lipids, respectively.

The Shahrokh et al. parameters were used for the heme moiety and Cys437 [62]. Simulations were done in the presence of the substrate androstenedione (ASD) in the active site and of glyphosate in the allosteric pockets for which the general Amber FF (GAFF) was employed [63]. For the organic ligands the electrostatic potential (ESP) charges [64] were calculated by performing geometry optimization of the substrates at the Hartree-Fock level of theory using a 6-31G* basis set with the Gaussian 09 software (Gaussian Inc., Wallingford, CT, USA) [65]. These were later transformed in RESP charges by using the Antechamber tool [66].

The system was then explicitly solvated using the TIP3P water model, leading to a total of 131,454 atoms. Topology, built with AmberTools 18, was later converted in a GROMACS format using the acpype algorithm [67]. MD simulations were performed with GROMACS 5.0.4 [68]. An integration time step of 2 fs was used and all covalent bonds involving hydrogen atoms were constrained with the LINCS algorithm. The Particle Mesh Ewald algorithm [69] was used in order to account for electrostatic interactions. Simulations were done in the isothermal-isobaric NPT ensemble, at a temperature of 300 K, using a velocity-rescaling thermostat [70]. Preliminary energy minimization was done with the steepest descend algorithm.

An initial equilibration of the membrane was performed for 100 ns with the protein atoms harmonically restrained with a force constant of 1000 kJ mol^{-1} nm^{-2}, reaching a constant value ($92 \times 92 \times 151$ $Å^3$) of the simulation box size. Constraints were then slowly released, and the system was thermalized to the target temperature of 300 K in about 10 ns. Then, the aromatase in complex with glyphosate was relaxed by performing a 100 ns MD simulation rescaling the motion of the center of mass of aromatase and the ligand, followed by an unbiased 100 ns MD simulation.

2.4. MELN cell Culture

MELN cells were provided by Dr. P. Balaguer (INSERM, Montpellier, France). They are estrogen-sensitive human breast cancer cells (MCF-7) transfected with the ERE-βGlob-Luc-SVNeo plasmid (ERE-*β*Glob-Luc-SVNeo) [71,72]. The integrated plasmid contains a luciferase reporter gene, the estrogen-responsive elements (ERE) and an antibiotic resistance selection gene (SVNeo). MELN cells were cultured at 37 °C and 5% CO_2 in Dulbecco's Modified Eagle's Medium Nutrient Mixture F12-Ham (DMEM-F12), supplemented with phenol red, fetal bovine serum (FBS) (5% v/v), L-glutamine (4 mM), penicillin-streptomycin (100 U/mL–100 μg/mL), and G418 (1 mg/mL).

2.5. MELN Gene Reporter Assay

The assay was carried out as described by Balaguer et al., 1999 [73] with slight modifications [74]. For three days the cells were adapted to a test medium: DMEM-F12 without phenol red and supplemented with dextran-coated charcoal-treated FBS (5% v/v), L-glutamine (4 mM), and penicillin-streptomycin (100 U/mL-100 µg/mL). Then, the cells were seeded at a density of 40,000 cells/well, in 96-well plates (100 µL/well). After 24 h, the test medium of each well was replaced with a test medium containing pesticides (100 µL/wells), and the cells were incubated for 16 h. After the incubation, the luciferase activity was assessed adding 100 µL/well of the One Glo Reagent (One-Glo Luciferase Assay System, Promega, Madison, USA), mixing (5 min) and measuring the luminescence of each well by a luminometer (Infinite Reader M200 Pro, Tecan, Männedorf, Switzerland).

The stock solutions of thiacloprid and imidacloprid were prepared in DMSO, while the stock solution of glyphosate was prepared in a test medium. The stock solutions were stored at −20 °C and, shortly before exposure, different concentrations of pesticides were prepared in a test medium (glyphosate and imidacloprid: From 10^{-8} to 10^{-3} M; thiacloprid from 10^{-8} to 5×10^{-4} M, due to lower solubility). The final DMSO concentration was less than 0.1%. Cells exposed to the test medium were used as a negative control and five concentrations of E2 (from 10^{-12} to 10^{-8} M) were tested to obtain a standard positive curve of the reference compound (E2).

The estrogenic activity was calculated as the ratio of the activity induced by the treatment over the activity induced by the positive control with 17-βestradiol (E2). It was expressed in percentage considering the relative luciferase activity of E2 (10^{-8} M) as 100%. Since all experiments were performed in quadruplicate (four wells for each experimental condition), the estrogenic activity was expressed as the mean and standard deviation of four values. The estrogenic activity of pesticides was also evaluated by the determination of the relative potency of each pesticide in comparison with the reference compound (E2) and it was expressed as the E2 equivalency factor (EEF) [75]. The EEF was calculated using the concentrations of E2 and pesticides at which 50% of biological effect is achieved (EC50) through the formula: EEF = E2 EC50/pesticide EC50.

Three concentrations of pesticides (10^{-5}, 2.5×10^{-4}, and 5×10^{-4} M) were also tested: In combination with an ER-antagonist (tamoxifen 10^{-6} M), in order to confirm whether the observed effects were due to the ER activation, and in combination with E2 (10^{-10} M), in order to investigate the interaction between pesticides and E2 in MELN cells. The estrogenic activity of these treatments was expressed as relative luciferase activity and it was calculated as percentage of activity induced by the treatment with respect to the activity induced by the E2 10^{-10} M (relative luciferase activity of E2 10^{-10} M = 100%). The stock solutions of E2 and tamoxifen were prepared in ethanol and stored at −20 °C.

2.6. Data Analysis

Statistical analysis was performed using IBM SPSS Statistics 25.0 (IBM, Armonk, USA). The EC50 of E2 and pesticides was calculated by dose–response curves, which were estimated through a probit regression between the relative luciferase activity and Log transformed-concentrations of E2 or pesticides.

Data collected with the MELN gene reporter assay were not normally distributed, so the non-parametric Kruskal-Wallis test followed by the post-hoc Dunnett test was used to assess significant differences among the different experimental conditions. The differences were considered significant with p-value < 0.05.

3. Results

3.1. Effect of Pesticides on Aromatase Activity

In order to study the effect of pesticide compounds on aromatase activity, a direct competitive estrone ELISA was performed using the purified cytochrome P450 reductase (CPR), as an electron donor from NADPH, and aromatase. The aromatase activity was evaluated by measuring the estrone production in the absence and presence of three different concentrations of pesticides (0.5, 1, and 5 µM). As a control, anastrozole, a known aromatase inhibitor, was applied at a concentration of 1000 nM

and the residual aromatase activity detected was 0.7%. As can be seen in Table 1, glyphosate partially reduced the aromatase activity at the concentrations tested. The enzyme activity decreased with the increase of glyphosate concentration. When adding 5 µM of glyphosate, the residual aromatase activity was 36%. Unlike glyphosate, imidacloprid and thiacloprid did not inhibit the enzyme activity (Table 1).

Table 1. Effect of pesticides on the aromatase activity.

	Pesticide	Relative Activity (%)		
		500 nM	1000 nM	5000 nM
1	Glyphosate	76.6 ± 11.3 *	74.5 ± 7.6 *	36.0 ± 19.5 *
2	Imidacloprid	100.1 ± 8.8	92.9 ± 28.0	120.5 ± 17.6
3	Thiacloprid	100.9 ± 11.9	153.6 ± 56.9	146.9 ± 42.1

Statistical significance *: p-value < 0.05 versus positive control (C^+).

3.2. Effect of Glyphosate Concentration on Aromatase Activity

The effect of glyphosate on aromatase activity was further studied by exploring the concentration range of glyphosate applied from 50 to 1500 nM. Such concentrations of glyphosate were selected since they resemble the ones detected in human urine samples [76]. The experiment was carried out by the ELISA assay at the concentration of 50 and 400 nM androstenedione, respectively. The two different concentrations were chosen on the basis of the kinetic parameters of aromatase: The first one (50 nM) is close to the enzyme K_M and the second one (400 nM) is saturating the enzyme (see next paragraph).

As shown in Figure 1, the activity of Aro is inhibited by 30% when the glyphosate concentration is ≥1000 nM. However, when the substrate concentration is 50 nM (black squares in Figure 1), the maximal inhibitory effect is already achieved when the glyphosate concentration is 100 nM. Therefore, the inhibitory effect of glyphosate strongly depends on the substrate concentration and it is only partial, indicating that this compound can be considered as a weak inhibitor.

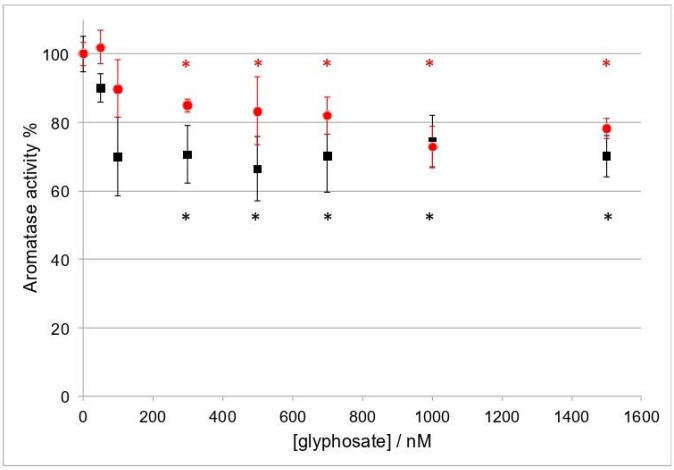

Figure 1. Aromatase activity in the presence of different concentrations of glyphosate and 50 nM (black squares) or 400 nM (red circles) of the substrate androstenedione. Statistical significance *: p-value < 0.05 versus C^+.

3.3. Effect of Glyphosate on the Catalytic Parameters of Aro

In order to investigate the mechanism of aromatase inhibition by glyphosate, the kinetic parameters of the enzyme were evaluated using the estrone ELISA assay in the absence and presence of two different concentrations of the pesticide (1000 and 5000 nM). Different substrate concentrations were applied and the product formation rate was plotted as a function of the substrate concentration (Figure 2A). The plot showed hyperbolic trends and the catalytic parameters, shown in Table 2, were obtained by fitting the experimental data to the Michaelis-Menten equation.

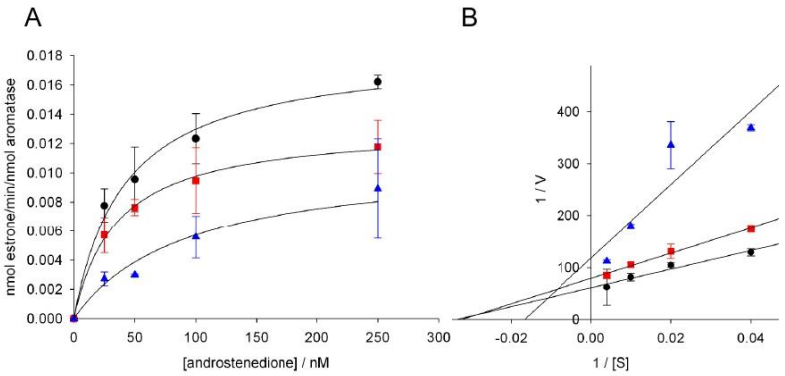

Figure 2. (**A**) Michaelis-Menten plots and (**B**) Lineweaver-Burk linearization for aromatase activity in the absence (black circles) and presence of 1000 nM (red squares) and 5000 nM (blue triangles) of glyphosate. In Panel (**A**), the data were fitted to the Michaelis-Menten equation using the Sigma Plot software to obtain the kinetic parameters.

When glyphosate is not present, the resulting K_M and V_{max} are 41.3 ± 8.2 nM and 0.018 ± 0.001 min^{-1}, respectively. When 1000 nM of glyphosate was added, the V_{max} value was significantly decreased whereas the K_M value was not significantly affected. Interestingly, when the glyphosate concentration was increased to 5000 nM, both K_M and V_{max} were affected. Compared to the reaction without glyphosate, K_M was increased by 2.2 folds, while V_{max} was decreased to 0.011 ± 0.002 min^{-1} (Table 2).

Table 2. Kinetic parameters obtained from the fitting of the data in Figure 2A to a Michaelis-Menten curve. The kinetic parameters are calculated for aromatase activity in the absence and presence of 1000 and 5000 nM of glyphosate.

Glyphosate (nM)	K_M (nM)	V_{max} (min^{-1})
0	41.3 ± 8.2	0.018 ± 0.001
1000	35.3 ± 3.5	0.013 ± 0.001 *
5000	92.3 ± 20.7 *	0.011 ± 0.002 *

Statistical significance*: p-value < 0.05 versus the values obtained in the absence of glyphosate.

The kinetic parameters show that the type of inhibition of aromatase by glyphosate depends on the herbicide concentration applied. Indeed, when using 1000 nM of glyphosate, the V_{max} was decreased while K_M did not change, indicating a non-competitive inhibition mechanism, meaning that, at this concentration, glyphosate does not compete with the substrate and binds to a site different from that where the substrate binds. When the concentration of glyphosate was increased to 5000 nM, both K_M and V_{max} were affected, and the Lineweaver-Burk plot shows a trend typical of a mixed inhibition mechanism (Figure 2B). Mixed inhibition is considered a more general case of

non-competitive inhibition, in which the inhibitor exhibits unequal affinity for the free enzyme and for the enzyme-substrate complex.

3.4. Molecular Dynamics Simulations on Aromatase

Grounding on recent evidence demonstrating the existence of allosteric binding sites [50] and their possible exploitation for a non-competitive/mixed inhibition mechanism [54] we docked glyphosate into the two allosteric cavities. Namely, we docked it to Site 1, which lies along the most relevant access channel to the enzyme active site [77] and to Site 2, which instead lies at the interface with the cytochrome P450 reductase (CPR), supplying the electrons necessary for catalysis (Figure 3) [78]. In the docking pose in Site 1 and during MD simulations glyphosate engages a salt bridge interaction with its phosphate group and Arg192, as well as the formation of a hydrogen (H)-bond between Gln218 and the carboxylic group of the pesticide. Most importantly, the phosphate group of glyphosate makes up to two simultaneous H-bonds with Asp309 (Figure 3), which normally is engaged in stabilizing the binding of aromatase substrates.

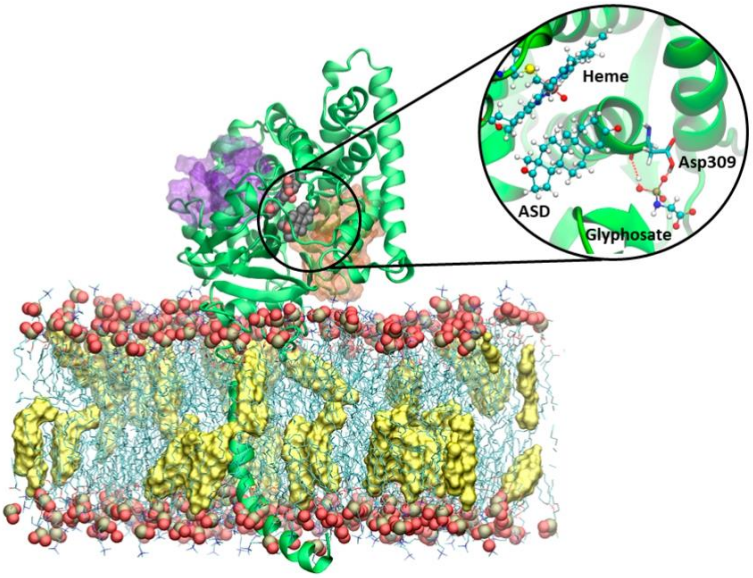

Figure 3. Representative structure of aromatase embedded in a POPC (1-palmitoyl-2-oleoyl-sn-glycero-3-phosphocholine) membrane, with phosphorous and oxygen atoms shown as tan and red van der Waals (vdw) spheres, and cholesterol (yellow surface) membrane. Sites 1 and 2 are shown as orange and purple transparent surfaces, respectively. The heme and androstenedione (ASD) are displayed in a vdw representation. The protein is shown as green new cartoons. The inset reports a close view of structure of aromatase in complex with glyphosate, as obtained from the most representative cluster of the molecular dynamics simulation trajectory. The heme moiety, ASD, and glyphosate are depicted in balls and sticks. The key catalytic residue Asp309, lining the binding cavity, is shown in licorice and colored by the atom name.

Due to these interactions the molecule remains stably bound in the pocket for the whole MD simulation, in line with its inhibitory activity in the μM range. Remarkably, it was recently suggested that the binding of a small molecule in Site 1 triggered the displacement of the water molecule needed

for the catalytic activity, which are normally H-bonding with the Asp309 and Arg192 residues, both being critical residues for the catalytic activity [41,57], thus inhibiting estrogen biosynthesis. Conversely, the docking pose obtained in Site 2, did not establish any relevant H-bond/salt bridge. As a result, the glyphosate dissociated from the pocket within the first few ns of MD simulations.

3.5. Detection of Estrogenic Activity with the MELN Gene Reporter Assay

The MELN gene reporter assay was carried out to evaluate the estrogenic activity of glyphosate, imidacloprid, and thiacloprid on MELN cells. In this study, different concentrations of each pesticide were tested. Concentrations similar to the pesticide levels measured in human urine [76] were selected as the lowest concentrations (10^{-8} and 10^{-7} M), while concentrations up to 10^{-3} M were selected as the highest concentrations, in order to assess the effect induced by each pesticide in a wide range of concentrations.

Our results showed that glyphosate did not increase the relative luciferase activity with respect to the negative control; therefore no estrogenic activity was detected testing this pesticide on MELN cells (Figure 4). On the contrary, the highest concentrations of glyphosate induced a small decrease of the relative luciferase activity, which may be due to a toxic effect of the pesticide on cells.

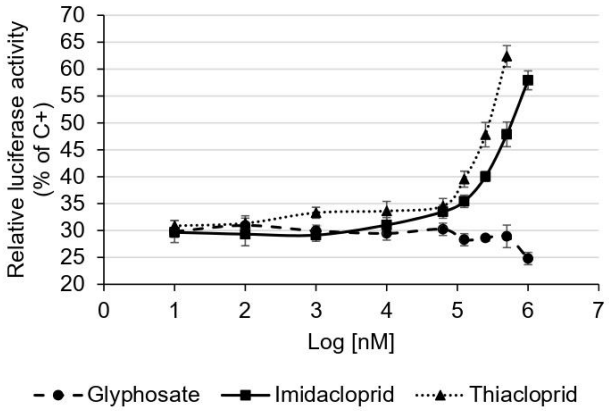

Figure 4. Estrogenic activity of pesticides measured with the MELN gene reporter assay. Data are expressed as means and standard deviations of the relative luciferase activity (% of C+, E2 10^{-8} M). The relative luciferase activity of the C+ is 100.0 ± 5.9%, while the relative luciferase activity of the negative control (test medium) is 30.5 ± 1.1%.

The null estrogenic activity induced by glyphosate was confirmed also by the exposure of cells to glyphosate in combination with tamoxifen (ER-antagonist) or with E2. Indeed, the wells treated with glyphosate and tamoxifen showed a relative luciferase activity equal to the wells treated with tamoxifen alone, and the wells treated with glyphosate and E2 showed a relative luciferase activity equal to the wells treated with E2 alone (data not shown). These results suggest that glyphosate does not interfere with the binding between ER and E2.

Regarding the neonicotinoid pesticides, in the present study, imidacloprid and thiacloprid significantly increased the relative luciferase activity with respect to the negative control, starting from 6.3×10^{-5} M (Log[nM] = 4.79) and 10^{-6} M (Log[nM] = 3), respectively (Kruskal-Wallis test followed by the post-hoc Dunnett test, $p < 0.05$). Since both the neonicotinoid pesticides induced a dose-dependent increase of the relative luciferase activity, in particular from 10^{-4} M (Log[nM] = 5) to the highest tested dose (Figure 4), a significant estrogenic activity of these two pesticides was detected on MELN cells.

The estrogenic activity of imidacloprid and thiacloprid was also quantitatively evaluated by the estimate of the concentrations of E2 and pesticides at which 50% of biological effect is achieved (EC50) and the E2 equivalency factor (EEF). The EC50 of E2 and pesticides was calculated by dose-response curves whereas the EEF was calculated through the formula: EEF = E2 EC50/pesticide EC50. The EC50 of imidacloprid and thiacloprid was 1.0×10^{-2} M (IC 95% 1.7×10^{-3}–2.2×10^{-1} M) and 1.5×10^{-3} M (IC 95% 2.5×10^{-4}–3.6×10^{-2} M), respectively, while the EEF was 5.4×10^{-10} (IC 95% 3.3×10^{-9}–2.5×10^{-11}) and 3.7×10^{-9} (IC 95% 2.2×10^{-8}–1.5×10^{-10}), respectively.

The exposure of cells to imidacloprid and thiacloprid in combination with tamoxifen confirmed that the estrogenic activity of the two pesticides was induced by the activation of ER. Indeed, the wells treated with the neonicotinoid pesticides and tamoxifen showed a relative luciferase activity that was lower compared to the wells treated with these pesticides alone. Furthermore, the relative luciferase activity of wells treated with the neonicotinoid pesticides and tamoxifen was similar to the relative luciferase activity measured in the negative control (Figure 5A,C).

Finally, the exposure of cells to imidacloprid and thiacloprid in combination with E2 induced an increase of the relative luciferase activity with respect to the E2 alone (Figure 5B,D). The increase was slight for imidacloprid while it was stronger for thiacloprid, suggesting a possible additive effect exerted by these pesticides in combination with E2.

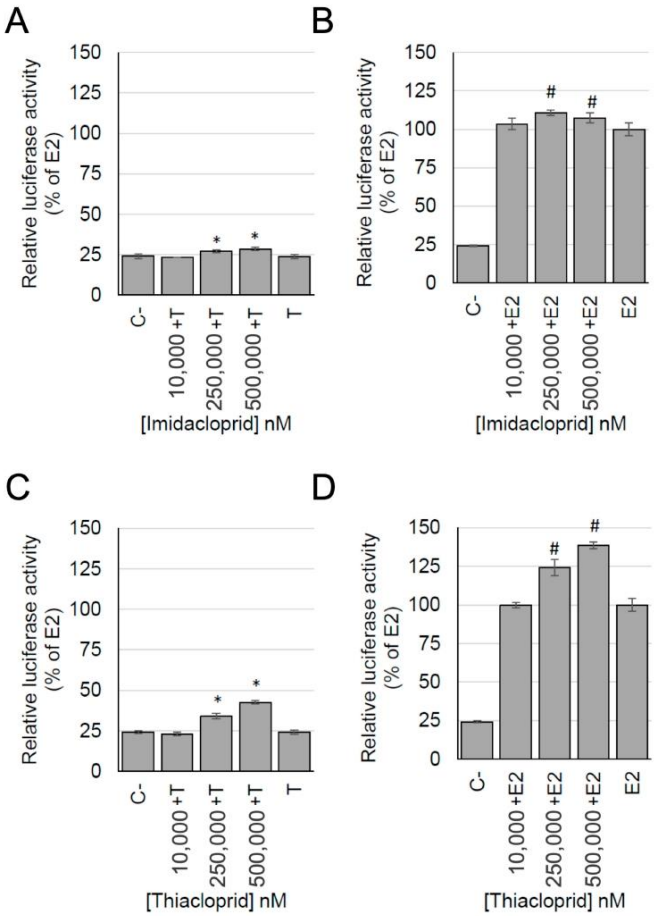

Figure 5. Estrogenic activity, measured with the MELN gene reporter assay, of imidacloprid (**A**,**B**) and thiacloprid (**C**,**D**) in combination with E2 (10^{-10} M) (**B**,**D**) or in combination with tamoxifen (10^{-6} M) (**A**,**C**). Data are expressed as the relative luciferase activity (% of E2 10^{-10} M). C−: Negative control; E2: E2 10^{-10} M; T: Tamoxifen 10^{-6} M. * $p < 0.05$ vs. C−; # $p < 0.05$ vs. E2; Kruskal-Wallis test followed by the post-hoc Dunnett test.

3.6. Docking Calculation on ERα

In order to provide a rationale for the estrogenic activity exerted by the two neonicotinoids, thiacloprid and imidacloprid, we have performed docking calculations on ERα. First, the two molecules were docked into the ERαs estrogen binding site, using the crystal structure of 17-β-estradiol bound to the ERα dimer (PDB id: 1qku) [52]. Both neonicotinoids fit inside the estrogen binding pocket (Figure 6). In particular, imidacloprid forms a H-bond with the backbone of Gly521, while in thiacloprid, the Cl atom makes halogen bonds with the guanidinium group of Arg394 and the aromatic rings of Phe404

and Trp393. Halogen bonds are attractive interactions between the electrophilic region associated with the Cl halogen atom and the nucleophilic regions of the surrounding protein residues [79].

Next, in order to disclose if and how the two neonicotinoids exert an additive effect to estrogen binding, by occupying an allosteric cavity, we looked for the presence of druggable allosteric pockets in the protein. Interestingly, a high-ranking binding pocket was found in the proximity of the estrogen binding site of one monomer of ERα (Figure 6). The docking calculation performed on this pocket, strikingly revealed that imidacloprid can H-bond with Lys449 and Glu323. As well thiacloprid H-bonds with Lys449 and Trp393.

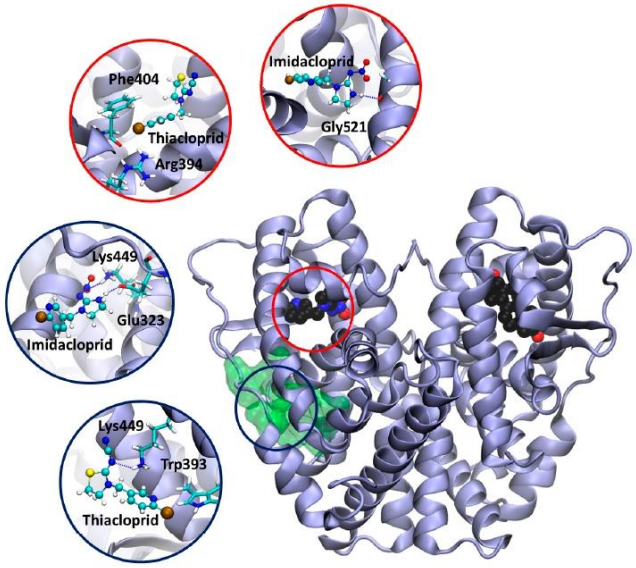

Figure 6. Model of estrogen receptor α dimer (PDB ID 1qku [52]) in complex with the neonicotinoids, imidacloprid and thiacloprid. The allosteric pocket is shown as a green transparent surface. Imidacloprid, thiacloprid, and 17-β-estradiol are displayed in a van der Waals representation and colored by the atom name. The protein is shown as violet new cartoons. The insets report a close view of docking poses of imidacloprid and thiacloprid inside the estrogen binding site (red circles) and onto the newly identified allosteric pocket (dark blue circles). The ligand and the residues establishing the most important interactions are depicted in balls and sticks and licorice representations, respectively, and colored by the atom name.

4. Discussion

In this study, the effect of three pesticides on two key targets of the endocrine system was evaluated using a combination of experimental and in silico methods that allowed an investigation at the molecular level.

The first target considered was aromatase, the key enzyme for estrogen production that resulted in being partially inhibited by glyphosate. The increase obtained in the aromatase activity in the presence of imidacloprid and thiacloprid, even if not statistically significant, can be interesting to be further investigated. Indeed, these two compounds could directly act on aromatase as allosteric activators or they could exert their action indirectly on CPR that has an essential role in catalysis and acts as an effector on human aromatase conformation [80,81].

Glyphosate is the most widely used active compound among herbicides and was already reported to affect aromatase expression and activity in cells [33,35]. The impact for human health has already been demonstrated: Indeed, an alteration in androgens/estrogens balance due to a lower aromatase expression as a consequence of the glyphosate presence changed the sperm nuclear quality impacting mammalian reproduction [82].

However, the direct interaction between glyphosate and the enzyme together with the inhibition mechanism was not reported yet. In this study, the ELISA assay revealed that the inhibition of aromatase by glyphosate is partial and weak and strongly depends on the substrate concentration. Moreover, at the lower concentration of glyphosate tested (1 μM), the inhibition was found to be non-competitive, while at the higher concentration used (5 μM), the inhibition turned into a mixed inhibition mode. These data suggest that glyphosate binds to an allosteric site both when the enzyme is free and in complex with the substrate. Classical MD simulations supply a structural model for glyphosate binding to aromatase, explaining at the atomic-level that this pollutant may exert its inhibitory activity at a low concentration by binding to the allosteric Site 1 previously identified by Magistrato et al. [50] and demonstrated to bind small-molecules inhibitors [54]. When the concentration increases, a mixed inhibition is observed again compatible with the presence of an allosteric site. The binding of glyphosate probably becomes stronger or another allosteric site is occupied by the inhibitor. However, MD simulations showed that glyphosate did not stably bind to the second allosteric pocket (Site 2) identified in previous studies.

The second important target studied was the estrogen receptor that is responsible for estrogen binding and signal transduction in cells. MCF-7 cells, stably transfected with an estrogen-regulated luciferase gene (MELN cells), were used to assess the estrogenic activity of the pesticides. Glyphosate induced no estrogenic activity on MELN cells, moreover glyphosate did not change the effect induced by tamoxifen or E2. These results are in accordance with the results of the studies of Kojima et al., 2004 [46] and Gasnier et al., 2009 [35], who did not find any agonistic or antagonistic effect of glyphosate on ER. On the contrary, our results are different than the results of Thongprakaisang et al., 2013 [44] and Mesnage et al., 2017 [45] who found a significant increase of ER-induced estrogenic activity. A possible explanation of this discrepancy could be that in our study the estrogenic activity was evaluated on MELN cells while the other two studies applied T47D-KBluc cells, which might be more sensitive to the glyphosate activity than MELN cells. Moreover, our results are consistent with the results of the Endocrine Disruptor Screening Program (EDSP) conducted by the United States Environmental Protection Agency (US EPA, 2015) which concluded that "there is no convincing evidence of a potential interaction with the estrogen pathway for glyphosate".

In the present study, both imidacloprid and thiacloprid induced a dose-response estrogenic activity mediated by the ER activation, in particular starting from 10^{-4} M. A consistent result was found in the study of Kojima et al., 2004 [46] in which no estrogenic activity was detected exposing transfected-cells to imidacloprid at concentrations lower than 10^{-5} M; a contradicting result was found by Westlund and Yargeau, 2017 [48], who did not find any estrogenic activity testing thiacloprid at concentrations comparable to ours. The conflicting results of thiacloprid should be interpreted considering the different cell models applied in our study with respect to the study of Westlund and Yargeau, 2017 (i.e., the present study was performed on mammalian cells while the previous one on yeast cells) [48]. Indeed, yeast cells are characterized by a different membrane permeability, transport proteins, and signal transduction pathways with respect to mammalian cells which may have influenced the results [42], as reported before also for other nuclear receptors [83].

The estrogenic activity of imidacloprid and thiacloprid was observed at concentrations higher than the pesticide levels measured in human biological samples [76,84]. Although such high levels of pesticides are not found in human biological samples, low doses of these pesticides should not be considered harmless. Indeed, in biological fluids these pesticides may be present in combination with other EDCs with a similar action mode and, thus, these pesticides together with other EDCs might cause an overall estrogenic effect. Moreover, these high concentrations of pesticides are similar

to levels in some environmental matrices, where they could cause adverse health effects on wildlife animals. For example, in guttation water or morning dew of plants, imidacloprid was found to be present at a concentration up to 346 mg/L [85].

Interestingly, the results of the present study showed that, when the ER-antagonist tamoxifen was added to these pesticides, the estrogenic activity was still higher than the negative control. This result can be explained by the competition between each pesticide and tamoxifen for ER binding. Moreover, in the presence of high concentrations of imidacloprid and thiacloprid, an additive effect with E2 was also observed. The docking calculation suggested that these two neonicotinoids may bind to both the orthosteric and allosteric pockets of ERα, suggesting a putative mechanism to rationalize their observed estrogenic activity.

5. Conclusions

In conclusion, this study provides further evidence about the action of some pesticides as endocrine disrupting chemicals (EDCs) targeting important proteins of the endocrine system. In particular, it shows that the inhibitory effects of the three compounds tested on aromatase are partial and their estrogenic effects occur at relatively high concentrations. However, possible additive estrogenic effects with the physiological hormone 17-βestradiol are present. Furthermore, it has to be taken into account that pesticides are usually introduced in the environment with their co-formulants that can be also biologically active as EDCs. Previous studies already showed that aromatase is inhibited by co-formulants of glyphosate-based herbicides [33,86]. Moreover, more studies are needed to investigate a possible additive effect of different pesticides that can be contemporarily present in the environment.

Our study also provides an integrated approach based on different assays and computational methods that allowed gaining new information about the possible interaction of pesticides and key targets at a molecular level. Such information can be exploited to predict the possible impact of other compounds on estrogen production and signaling in order to develop safer compounds for human health and environment.

Author Contributions: Conceptualization, T.S., A.S., A.M., G.G., and G.D.N.; data curation, C.Z., T.S., M.G., A.M., and G.D.N.; formal analysis, C.Z., T.S., M.G., A.S., A.M., and G.D.N.; funding acquisition, A.M., G.G., and G.D.N.; investigation, C.Z., T.S., M.G., S.B., A.S., A.M., G.G., and G.D.N.; methodology, C.Z., M.G., S.B., A.S., and A.M.; project administration, G.D.N.; resources, T.S., A.M., and G.G.; software, C.Z., M.G., S.B., A.S., and A.M.; supervision, T.S., A.M., G.G., and G.D.N.; validation, C.Z., M.G., and S.B.; visualization, C.Z., M.G., and A.S.; writing—original draft, C.Z. and G.D.N.; writing—review and editing, C.Z., T.S., M.G., A.S., A.M., G.G., and G.D.N. All authors have read and agreed to the published version of the manuscript.

Funding: This research was funded by the CRT Foundation grant (project "Exposome" RF = 2016.2780) to G.D.N., by the Italian Association for Cancer Research (MFAG 17134), "Mario and Valeria Rindi" fellowship for Italy, and by the "Against bRain cancEr: Finding personalized therapies with in silico and in vitro strategies" (ARES) CUP: D93D19000020007 POR FESR 2014 2020—1.3.b—Friuli Venezia Giulia.

Conflicts of Interest: The authors declare no conflict of interest.

References

1. Mie, A.; Andersen, H.R.; Gunnarsson, S.; Kahl, J.; Kesse-Guyot, E.; Rembiałkowska, E.; Quaglio, G.; Grandjean, P. Human health implications of organic food and organic agriculture: A comprehensive review. *Environ. Health* **2017**, *16*, 111. [CrossRef] [PubMed]
2. Prüss-Ustün, A.; Vickers, C.; Haefliger, P.; Bertollini, R. Knowns and unknowns on burden of disease due to chemicals: A systematic review. *Environ. Health* **2011**, *10*, 9. [CrossRef]
3. Kortenkamp, A.; Faust, M.; Scholze, M.; Backhaus, T. Low-level exposure to multiple chemicals: Reason for human health concerns? *Environ. Health Perspect.* **2007**, *115*, 106–114. [CrossRef] [PubMed]
4. Yang, M.; Park, M.S.; Lee, H.S. Endocrine disrupting chemicals: Human exposure and health Risks. *J. Environ. Sci. Health C Environ. Carcinog. Ecotoxicol. Rev.* **2006**, *24*, 183–224. [CrossRef] [PubMed]
5. Schug, T.T.; Janesick, A.; Blumberg, B.; Heindel, J.J. Endocrine disrupting chemicals and disease susceptibility. *J. Steroid Biochem. Mol. Biol.* **2011**, *127*, 204–215. [CrossRef] [PubMed]

6. Vandenberg, L.N.; Colborn, T.; Hayes, T.B.; Heindel, J.J.; Jacobs, D.R.; Lee, D.H.; Shioda, T.; Soto, A.M.; Vom, S.F.; Welshons, W.V.; et al. Hormones and endocrine-disrupting chemicals: Low-dose effects and nonmonotonic dose responses. *Endocr. Rev.* **2012**, *33*, 378–455. [CrossRef]
7. Takayanagi, S.; Tokunaga, T.; Liu, X.; Okada, H.; Matsushima, A.; Shimohigashi, Y. Endocrine disruptor bisphenol A strongly binds to human estrogen-related receptor γ (ERRγ) with high constitutive activity. *Toxicol. Lett.* **2006**, *167*, 95–105. [CrossRef]
8. Mnif, W.; Hassine, A.I.H.; Bouaziz, A.; Bartegi, A.; Thomas, O.; Roig, B. Effect of endocrine disruptor Pesticides: A Review. *Int. J. Environ. Res. Public Health* **2011**, *8*, 2265–2303. [CrossRef]
9. Bernhardt, E.S.; Rosi, E.J.; Gessner, M.O. Synthetic chemicals as agents of global change. *Front. Ecol. Environ.* **2017**, *15*, 84–90. [CrossRef]
10. Storck, V.; Karpouzas, D.G.; Martin-Laurent, F. Towards a better pesticide policy for the European Union. *Sci. Total Environ.* **2017**, *575*, 1027–1033. [CrossRef]
11. Amrhein, N.; Deus, B.; Gehrke, P.; Steinrücken, H.C. The Site of the Inhibition of the Shikimate Pathway by glyphosate: ii. interference of glyphosate with chorismate formation in vivo and in vitro. *Plant Physiol.* **1980**, *66*, 830–834. [CrossRef] [PubMed]
12. Herrmann, K.M.; Weaver, L.M. The Shikimate Pathway. *Annu. Rev. Plant Phys.* **1999**, *50*, 473–503. [CrossRef] [PubMed]
13. Simon-Delso, N.; Amaral-Rogers, V.; Belzunces, L.P.; Bonmatin, J.M.; Chagnon, M.; Downs, C.; Furlan, L.; Gibbons, D.W.; Giorio, C.; Girolami, V.; et al. Systemic insecticides (neonicotinoids and fipronil): Trends, uses, mode of action and metabolites. *Environ. Sci. Pollut. Res. Int.* **2015**, *22*, 5–34. [CrossRef] [PubMed]
14. Matsuda, K.; Ihara, M.; Sattelle, D.B. Neonicotinoid Insecticides: Molecular Targets, Resistance, and Toxicity. *Annu. Rev. Pharmacol. Toxicol.* **2020**, *60*, 241–255. [CrossRef] [PubMed]
15. Sánchez-Bayo, F.; Tennekes, H.A. Time-Cumulative Toxicity of Neonicotinoids: Experimental Evidence and Implications for Environmental Risk Assessments. *Int. J. Environ. Res. Public Health* **2020**, *17*, 1629. [CrossRef]
16. Mensah, P.K.; Palmer, C.G.; Odume, O.N. Ecotoxicology of glyphosate and glyphosate-based herbicides — toxicity to wildlife and humans. In *Toxicity and Hazard of Agrochemicals*; Larramendy, M.L., Soloneski, S., Eds.; Intech: Rijeka, Croatia, 2015; pp. 281–304.
17. Gibbons, D.; Morrissey, C.; Mineau, P. A review of the direct and indirect effects of neonicotinoids and fipronil on vertebrate wildlife. *Environ. Sci. Pollut. Res.* **2015**, *22*, 103–118. [CrossRef]
18. Thompson, D.A.; Lehmler, H.-J.; Kolpin, D.W.; Hladik, M.L.; Vargo, J.D.; Schilling, K.E.; LeFevre, G.H.; Peeples, T.L.; Poch, M.C.; LaDuca, L.E.; et al. A critical review on the potential impacts of neonicotinoid insecticide use: Current knowledge of environmental fate, toxicity, and implications for human health. *Environ. Sci. Processes Impacts* **2020**, *22*, 1315–1346. [CrossRef]
19. Bass, C.; Denholm, I.; Williamson, M.S.; Nauen, R. The global status of insect resistance to neonicotinoid insecticides. *Pestic. Biochem. Physiol.* **2015**, *121*, 78–87. [CrossRef]
20. Jeschke, P.; Nauen, R.; Schindler, M.; Elbert, A. Overview of the status and global strategy for neonicotinoids. *J. Agric. Food Chem.* **2011**, *59*, 2897–2908. [CrossRef]
21. The European Commission. Legislation 132. *Off. J. Eur. Union* **2018**, *61*, 31–40.
22. Zhang, Q.; Li, Z.; Chang, C.H.; Lou, J.L.; Zhao, M.R.; Lu, C. Potential human exposures to neonicotinoid insecticides: A review. *Environ. Pollut.* **2018**, *236*, 71–81. [CrossRef] [PubMed]
23. Annett, R.; Habibi, H.R.; Hontela, A. Impact of glyphosate and glyphosate-based herbicides on the freshwater environment: Impact of glyphosate-based herbicides. *J. Appl. Toxicol.* **2014**, *34*, 458–479. [CrossRef] [PubMed]
24. Bai, S.H.; Ogbourne, S.M. Glyphosate: Environmental contamination, toxicity and potential risks to human health via food contamination. *Environ. Sci. Pollut. Res.* **2016**, *23*, 18988–19001. [CrossRef] [PubMed]
25. Van Bruggen, A.H.C.; He, M.M.; Shin, K.; Mai, V.; Jeong, K.C.; Finckh, M.R.; Morris, J.G. Environmental and health effects of the herbicide glyphosate. *Sci. Total Environ.* **2018**, *616–617*, 255–268. [CrossRef]
26. Morrissey, C.A.; Mineau, P.; Devries, J.H.; Sanchez-Bayo, F.; Liess, M.; Cavallaro, M.C.; Liber, K. Neonicotinoid contamination of global surface waters and associated risk to aquatic invertebrates: A review. *Environ. Int.* **2015**, *74*, 291–303. [CrossRef]
27. Lu, C.; Chang, C.-H.; Palmer, C.; Zhao, M.; Zhang, Q. Neonicotinoid residues in fruits and vegetables: An integrated dietary exposure assessment approach. *Environ. Sci. Technol.* **2018**, *52*, 3175–3184. [CrossRef]

28. Hladik, M.L.; Main, A.R.; Goulson, D. Environmental risks and challenges associated with neonicotinoid insecticides. *Environ. Sci. Technol.* **2018**, *52*, 3329–3335. [CrossRef]
29. Vencill, W.K. *Herbicide Handbook*, 8th ed.; Vencill, W.K., Ed.; Weed Science Society of America: Lawrence, KS, USA, 2002; pp. 231–234.
30. Agostini, L.P.; Dettogni, R.S.; dos Reis, R.S.; Stur, E.; dos Santos, E.V.W.; Ventorim, D.P.; Garcia, F.M.; Cardoso, R.C.; Graceli, J.B.; Louro, I.D. Effects of glyphosate exposure on human health: Insights from epidemiological and in vitro studies. *Sci. Total Environ.* **2020**, *705*, 135808. [CrossRef]
31. Di Nardo, G.; Gilardi, G. Human aromatase: Perspectives in biochemistry and biotechnology: Human Aromatase. *Biotechnol. Appl. Biochem.* **2013**, *60*, 92–101. [CrossRef]
32. Benachour, N.; Sipahutar, H.; Moslemi, S.; Gasnier, C.; Travert, C.; Séralini, G.E. Time- and dose-dependent effects of roundup on human embryonic and placental Cells. *Arch. Environ. Contam. Toxicol.* **2007**, *53*, 126–133. [CrossRef]
33. Richard, S.; Moslemi, S.; Sipahutar, H.; Benachour, N.; Seralini, G.-E. Differential effects of glyphosate and roundup on human placental cells and aromatase. *Environ. Health Perspect.* **2005**, *113*, 716–720. [CrossRef] [PubMed]
34. Benachour, N.; Séralini, G.E. Glyphosate formulations induce apoptosis and necrosis in human umbilical, embryonic, and placental cells. *Chem. Res. Toxicol.* **2009**, *22*, 97–105. [CrossRef] [PubMed]
35. Gasnier, C.; Dumont, C.; Benachour, N.; Clair, E.; Chagnon, M.C.; Séralini, G.E. Glyphosate-based herbicides are toxic and endocrine disruptors in human cell lines. *Toxicology* **2009**, *262*, 184–191. [CrossRef]
36. Caron-Beaudoin, E.; Viau, R.; Hudon-Thibeault, A.A.; Vaillancourt, C.; Sanderson, J.T. The use of a unique co-culture model of fetoplacental steroidogenesis as a screening tool for endocrine disruptors: The effects of neonicotinoids on aromatase activity and hormone production. *Toxicol. Appl. Pharmacol.* **2017**, *332*, 15–24. [CrossRef] [PubMed]
37. Caron-Beaudoin, É.; Denison, M.S.; Sanderson, J.T. Effects of neonicotinoids on promoter-specific expression and activity of aromatase (CYP19) in human adrenocortical carcinoma (H295R) and primary umbilical vein endothelial (HUVEC) cells. *Toxicol. Sci.* **2016**, *149*, 134–144. [CrossRef]
38. Caron-Beaudoin, É.; Viau, R.; Sanderson, J.T. Effects of neonicotinoid pesticides on promoter-specific aromatase (CYP19) expression in Hs578t breast cancer cells and the role of the VEGF pathway. *Environ. Health Perspect.* **2018**, *126*, 047014. [CrossRef]
39. Di Nardo, G.; Breitner, M.; Sadeghi, S.J.; Castrignanò, S.; Mei, G.; Di Venere, A.; Nicolai, E.; Allegra, P.; Gilardi, G. Dynamics and flexibility of human aromatase probed by FTIR and time resolved fluorescence spectroscopy. *PLoS ONE* **2013**, *8*, e82118. [CrossRef]
40. Baravalle, R.; Ciaramella, A.; Baj, F.; Di Nardo, G.; Gilardi, G. Identification of endocrine disrupting chemicals acting on human aromatase. *Biochim. Biophys. Acta - Proteins Proteomics* **2018**, *1866*, 88–96. [CrossRef]
41. Lo, J.; Di Nardo, G.; Griswold, J.; Egbuta, C.; Jiang, W.; Gilardi, G.; Ghosh, D. Structural basis for the functional roles of critical residues in human cytochrome P450 aromatase. *Biochemistry* **2013**, *52*, 5821–5829.
42. Kiyama, R.; Wada-Kiyama, Y. Estrogenic endocrine disruptors: Molecular mechanisms of action. *Environ. Int.* **2015**, *83*, 11–40. [CrossRef]
43. Pavlin, M.; Spinello, A.; Pennati, M.; Zaffaroni, N.; Gobbi, S.; Bisi, A.; Colombo, G.; Magistrato, A. A computational assay of estrogen receptor α antagonists reveals the key common structural traits of drugs effectively fighting refractory breast Cancers. *Sci. Rep.* **2018**, *8*, 649. [CrossRef] [PubMed]
44. Thongprakaisang, S.; Thiantanawat, A.; Rangkadilok, N.; Suriyo, T.; Satayavivad, J. Glyphosate induces human breast cancer cells growth via estrogen receptors. *Food Chem. Toxicol.* **2013**, *59*, 129–136. [CrossRef] [PubMed]
45. Mesnage, R.; Phedonos, A.; Biserni, M.; Arno, M.; Balu, S.; Corton, J.C.; Ugarte, R.; Antoniou, M.N. Evaluation of estrogen receptor alpha activation by glyphosate-based herbicide constituents. *Food Chem. Toxicol.* **2017**, *108*, 30–42. [CrossRef]
46. Kojima, H.; Katsura, E.; Takeuchi, S.; Niiyama, K.; Kobayashi, K. Screening for estrogen and androgen receptor activities in 200 pesticides by in vitro reporter gene assays using Chinese hamster ovary cells. *Environ. Health Perspect.* **2004**, *112*, 524–531. [CrossRef] [PubMed]
47. Mesnage, R.; Biserni, M.; Genkova, D.; Wesolowski, L.; Antoniou, M.N. Evaluation of neonicotinoid insecticides for oestrogenic, thyroidogenic and adipogenic activity reveals imidacloprid causes lipid accumulation. *J. Appl. Toxicol.* **2018**, *38*, 1483–1491. [CrossRef]

48. Westlund, P.; Yargeau, V. Investigation of the presence and endocrine activities of pesticides found in wastewater effluent using yeast-based bioassays. *Sci. Total Environ.* **2017**, *607–608*, 744–751. [CrossRef]
49. Huang, N.; Pandey, A.V.; Agrawal, V.; Reardon, W.; Lapunzina, P.D.; Mowat, D.; Jabs, E.W.; Vliet, G.V.; Sack, J.; Flück, C.E.; et al. Diversity and Function of Mutations in P450 Oxidoreductase in Patients with Antley-Bixler Syndrome and Disordered Steroidogenesis. *Am. J. Hum. Genet.* **2005**, *76*, 729–749. [CrossRef]
50. Sgrignani, J.; Bon, M.; Colombo, G.; Magistrato, A. Computational approaches elucidate the allosteric mechanism of human aromatase inhibition: A novel possible route to small-molecule regulation of CYP450s activities? *J. Chem. Inf. Model.* **2014**, *54*, 2856–2868. [CrossRef]
51. Friesner, R.A.; Murphy, R.B.; Repasky, M.P.; Frye, L.L.; Greenwood, J.R.; Halgren, T.A.; Sanschagrin, P.C.; Mainz, D.T. Extra precision Glide: Docking and scoring incorporating a model of hydrophobic enclosure for protein-ligand complexes. *J. Med. Chem.* **2006**, *49*, 6177–6196.
52. Gangloff, M.; Ruff, M.; Eiler, S.; Duclaud, S.; Wurtz, J.M.; Moras, D. Crystal structure of a mutant hERα ligand-binding domain reveals key structural features for the mechanism of partial agonism. *J. Biol. Chem.* **2001**, *276*, 15059–15065. [CrossRef]
53. Halgren, T. New method for fast and accurate binding-site identification and analysis. *Chem. Biol. Drug Des.* **2007**, *69*, 146–148. [CrossRef] [PubMed]
54. Spinello, A.; Martini, S.; Berti, F.; Pennati, M.; Pavlin, M.; Sgrignani, J.; Grazioso, G.; Colombo, G.; Zaffaroni, N.; Magistrato, A. Rational design of allosteric modulators of the aromatase enzyme: An unprecedented therapeutic strategy to fight breast cancer. *Eur. J. Med. Chem.* **2019**, *168*, 253–262. [CrossRef] [PubMed]
55. Jo, S.; Kim, T.; Iyer, V.G.; Im, W. CHARMM-GUI: A web-based graphical user interface for CHARMM. *J. Comput. Chem.* **2008**, *29*, 1859–1865. [CrossRef] [PubMed]
56. Anandakrishnan, R.; Aguilar, B.; Onufriev, A.V. *H*++ 3.0: Automating pK prediction and the preparation of biomolecular structures for atomistic molecular modeling and simulations. *Nucl. Aci. Res.* **2012**, *40*, W537–W541. [CrossRef]
57. Spinello, A.; Pavlin, M.; Casalino, L.; Magistrato, A. A dehydrogenase dual hydrogen abstraction mechanism promotes estrogen biosynthesis: Can we expand the functional annotation of the aromatase enzyme? *Chem. Eur. J.* **2018**, *24*, 10840–10849. [CrossRef]
58. Liu, B.; Dong, L.; Yu, Q.; Li, X.; Wu, F.; Tan, Z.; Luo, S. Thermodynamic study on the protonation reactions of glyphosate in aqueous solution: Potentiometry, calorimetry and NMR spectroscopy. *J. Phys. Chem. B* **2016**, *120*, 2132–2137. [CrossRef]
59. Wickstrom, L.; Okur, A.; Simmerling, C. Evaluating the performance of the ff99SB force field based on NMR scalar coupling data. *Biophys. J.* **2009**, *97*, 853–856. [CrossRef]
60. Lindorff-Larsen, K.; Piana, S.; Palmo, K.; Maragakis, P.; Klepeis, J.L.; Dror, R.O.; Shaw, D.E. Improved side-chain torsion potentials for the Amber ff99SB protein force field. *Proteins* **2010**, *78*, 1950–1958. [CrossRef]
61. Dickson, C.J.; Madej, B.D.; Skjevik, Å.A.; Betz, R.M.; Teigen, K.; Gould, I.R.; Walker, R.C. Lipid14: The Amber Lipid Force Field. *J. Chem. Theory Comput.* **2014**, *10*, 865–879. [CrossRef]
62. Shahrokh, K.; Orendt, A.; Yost, G.S.; Cheatham, T.E. Quantum mechanically derived AMBER-compatible heme parameters for various states of the cytochrome P450 catalytic cycle. *J. Comput. Chem.* **2012**, *33*, 119–133. [CrossRef]
63. Wang, J.; Wolf, R.M.; Caldwell, J.W.; Kollman, P.A.; Case, D.A. Development and testing of a general amber force field. *J. Comput. Chem.* **2004**, *25*, 1157–1174. [CrossRef] [PubMed]
64. Bayly, C.I.; Cieplak, P.; Cornell, W.; Kollman, P.A. A well-behaved electrostatic potential based method using charge restraints for deriving atomic charges: The RESP model. *J. Phys. Chem.* **1993**, *97*, 10269–10280. [CrossRef]
65. Frisch, M.J.; Trucks, G.W.; Schlegel, H.B.; Scuseria, G.E.; Robb, M.A.; Cheeseman, J.R.; Scalmani, G.; Barone, V.; Petersson, G.A.; Nakatsuji, H.; et al. *Gaussian 09, Revision A.02*; Gaussian, Inc.: Wallingford, CT, USA, 2009.
66. Wang, J.; Wang, W.; Kollman, P.A.; Case, D.A. Automatic atom type and bond type perception in molecular mechanical calculations. *J. Mol. Graphics Model.* **2006**, *25*, 247–260. [CrossRef] [PubMed]
67. Sousa da Silva, A.W.; Vranken, W.F. ACPYPE - Antechamber Python Parser Interface. *BMC Res. Notes* **2012**, *5*, 367. [CrossRef] [PubMed]
68. Van Der Spoel, D.; Lindahl, E.; Hess, B.; Groenhof, G.; Mark, A.E.; Berendsen, H.J. GROMACS: Fast, flexible, and free. *J. Comput. Chem.* **2005**, *26*, 1701–1718. [CrossRef] [PubMed]

69. Darden, T.; York, D.; Pedersen, L. Particle mesh Ewald: An N-log(N) method for Ewald sums in large systems. *J. Chem. Phys.* **1993**, *98*, 10089–10092. [CrossRef]
70. Bussi, G.; Donadio, D.; Parrinello, M. Canonical sampling through velocity rescaling. *J. Chem. Phys.* **2007**, *126*, 014101. [CrossRef]
71. Balaguer, P.; Boussioux, A.-M.; Demirpence, E.; Nicolas, J.C. Reporter cell lines are useful tools for monitoring biological activity of nuclear receptor ligands. *Luminescence* **2001**, *16*, 153–158. [CrossRef]
72. Berckmans, P.; Leppens, H.; Vangenechten, C.; Witters, H. Screening of endocrine disrupting chemicals with MELN cells, an ER-transactivation assay combined with cytotoxicity assessment. *Toxicol. In Vitro* **2007**, *21*, 1262–1267. [CrossRef]
73. Balaguer, P.; François, F.; Comunale, F.; Fenet, H.; Boussioux, A.-M.; Pons, M.; Nicolas, J.C.; Casellas, C. Reporter cell lines to study the estrogenic effects of xenoestrogens. *Sci. Total. Environ.* **1999**, *233*, 47–56. [CrossRef]
74. Schilirò, T.; Porfido, A.; Longo, A.; Coluccia, S.; Gilli, G. The E-screen test and the MELN gene-reporter assay used for determination of estrogenic activity in fruits and vegetables in relation to pesticide residues. *Food Chem. Toxicol.* **2013**, *62*, 82–90. [CrossRef] [PubMed]
75. Körner, W.; Hanf, V.; Schuller, W.; Kempter, C.; Metzger, J.; Hagenmaier, H. Development of a sensitive E-screen assay for quantitative analysis of estrogenic activity in municipal sewage plant effluents. *Sci. Total Environ.* **1999**, *225*, 33–48. [CrossRef]
76. Gillezeau, C.; Van Gerwen, M.; Shaffer, R.M.; Rana, I.; Zhang, L.; Sheppard, L.; Taioli, E. The evidence of human exposure to glyphosate: A review. *Environ. Health* **2019**, *18*, 2. [CrossRef] [PubMed]
77. Magistrato, A.; Sgrignani, J.; Krause, R.; Cavalli, A. Single or multiple access channels to the CYP450s active Site? An answer from free energy simulations of the human aromatase enzyme. *J. Phys. Chem. Lett.* **2017**, *8*, 2036–2042. [CrossRef]
78. Ritacco, I.; Saltalamacchia, A.; Spinello, A.; Ippoliti, E.; Magistrato, A. All-atom simulations disclose how cytochrome reductase reshapes the substrate access/egress routes of its partner CYP450s. *J. Phys. Chem. Lett.* **2020**, *11*, 1189–1193. [CrossRef]
79. Scholfield, M.R.; Vander Zanden, C.M.; Carter, M.; Ho, P.S. Halogen bonding (X-bonding): A biological perspective: Halogen Bonding (X-Bonding). *Protein Sci.* **2013**, *22*, 139–152. [CrossRef]
80. Parween, S.; Di Nardo, G.; Baj, F.; Zhang, C.; Gilardi, G.; Pandey, A.V. Differential effects of variations in human P450 oxidoreductase on the aromatase activity of CYP19A1 polymorphisms R264C and R264H. *J. Steroid Biochem. Mol. Biol.* **2020**, *196*, 105507. [CrossRef]
81. Zhang, C.; Catucci, G.; Di Nardo, G.; Gilardi, G. Effector role of cytochrome P450 reductase for androstenedione binding to human aromatase. *Int. J. Biol. Macromol.* **2020**, *164*, 510–517. [CrossRef]
82. Cassault-Meyer, E.; Gress, S.; Séralini, G.-É.; Galeraud-Denis, I. An acute exposure to glyphosate-based herbicide alters aromatase levels in testis and sperm nuclear quality. *Environ. Toxicol. Pharmacol.* **2014**, *38*, 131–140. [CrossRef]
83. Bureik, M.; Brück, N.; Hübel, K.; Bernhardt, R. The human mineralocorticoid receptor only partially differentiates between different ligands after expression in fission yeast. *FEMS Yeast Res.* **2005**, *5*, 627–633. [CrossRef]
84. Wang, L.; Liu, T.; Liu, F.; Zhang, J.; Wu, Y.; Sun, H. Occurrence and profile characteristics of the pesticide imidacloprid, preservative parabens, and their metabolites in human urine from rural and urban China. *Environ. Sci. Technol.* **2015**, *49*, 14633–14640. [CrossRef] [PubMed]
85. Tapparo, A.; Giorio, C.; Marzaro, M.; Marton, D.; Soldà, L.; Girolami, V. Rapid analysis of neonicotinoid insecticides in guttation drops of corn seedlings obtained from coated seeds. *J. Environ. Monit.* **2011**, *13*, 1564. [CrossRef] [PubMed]
86. Defarge, N.; Takács, E.; Lozano, V.; Mesnage, R.; Spiroux de Vendômois, J.; Séralini, G.E.; Székács, A. Co-formulants in glyphosate-based herbicides disrupt aromatase activity in human cells below toxic levels. *Int. J. Environ. Res. Public Health* **2016**, *13*, 264. [CrossRef] [PubMed]

Chapter 7

General conclusions

Aromatase is an important cytochrome P450 enzyme involved in human hormone biosynthesis and androgen/estrogen balance. Not only it catalyzes traditional hydroxylation reactions, but it also mediates the scission of the carbon-carbon bond to construct an aromatic ring. The mechanism of its catalytic reaction is still elusive and has not been fully explained.

The reactive oxoferryl species has not been captured and characterized yet in a human cytochrome P450. Chapter 2 of this thesis deals with the capture and characterization of aromatase compound I in the stopped-flow spectrometer using the “peroxide shunt pathway”. Using this strategy, the product estrone was obtained by using 19-oxo ASD as the substrate, which supports the theory that compound I is the active species in the aromatization reaction. The function of some important amino acids in proton transfer was also investigated. The conserved “acid-alcohol” pair in P450s was proven to be crucial for protonation. The active site residue Asp-309 releases protons through a protonation-deprotonation equilibrium. The effect of Thr-310 mutation was not as obvious as that in P450cam. The T310A mutant can still form compound I and retain some catalytic activity. Threonine is thought to form a hydrogen bond with compound 0 to stabilize and promote the formation of compound I. But in the results presented in this thesis, it also shows to affect the stability of compound I. Another important amino acid Arg-192, located in the proton transfer network, its mutation results in the decrease of proton transfer efficiency. An alternative and less efficient proton transfer path is also proposed.

Aromatase mediated reactions require the redox partner CPR to provide electrons. Whether CPR has other roles besides an electron donor has always been a controversial topic. To answer this question, the possible functions of CPR was investigated in Chapter 3. In kinetic studies of substrate binding, aromatase was found to follow the conformational selection mechanism. Interestingly, this mechanism enhanced by CPR’s presence, and the substrate binding rate of aromatase increased. In the ITC experiment, CPR was found to prefer to bind to substrate-free aromatase, and the change of enthalpy was relatively higher than that of substrate-bound aromatase. The data suggest that the binding of CPR changed the aromatase motions, promoting aromatase conformation optimal for substrate binding, and thus accelerated the substrate-binding rate.

The formation of CPR-aromatase catalytic complex is predicted to be through electrostatic interaction. In Chapter 4, these amino acids in contact with CPR were found to be non-conserved through sequence alignment and structural analysis of aromatase from different vertebrate species and invertebrates. In the course of evolution, positive amino acids and residues forming hydrogen bonds with reductase were introduced on aromatase surface forming the interface with CPR. In mammals, CPR serves not only aromatase but also other P450s. However, the number of CPR *in vivo* is limited. The continuous optimization of aromatase contact interface in the evolution process could have made it more competitive. In this chapter, it is also concluded that the high substrate specificity of aromatase is due to the conserved sequences of its active center and substrate recognition sites.

Chapter 5 provides evidence that aromatase has a more compact three-dimensional structure after binding with the ligand through FTIR and fluorescence experiments. However, the two SNPs (R264C and R264H) didn't show the same behavior. The data suggested that the substitution of Arg-264 changes the flexibility of G-helix and affects its interaction with F-helix. It leads to the incorrect incorporation of the substrate that it is not retained in the active site as in the WT enzyme.

Due to the role of aromatase in human health, in Chapter 6, the effects of pesticides on aromatase and estrogen receptor were studied by using two key targets of the endocrine system. Glyphosate can inhibit aromatase activity by binding different allosteric sites on aromatase, which shows non-competitive inhibition or mixed inhibition mechanism. Both imidacloprid and thiacloprid can activate the estrogen receptor in MELN cells. Docking experiments show the presence of allosteric sites in both aromatase and ERα. These three pesticides are potential endocrine disruptors and harmful to human health.

In conclusion, the data presented in this thesis add new information about the catalytic mechanism of human aromatase and highlights the role of three residues in oxygen activation and reactive species stabilization. Moreover, the results show how SNPs or exogenous molecules can affect the functionality of this important enzyme that is crucial to maintain the correct hormonal levels and prevent estrogen-related pathologies.